TU/e EINDHOVEN UNIVERSITY OF TECHNOLOGY

Ohmic resistance and current distribution at gas-evolving electrodes

Citation for published version (APA):
Bongenaar-Schlenter, B. E. (1984). *Ohmic resistance and current distribution at gas-evolving electrodes*. [Phd Thesis 1 (Research TU/e / Graduation TU/e), Applied Physics and Science Education]. Technische Hogeschool Eindhoven. https://doi.org/10.6100/IR108330

DOI:
10.6100/IR108330

Document status and date:
Published: 01/01/1984

Document Version:
Publisher's PDF, also known as Version of Record (includes final page, issue and volume numbers)

Please check the document version of this publication:

• A submitted manuscript is the version of the article upon submission and before peer-review. There can be important differences between the submitted version and the official published version of record. People interested in the research are advised to contact the author for the final version of the publication, or visit the DOI to the publisher's website.
• The final author version and the galley proof are versions of the publication after peer review.
• The final published version features the final layout of the paper including the volume, issue and page numbers.

Link to publication

General rights
Copyright and moral rights for the publications made accessible in the public portal are retained by the authors and/or other copyright owners and it is a condition of accessing publications that users recognise and abide by the legal requirements associated with these rights.

• Users may download and print one copy of any publication from the public portal for the purpose of private study or research.
• You may not further distribute the material or use it for any profit-making activity or commercial gain
• You may freely distribute the URL identifying the publication in the public portal.

If the publication is distributed under the terms of Article 25fa of the Dutch Copyright Act, indicated by the "Taverne" license above, please follow below link for the End User Agreement:

www.tue.nl/taverne

Take down policy
If you believe that this document breaches copyright please contact us at:

openaccess@tue.nl

providing details and we will investigate your claim.

Download date: 04. Oct. 2023

OHMIC RESISTANCE AND CURRENT DISTRIBUTION AT GAS-EVOLVING ELECTRODES

B.E. BONGENAAR-SCHLENTER

OHMIC RESISTANCE AND CURRENT DISTRIBUTION AT GAS-EVOLVING ELECTRODES

OHMSE WEERSTAND EN STROOMVERDELING AAN GASONTWIKKELENDE ELEKTRODEN

PROEFSCHRIFT

TER VERKRIJGING VAN DE GRAAD VAN DOCTOR
IN DE TECHNISCHE WETENSCHAPPEN
AAN DE TECHNISCHE HOGESCHOOL EINDHOVEN,
OP GEZAG VAN DE RECTOR MAGNIFICUS
PROF. DR. S. T. M. ACKERMANS,
VOOR EEN COMMISSIE AANGEWEZEN DOOR HET COLLEGE
VAN DEKANEN IN HET OPENBAAR TE VERDEDIGEN OP
VRIJDAG 7 DECEMBER 1984 TE 14.00 UUR

DOOR

BERNADETTE ELISABETH BONGENAAR-SCHLENTER

GEBOREN TE EINDHOVEN

Dit proefschrift is goedgekeurd
door de promotoren:
Prof. E. Barendrecht
Prof.dr. D.A. de Vries

copromotor:
Dr. L.J.J. Janssen

Druk: Dissertatie Drukkerij Wibro, Helmond, Telefoon 04920-23981.

VOORWOORD

Bij het gereedkomen van dit proefschrift wil ik niet nalaten een woord van dank te richten tot allen die aan de totstandkoming hiervan hebben bijgedragen. Veel dank ben ik verschuldigd aan Han Verbunt, die mij voortdurend met enorme inzet terzijde heeft gestaan en aan Charles Smeyers en Leon Konings, die mij, met name in de eerste fasen van het onderzoek, voortreffelijk geholpen hebben. Han, Charles, Leon, zonder jullie collegialiteit en hulp was het mij niet mogelijk geweest het onderzoek in deze beperkte tijd te verrichten.
Jos Janssen ben ik bijzonder erkentelijk voor de prettige en kundige begeleiding. Jos, de discussies met jou waren bronnen van inspiratie en gaven richting aan het onderzoek. Je enthousiasme voor het onderzoek werkte aanstekelijk.
Pim Sluyter en Kees Copray dank ik bijzonder voor de technische adviezen, de hulp en de nuttige discussies.
Rob Blokland en Kees van der Geld dank ik voor de discussies op het gebied van stromingsverschijnselen.
Voor het vervaardigen van de vele tekeningen dank ik Ruth Gruyters en Leon Konings.
Mijn dank gaat eveneens uit naar Marjon Dahlmans voor de snelle en correcte verzorging van het typewerk.
De technici van de verschillende werkplaatsen en de elektronicagroep dank ik voor hun grote hulpvaardigheid bij het oplossen van experimentele problemen.
Tenslotte wil ik alle leden van de vakgroepen Transportfysica en Elektrochemie bedanken voor de plezierige werksfeer. De soms verhitte tafeltennis-sessies tijdens de lunchpauze zal ik niet snel vergeten.

Een gedeelte van het hier beschreven onderzoek
is uitgevoerd in het kader van een contract tussen
de Technische Hogeschool Eindhoven en de
Commissie van de Europese Gemeenschap te Brussel.

TABLE OF CONTENTS

LIST OF SYMBOLS AND SI-UNITS 5

1. INTRODUCTION 9
   1.1 The electrolytic cell 9
   1.2 Gas-evolving electrodes 10
   1.3 Water electrolysis 11
   1.4 Present investigation 14

2. GAS BUBBLE BEHAVIOUR ON A TRANSPARENT GOLD ELECTRODE AND BUBBLE DISTRIBUTION IN THE ELECTROLYTE 17
   2.1 Introduction 17
   2.2 Literature survey 17
      2.2.1 Nucleation 17
      2.2.2 Growth 18
      2.2.3 Departure and rise 20
   2.3 Experimental set-up 21
   2.4 Results 24
      2.4.1 Bubble behaviour on the electrode surface 24
         2.4.1.1 Introduction 24
         2.4.1.2 Effect of current density 24
         2.4.1.3 Effect of solution flow velocity 26
         2.4.1.4 Effect of height 28
         2.4.1.5 Conclusions 29
      2.4.2 Bubble distribution in the electrolyte 30
         2.4.2.1 Introduction 30
         2.4.2.2 Effect of current density 31
         2.4.2.3 Effect of solution flow velocity 33
         2.4.2.4 Effect of height 35
         2.4.2.5 Conclusions 38

3. SPECIFIC RESISTANCE OF A BUBBLE-ELECTROLYTE MIXTURE AND CURRENT DISTRIBUTION AT A SEGMENTED NICKEL ELECTRODE 39
   3.1 Introduction 39
   3.2 Literature survey 39

3.2.1 Conductivity of dispersions 39
3.2.2 Current density distribution 42
3.2.3 Application to electrolysis processes 46
3.3 Bubble diffusion model 54
3.4 Experimental set-up 59
3.5 Results 62
3.5.1 Current density distribution 62
3.5.1.1 Effect of current 62
3.5.1.2 Effect of solution flow velocity 63
3.5.1.3 Effect of electrolyte concentration 65
3.5.1.4 Effect of nature of gas evolved at the working electrode 66
3.5.2 Ohmic resistance 66
3.5.2.1 Effect of current density 66
3.5.2.2 Effect of solution flow velocity 68
3.5.2.3 Effect of height 69
3.6 Discussion 69

4. SPECIFIC RESISTANCE OF A BUBBLE-ELECTROLYTE MIXTURE DURING WATER ELECTROLYSIS UNDER PRACTICAL CONDITIONS 75
4.1 Introduction 75
4.2 Experimental set-up 75
4.2.1 Electrolysis cells 75
4.2.2 Electrolytic flow circuits 77
4.2.3 Determination of ohmic potential drop 78
4.2.4 Experimental conditions 78
4.3 Results 79
4.3.1 Effect of the gas to liquid volumetric ratio at the outlet of the electrolysis cell 79
4.3.2 Effect of nature of the electrode surface 82
4.3.3 Effect of temperature 83
4.3.4 Effect of KOH-concentration 84
4.3.5 Effect of pressure 84
4.3.6 Effect of distance between working electrode and diaphragm 85
4.3.7 Effect of geometry of the electrode 87
4.4 Discussion 90

5. AVERAGE RADII AND RADIUS DISTRIBUTIONS OF BUBBLES EVOLVED DURING WATER ELECTROLYSIS AT THE OUTLET OF THE CELL 93

5.1 Introduction 93

5.2 Experimental set-up 93

5.3 Results 94

5.3.1 Introduction 94

5.3.2 Effect of current density 95

5.3.3 Effect of solution flow velocity 99

5.3.4 Effect of the nature of the electrode surface 100

5.3.5 Effect of temperature 102

5.3.6 Effect of KOH-concentration 102

5.3.7 Effect of pressure 102

5.3.8 Effect of distance between the working electrode and the diaphragm 104

5.4 Discussion 104

6. SUGGESTIONS FOR FURTHER WORK 107

REFERENCES 108

ABSTRACT 115

SAMENVATTING 117

CURRICULUM VITAE 119

LIST OF SYMBOLS AND SI-UNITS

a	constant	(-)
A_ℓ	electrolyte area	(m^2)
b	constant	(-)
c	constant	(-)
C_{bu}	proportionality factor in Eq. 3.2.3.19	(-)
ΔC_w	supersaturation of dissolved gas at the bubble wall	(kg/m^3)
ΔC_x	supersaturation of dissolved gas at a distance x from the electrode surface	(kg/m^3)
d	distance between the electrodes	(m)
D	diffusion coefficient	(m^2/s)
d_b	bubble diameter	(m)
d_{bm}	distance between the backwall of the working electrode compartment and the diaphragm	(m)
d_{hyd}	hydraulic diameter of the working electrode compartment	(m)
d_{wm}	distance between the working electrode and the diaphragm resp. the tip of the Luggin capillary	(m)
D_{wm}	reduced distance between the working electrode and the diaphragm; $D_{wm} = d_{wm}/d_{bm}$	(-)
E	tension of an operating cell	(V)
E_c	tension needed to overcome concentration polarization	(V)
E_p	tension needed to overcome electrode polarization	(V)
E_R	tension needed to overcome ohmic resistance	(V)
E_T	theoretical minimum tension at which electrolysis can occur	(V)
f	gas void fraction	(-)
F	Faraday constant	(C/mol)
f_0	gas void fraction at the electrode surface	(-)
f_b	gas void fraction in the bulk electrolyte	(-)
F_b	upward buoyancy force	(N)
F_{drag}	drag force	(N)
F_G	force due to velocity gradient	(N)
F_{inert}	inertia force	(N)
F_{R_b}	bubble radius distribution function	(m^{-1})
F_{up}	upward force	(N)
F_σ	downward component of the adhesion force	(N)

g	gravitational acceleration	(m/s^2)
ΔG	change in Gibbs' free energy	(f/mol)
h	height from the bottom of the working electrode	(m)
h_r	reference height (= 1 cm)	(m)
H	total height of the electrode	(m)
H^*	dimensionless height; $H^* = h/H$	(-)
ΔH	change in enthalpy	(J/mol)
i	current density	(A/m^2)
I	total current through the cell	(A)
i_{av}	average current density	(A/m^2)
i_0	exchange current density	(A/m^2)
i_∞	current density far from the edge of the electrode	(A/m^2)
i_r	reference current density (= 1 kA/m^2)	(A/m^2)
Ja	Jakob number; $Ja = \Delta C_0/\rho_2$	(-)
K	gas effect parameter	(-)
K_c	conductivity of the continuous medium	(Ω^{-1})
K_d	conductivity of the dispersed phase	(Ω^{-1})
K_e	effective conductivity	(Ω^{-1})
K_s	specific conductivity	$(\Omega^{-1}m^{-1})$
K_T	turbulent diffusion coefficient	(m^2/s)
K_i	empirical constant	(-)
Mg	atomic mass of gas	(kg/mol)
n	number of electrons transferred in reaction	(-)
N	number of bubbles	(-)
n_i	empirical constant	(-)
p	pressure	(N/m^2)
p_0	atmospheric pressure	(N/m^2)
P	reduced pressure; $P = p/p_0$	(-)
Δp	excess pressure	(N/m^2)
r	cavity mouth radius	(m)
R	resistance	(Ω)
R'	specific resistance	(Ωm)
R"	unit surface resistance	(Ωm^2)
R_1	resistance of the first bubble layer	(Ω)
R_2	resistance of the second bubble layer	(Ω)
R_{cell}	ohmic resistance in the cell	(Ω)
R_b	bubble radius	(m)
R_d	bubble departure radius	(m)

R_e	equilibrium bubble radius	(m)
R_G	gas constant	(J/molK)
R_p	resistance of the pure electrolyte	(Ω)
R_p'	specific resistance of the pure electrolyte	(Ωm)
R_p''	unit surface resistance of the pure electrolyte	(Ωm^2)
$\bar{R}$	average bubble radius	(m)
$\bar{R}_s$	average Sauter radius	(m)
Re	Reynolds number	(-)
s	degree of screening by attached bubbles	(-)
s_0	maximum degree of screening	(-)
s_ℓ	degree of screening by bubbles in the electrolyte	(-)
ΔS	change in entropy	(J/molK)
t	time	(s)
T	temperature	(K)
u	constant depending on particle form	(Ω^{-1})
u_b	velocity of a bubble relative to the electrolyte	(m/s)
v	average rising velocity of a bubble	(m/s)
v_ℓ	liquid flow velocity	(m/s)
$v_{\ell,r}$	reference liquid flow velocity (= 1 m/s)	(m/s)
$V_{d,max}$	upper limit of the static departure volume	(m^3)
V_G	volumetric gas production rate	(m^3/s)
V_ℓ	volumetric liquid flow rate	(m^3/s)
V_M	molar gas volume	(m^3/mol)
ΔV	ohmic potential drop between the working electrode and the Luggin capillary	(V)
ΔV_{cell}	ohmic potential drop between anode and cathode	(V)
w	width of the electrode	(m)
x	distance from the electrode surface	(m)
Y_c	chemical yield of an electrolytic reactor	(-)
Y_E	energy yield of an electrolytic reactor	(kg/J)
Y_{st}	space-time yield of an electrolytic reactor	(kg/m^3s)
α	charge transfer coefficient	(-)
β	bubble growth parameter	(-)
γ	contact angle between the bubble and the wall	(degree)
δ	thickness of the bubble layer adjacent to the electrode	(m)
δ_A	thickness of the stagnant bubble layer at the anode	(m)
δ_C	thickness of the stagnant bubble layer at the cathode	(m)

δ_T	thickness of the theoretical bubble diffusion layer	(m)
$\delta_{v,bu}$	modified thickness of the velocity boundary layer	(m)
η	electrode overpotential	(V)
κ	Henry's constant	(m^2/s^2)
μ	polarization parameter	(-)
ν	kinematic viscosity	(m^2/s)
ρ_1	density of the liquid	(kg/m^3)
ρ_2	density of the gas	(kg/m^3)
σ	surface tension	(N/m)
Φ	potential	(V)
ψ	number of bubbles generated per unit surface area and unit time	$(m^{-2} s^{-1})$

CHAPTER 1: INTRODUCTION.

1.1. THE ELECTROLYTIC CELL.

In 1789 the Dutch chemists A. Paets van Troostwijk and J.R. Deimann were the first to decompose water in oxygen and hydrogen with the aid of electric charges produced by an electrostatic machine. Due to the limitations of this sort of electric generator they were, however, unable to detect the development of hydrogen and oxygen at the two poles and to interpret the nature of the electrochemical reaction they observed [1, 2].

The invention of the "copper zinc pile" by Alessandro Volta in 1800 [1], opened a totally new field of research: electrochemistry. Scientists were provided with a continuous source of direct current on which many processes could be based. The immediate effect of Volta's discovery was the construction of a pile by Nicholson and Carlisle [1, 2] with which they effected the decomposition of water.

Since the first electrolysis a number of improvements have been made to increase the efficiency of the electrolytic cells. In principal an electrolytic cell still consists of two electrodes dipping into a tank filled with electrolyte. An electrical current is passed through the cell, bringing about electrochemical reactions at both electrodes. Sometimes, the cell is divided into two parts to avoid the mixing of products formed at the electrodes [3].

To assess the performances of electrolytic reactors different quantitative criteria can be used. Three useful ones [4] are the space-time yield, Y_{st}, defined by:

$$Y_{st} = \frac{\text{amount of product obtained}}{\text{time x cell volume}} \qquad (1.1.1)$$

the chemical yield, Y_c, defined by:

$$Y_c = \frac{\text{actual amount of product obtained}}{\text{maximum amount obtainable for a given conversion}} \qquad (1.1.2)$$

and the energy yield, Y_E, defined by:

$$Y_E = \frac{\text{amount of product obtained}}{\text{energy consumed}} \qquad (1.1.3)$$

The respective yields are determined by a number of parameters such as electrode area per unit cell volume, current density, electrode potential, ohmic resistance of electrolyte and separator, mass and heat transfer and catalytic properties of the electrode surface. To increase the efficiency of the cell, electrodes, electrolytes and separators must be improved and new cell designs have to be introduced [4]. Studies in these areas are stimulated by the energy problem, the environmental problem and the materials problem with which industries all over the world are faced.

1.2. GAS-EVOLVING ELECTRODES.

Electrochemical reactions involving the evolution of gas have some special characteristics not shared by electrode reactions in general [5]. During the course of the process, gas bubbles nucleate, grow in size, depart from the electrode and rise in the solution. Since these phenomena can affect the electrochemical process considerably, a closer insight in the performance of gas-evolving electrodes is necessary. Gas evolution may favour a process in which diffusion of electro-active species to or from the electrode surface is the rate determining step, since it enhances the mass transfer and consequently the production capacity of the electrolytic reactor [5-8].

However, gas-evolving electrodes show a relatively high activation overpotential. Higher energy-efficiencies may be realized if the overpotential could be minimized by giving the electrodes better catalytic activity or a higher specific electrode area [4]. In recent years, the introduction of the dimensionally stable anode (DSA) has made a great contribution to diminish the activation overpotential of gas-evolving electrodes.

Gas bubbles attached to the electrode surfaces obstruct the passage of the current. Due to the presence of bubbles in the interelectrode gap, the ohmic resistance increases [9-13]. Therefore, the power demand increases and, hence, the energy efficiency of the process decreases. In industrial electrochemical processes involving gas evolving electrodes, e.g. the production of chlorine, aluminium or hydrogen, the energy consumption is high. Even a small improvement of the energy efficiency of these processes may cut down the expenses considerably.

1.3. WATER ELECTROLYSIS.

Although the water electrolysis process was already known in 1800, industrially it was not used until the beginning of this century. Because of the high cost of electrical energy, the price of electrolytic hydrogen is high. Therefore, large electrolysis plants are mostly located at sites where substantial amounts of low-cost electric power are available [14].

The sudden increase in the price of fossil fuels a number of years ago, resulted in an increased interest in alternative energy sources (wind, solar, nuclear, hydro, geothermal, tide). Since the energy produced by these sources has to be stored and transported, an additional energy carrier is needed. Hydrogen is considered to be a possible energy carrier in the future because of various advantages compared to other systems [15, 16].

Hydrogen can be produced from fossil fuels by water electrolysis or by the thermochemical splitting of water [17-19]. Due to various reasons it is expected that the thermochemical hydrogen production will not be able to compete with water electrolysis. Whether the use of electrolytic hydrogen will expand significantly in the future will therefore primarily be determined by the costs of electric energy and by the efficiency of the water electrolysis process.

Electrolysis of water occurs when a direct electric current is passed between two electrodes immersed in an aqueous electrolyte (cf. Fig. 1.3.1).

In cells with an alkaline electrolyte, the key reactions at the electrodes are:

cathode : $4e^- + 4H_2O \rightarrow 2H_2 + 4OH^-$ (1.3.1)
$E^\circ = 0.83$ V (NHE)

anode : $4OH^- \rightarrow O_2 + 2H_2O + 4e^-$ (1.3.2)
$E^\circ = 0.40$ V (NHE)

net reaction: $2H_2O \rightarrow 2H_2 + O_2$ (1.3.3)

In cells with an acid electrolyte the reactions are:

cathode : $4e^- + 4H^+ \rightarrow 2H_2$ (1.3.4)
$E^\circ = 0.00$ V (NHE)

anode : $2H_2O \rightarrow O_2 + 4H^+ + 4e^-$ (1.3.5)

$E^\circ = 1.23$ V (NHE)

net reaction: $2H_2O \rightarrow 2H_2 + O_2$ (1.3.6)

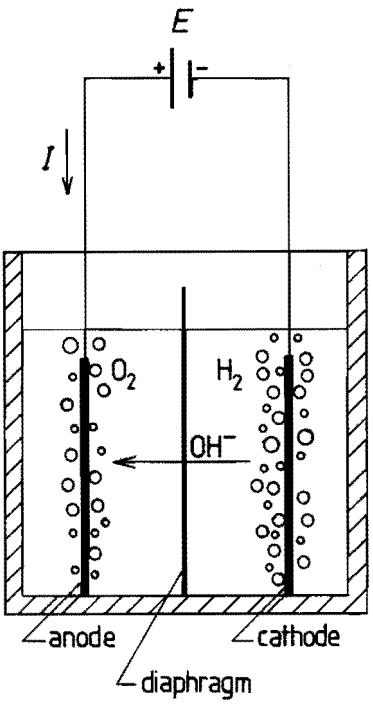

Fig. 1.3.1. Water electrolysis cell with alkaline electrolyte

Although the reactions on the electrodes depend on the nature of the electrolyte, the net reactions in both alkaline and acid electrolytes are the same. The hydroxyl and hydronium ions provide the electric conductivity in the respective electrolytes. The theoretical minimum cell tension necessary for the decomposition of water is determined by the Gibbs' free energy, ΔG, required to decompose water into its elements [1, 17, 18]

$$E_T = \frac{-\Delta G}{nF} \qquad (1.3.7)$$

where E_T = the theoretical minimum tension at which electrolysis can occur, F = the Faraday constant, n = the number of electrons transferred in the reaction and ΔG = the change in molar Gibbs' free energy for the reaction.
For an isobaric and isothermal reaction the Gibbs' free energy is related to the enthalpy and entropy changes by:

$$\Delta G = \Delta H - T\Delta S \qquad (1.3.8)$$

where ΔH = the enthalpy (heat contents) change for the reaction, ΔS = the entropy change for the reaction and T = the cell temperature. At increasing temperature the theoretical minimum tension decreases because the entropy change for the water electrolysis process is positive.
For water to decompose at practical rates, the tension across the electrodes must exceed the theoretical one by the tensions needed to overcome electrode polarization (E_p) and ohmic resistance (E_R). The tension of an operating cell can therefore be represented by [17]:

$$E = E_T + E_p + E_R \qquad (1.3.9)$$

with:

$$E_p = \eta_C + \eta_A + E_C \qquad (1.3.10)$$

and:

$$E_R = I \cdot R_{cell} \qquad (1.3.11)$$

where E = the tension necessary for the process, E_p = the tension needed to overcome the electrode polarization, E_R = the tension needed to overcome the ohmic resistance in the cell, η_C = the hydrogen activation overpotential, η_A = the oxygen activation overpotential, E_C = the tension necessary to overcome the concentration polarization, I = the total current in the cell and R_{cell} = the ohmic resistance in the cell.
The activation overpotentials, η_A and η_C, are a measure for the kinetic limitations of the charge transfer at the respective electrode-electrolyte interfaces. According to the Tafel equation [20] the overpotentials depend on current density, i, as:

$$i = i_0 \exp(\alpha n F \eta / R_G T) \qquad (1.3.12)$$

where i = the current density, i_0 = the exchange current density, η = the electrode overpotential and α = the charge transfer coefficient. The activation overpotential depends on the electrode reaction, the nature of the electrode material and of the electrode surface and on the temperature.

The concentration overpotential is due to a lack of electro-active species at the electrode surface. It may be minimized by the application of concentrated electrolyte, elevated temperature or forced convection.

The ohmic potential drop, $I \cdot R_{cell}$, is the product of the current, I, and the ohmic resistance of the cell, R_{cell}. R_{cell} is the sum of the ohmic resistances of the electrodes, the diaphragm and the bubble containing electrolyte. The resistance of the bubble-electrolyte mixture will exceed the resistance of the pure electrolyte. The extent of the increase in resistance due to the presence of the bubbles depends on the gas void fraction and on its distribution in the cell [9-13].

1.4. PRESENT INVESTIGATION.

The aim of the present study is to investigate the effect of gas bubbles evolved on the electrodes during alkaline water electrolysis on the ohmic resistance in the cell. Insight in the effects of various parameters on the gas bubble distribution and on the ohmic resistance is of utmost importance for the optimization of the water electrolysis process.

To obtain information on the bubble sizes and the gas void and bubble velocity distributions in a vertically placed cell, high speed motion pictures have been taken through small windows in a transparent gold electrode at various distances from the electrode surface and at various heights in the electrolysis cell. Results for a number of current densities and solution flow velocities are given in chapter 2. The behaviour of bubbles growing on the surface of a transparent gold electrode under various conditions is also described in this chapter.

The ohmic resistance and current distributions in the electrolysis

cell are determined using a segmented nickel working electrode. The experimental results under various conditions and a model relating the ohmic resistance and current distribution to the gas void fraction (ch. 2) is given in chapter 3.
A number of experiments have been carried out under semi-industrial conditions. In chapter 4 a dimensionless correlation for the reduced ohmic resistance between the working electrode and the diaphragm and the parameters of the electrolysis process is derived. The relation may be used to determine the optimum electrolysis conditions.
In chapter 5 a similar relation is derived for the reduced average bubble radius at the outlet of the electrolysis cell. Knowledge of the average bubble radius and of the bubble radius distribution at the outlet of the cell can help to solve the bubble-electrolyte separation problem.

CHAPTER 2: GAS BUBBLE BEHAVIOUR ON A TRANSPARENT GOLD ELECTRODE AND BUBBLE DISTRIBUTION IN THE ELECTROLYTE.

2.1. INTRODUCTION.

The mechanisms of the oxidation and the reduction reactions of water to, respectively, oxygen and hydrogen have been studied by several investigators [21-25].

These studies do, however, not include the processes that occur after the formation of dissolved gases. In the present study we are not concerned with the mechanisms of the oxidation and reduction reactions, but with the bubble behaviour and the influence of the bubbles on the ohmic resistance in the electrolysis cell.

In this chapter a brief survey on the nucleation, growth and departure of bubbles during water electrolysis is given (section 2.2). In section 2.3 experiments to establish the gas void distribution in the electrolysis cell are described. Section 2.4 contains the results of experiments that will be used for testing the model describing the effect of gas bubbles on the ohmic resistance, presented in chapter 3.

2.2. LITERATURE SURVEY.

2.2.1. Nucleation.

During water electrolysis, the electrolyte in the vicinity of the electrode surface will be supersaturated with dissolved gas. In the absence of convection or gas bubble formation, the supersaturation, ΔC_x, at a distance x from the electrode surface is determined by diffusion of the gas dissolved in the electrolyte. It can be represented as a function of time, t, after the start of the electrolysis process by [25]:

$$\Delta C_x = \frac{i}{nF(\pi D)^{\frac{1}{2}}} \int_0^t (t')^{-\frac{1}{2}} \exp(-\frac{x^2}{4Dt'})dt' \qquad (2.2.1.1)$$

Since the transfer of dissolved gas towards the bulk electrolyte is slow, the supersaturation at the electrode surface, ΔC_0, increases with time.

Analogous to the process of vapour bubble formation at a superheated wall [26], cavities at the electrode surface on which gas bubbles can originate, will be activated and bubbles are formed.
The pressure of the gas in a bubble has to exceed the pressure in the surrounding liquid to compensate for the surface tension at the interface. The excess pressure, Δp, is given by [27]:

$$\Delta p = 2\sigma/R_e \qquad (2.2.1.2)$$

where σ = the surface tension and R_e = the equilibrium bubble radius.
According to Henry's law the excess pressure is related to the supersaturation as:

$$\Delta p = \kappa.\Delta C_w \qquad (2.2.1.3)$$

with κ = Henry's constant and ΔC_w = the supersaturation of dissolved gas at the bubble wall. The relation between the equilibrium bubble radius and the supersaturation follows from Eqs. 2.2.1.2 and 2.2.1.3:

$$R_e = 2\sigma/(\kappa.\Delta C_w) \qquad (2.2.1.4)$$

According to Cole [26], cavities can, depending on their properties (wettability, steepness), entrap gas/vapour or liquid. For a vapour-filled cavity the equilibrium bubble radius often equals the mouth radius of the active cavity. Consequently, the supersaturation near the electrode determines whether a cavity is active or not. At small supersaturations, ΔC_0, only large cavities can be active, while at high supersaturations small cavities will also be activated.

2.2.2. Growth.

After nucleation, the gas bubble will grow at the electrode surface due to the supersaturation that still exists in the vicinity of the electrode. Bubble growth during electrolysis (mass transfer) is analogous to bubble growth in boiling liquids (heat transfer).

For the growth of a spherical bubble in an initially uniformly superheated infinite medium, Scriven [28] has derived theoretical expressions. In general, the theoretical treatment is based on the consideration of a force, a heat and a mass balance. However, a simultaneous solution of the three balance equations is not practical. For the special case of isothermal bubble growth and neglecting forces due to surface tension, viscosity etc., only the equation for the mass balance is retained. In that case the rate of growth of a bubble is limited by the rate of diffusion of the dissolved gas through the liquid phase. The bubble radius, R_b, is then given as a function of time by:

$$R_b = 2\beta(Dt)^{\frac{1}{2}} \qquad (2.2.2.1)$$

The growth parameter, β, depends on the initial supersaturation, ΔC_0, and on the density of the gas, ρ_2. It can be approximated by [29, 30]:

$$\beta = Ja\{1 + (1+2\pi/Ja)^{\frac{1}{2}}\}/(2\pi)^{\frac{1}{2}} \qquad (2.2.2.2)$$

with the Jakob number given by:

$$Ja = \Delta C_0/\rho_2 \qquad (2.2.2.3)$$

During electrolysis bubbles grow in an initially non-uniformly supersaturated liquid. Assuming an average supersaturation being approximately ten times the saturation concentration, the Jakob number for hydrogen evolution in water is 0.22, which is small compared to Jakob numbers in boiling processes.
Although true radial symmetry cannot exist during electrolysis, experimental results on electrolytic bubble growth reported in literature [27, 30-32] are in fair agreement with Scriven's equation.
The equation for bubble growth is derived for a single bubble. Obviously neighbouring bubbles will affect each other's growth. A slowing down of the rate of growth of the bubbles may occur because of the competition for the dissolved gas by adjacent

bubbles. On the other hand, the growth rate of bubbles may increase because of an increase in the rate of mass transfer of dissolved gas due to convection induced by neighbouring bubbles. The precise effect of the mutual interference of the bubbles is therefore hardly predictable [27].
When two bubbles, growing on the electrode surface, come into contact they may merge (coalesce) to form a new bubble. The volume of the new bubble is the sum of the volumes of the coalescing bubbles. After the coalescence, the new bubble may resume diffusional growth.

2.2.3. Departure and rise.

The departure mechanism of bubbles from the wall is governed by a number of forces as the buoyancy force, forces due to surface tension, viscosity, liquid inertia and, for electrolytically evolved bubbles, the electrostatic forces between the bubble and the electrode.
In 1935, Fritz [33] derived an expression for the departure radius, R_d, for slowly growing bubbles on a horizontal wall with a foot spreading beyond the mouth of the originating cavity:

$$R_d = 0.0104\ \gamma\{\sigma/g(\rho_1-\rho_2)\}^{\frac{1}{2}} \qquad (2.2.3.1)$$

where γ = the contact angle between the bubble and the wall, expressed in degrees. This equation results from a force balance considering the buoyancy and surface tension forces and a correction force accounting for the contact area, acting on a bubble at departure from a horizontal wall [34].
An experimental dynamic growth factor containing additional liquid inertia and viscosity effects was introduced by Cole and Shulman for the case of fast growing bubbles [35].
A number of other correlations have been derived, [34, 35], but they only deal with the departure of bubbles from a horizontal wall. The departure of bubbles from a vertical wall is, as yet, too complex to be described theoretically.
However, Slooten [34] recently derived an upper limit of the static departure volume, $V_{d,\ max}$, for a bubble growing from a cavity on a vertical wall with its foot attached to the mouth of

this cavity. His derivation is based on the force equation:

$$F_b - F_\sigma = 0 \qquad (2.2.3.2)$$

where $F_b = \rho g V$ = the upward buoyancy force and F_σ is the downward component of the adhesion force. At any moment of attachment this equation has to be satisfied.
F_σ reaches its maximum in the hypothetical case in which the tangent to the bubble profile at any point of the line of contact (at the bubble base) is parallel to the wall. Assuming a circular bubble foot, F_σ can be expressed by:

$$F_\sigma = 2\sigma \int_{\alpha=0}^{\pi} r \sin\alpha \, d\alpha = 4r\sigma \qquad (2.2.3.3)$$

where α is the circular parameter of the circle of contact. The maximum bubble volume is then obtained as:

$$V_{d,max} = 4r\sigma/\rho g \qquad (2.2.3.4)$$

This volume is a factor 2π smaller than the departure volume of a cavity bubble from a horizontal wall.
After the departure from the electrode surface, bubbles will rise in the electrolyte near the electrode. The natural rising velocity of a single bubble can be calculated using Stokes' equation:

$$v = 2R_b^{\,2}\rho g/9\eta \qquad (2.2.3.5)$$

When a forced electrolyte flow is applied, the rising velocity of the bubbles may increase. The ratio between the bubble velocity and the electrolyte velocity is called the slip ratio or phase velocity ratio [36]. It depends on various parameters, e.g. pressure, void fraction, channel area and orientation and gas/liquid density ratio. Generally, the slip ratio is unknown and is often taken to be unity (so called homogeneous model).

2.3. EXPERIMENTAL SET-UP.

The experimental set-up for bubble measurements is shown in Fig.

2.3.1. The electrolysis cell consists of two sections. One section is made of transparent acrylate resin and contains the counter electrode (perforated nickel plate, 50 x 2 cm^2), while the other section (stainless steel setting) incorporates the working electrode.

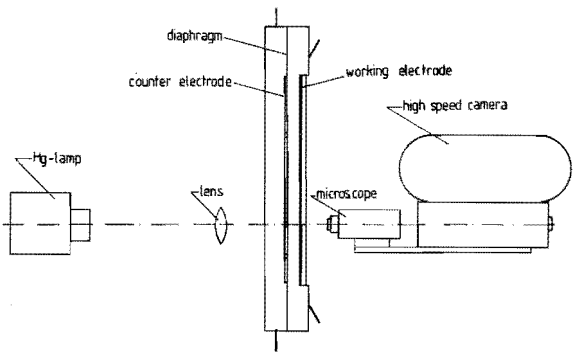

Fig. 2.3.1 Experimental set-up for bubble measurements.

The working electrode consists of a glass plate on which a thin gold layer is deposited. The glass plate is glued in the stainless steel setting and serves as the backwall of the working electrode section. The sections are separated by a transparent nafion (Du Pont) membrane. The counter electrode is placed against the membrane, while the distance between the working electrode and the membrane is 6 mm. The electrolysis cell is connected to a circuit for forced flow. Details of this circuit are given in chapter 3.
The bubble density and velocity distributions in the electrolysis cell are recorded using a high speed film camera (Hitachi, NAC 16D). To get optimally contrasted bubbles on the pictures, the light source, for which a mercury arc lamp (Oriel-HBO 100 W/2) is used, is placed at the opposite side of the electrolysis cell. A positive lens is used to focus the light beam in the recording area.
Because of the small sizes of the bubbles (10-100 μm) a microscope has to be used. The magnification factor is determined by the microscope objective and its distance to the camera (no ocular is used). Its value is established by measuring a recorded scale of one millimeter which is divided in 100 equal parts; it is found to be approximately 300.

To obtain sharp pictures, picture frequencies up to 8000 frames per second have to be used when forced flow up to 0.75 m/s is applied. Light marks on the edge of the film, initiated by the camera every millisecond, indicate the framing frequency.
Before a series of experiments, the microscope is focused on the surface of the gold electrode. The camera and the microscope can be translated simultaneously maintaining a constant magnification factor. From the displacement of the camera the focus point in the electrolysis cell is determined, taking into account the difference in refractive index between the electrolyte and air.
Unless mentioned otherwise, the experiments have been carried out galvanostatically with a hydrogen evolving gold electrode at atmospheric pressure, in 1 M KOH-solution at 303 K, at a current density of 0.75 kA/m^2 and with an applied flow velocity of 0.3 m/s. The current density is calculated by dividing the total current by the active geometrical surface area of the working electrode. The solution flow velocity is calculated by dividing the volumetric flow rate of the solution by the cross-sectional area of the compartment diminished by the cross-sectional area of the electrode in the compartment.
Only hydrogen bubbles have been studied since the thin gold layer crumbles from the glass plate at oxygen evolution.
The exposed films (Kodak 4-X reversal film 7277) are developed using a combilabor (Old Delft CMB-A-2). The bubbles on a frame are measured on the screen of a motion analyser (Hitachi, NAC MC-OB/PH-160B). The data are recorded on paper-tape and handled by the university computer (Burroughs 7700). Since one frame only represents the bubble situation at a distinct time and fluctuations, on a small time scale, in the bubble behaviour may occur, it is likely that the bubble situation on one frame does not represent the average bubble situation. Therefore bubble quantities are averaged over approximately 10 randomly taken frames for each experimental condition. In this way representative results are obtained.

2.4. RESULTS.

2.4.1. Bubble behaviour on the electrode surface.

2.4.1.1. Introduction.

To study the behaviour of hydrogen bubbles on the electrode surface, the transparency of the electrode has to be at least 10%. Although, relatively small gold electrodes with sufficient transparency and stability have been made, we did not succeed in making a lasting electrode of 2 x 50 cm^2 with more than 5% transparency.

The bubble behaviour of relatively small transparent nickel electrodes has been studied extensively by Sillen [32, 37] and Janssen [37, 38]. To check whether the results of these experiments can be used in the present experimental set-up, some experiments were carried out at relatively low current densities on a transparent electrode. At higher current densities the decay of the electrode would take place before a series of measurements could be made. The degree of screening of the electrode by attached bubbles, s, averaged over the observed surface area was determined and compared to the data obtained by Sillen [32, 37].

2.4.1.2. Effect of current density.

The effect of current density has only been studied in the range of 0.15 to 0.75 kA/m^2. Fig. 2.4.1 shows the measured screening of the gold working electrode surface by hydrogen bubbles as a function of current density at a solution flow of 0.3 m/s in 1 M KOH and at room temperature, together with results obtained by Sillen for hydrogen bubbles on transparent nickel electrodes [32] under similar conditions but in a wider current density range. The results of the present study agree well with the results obtained by Sillen.

In Fig. 2.4.2 the degree of screening by bubbles adhering to the electrode divided by the difference between the maximum possible degree of screening and the measured degree of screening, $s/(1-s)$, is plotted versus current density on a double logarithmic scale for a number of data obtained by Sillen for

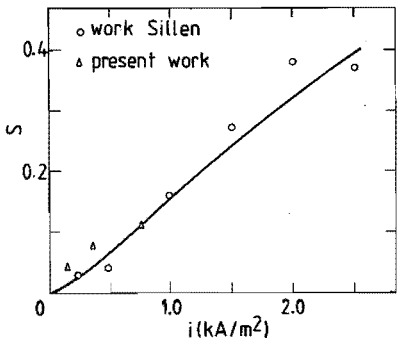

Fig. 2.4.1 The degree of screening of the gold electrode surface by hydrogen bubbles together with results on nickel electrodes obtained by Sillen. v_ℓ = 0.3 m/s, [KOH] = 1 M, T = 303 K.

hydrogen as well as for oxygen bubbles. From this Figure it follows that in the current density ranges 0.25-2.5 kA/m^2 for hydrogen and 0.5-5 kA/m^2 for oxygen, the dependence of the degree of screening on the current density can be represented by:

$$\frac{s}{1-s} \sim i^a \qquad (2.4.1.1)$$

where a is a constant depending on the nature of gas evolved, but, for oxygen, independent of solution flow velocity. Rearranging this equation, the degree of screening by bubbles adhering to the electrode is expressed as a function of current density by:

$$s = \frac{a_1 (i/i_r)^{a_2}}{1 + a_1 (i/i_r)^{a_2}} \qquad (2.4.1.2)$$

where i_r is the reference current density (= 1 kA/m^2).
The data of Sillen for hydrogen evolution at a solution flow velocity of 0.3 m/s in Fig. 2.4.1 are fitted by:

$$s = \frac{0.19\ (i/i_r)^{1.4}}{1 + 0.19\ (i/i_r)^{1.4}} \qquad (2.4.1.3)$$

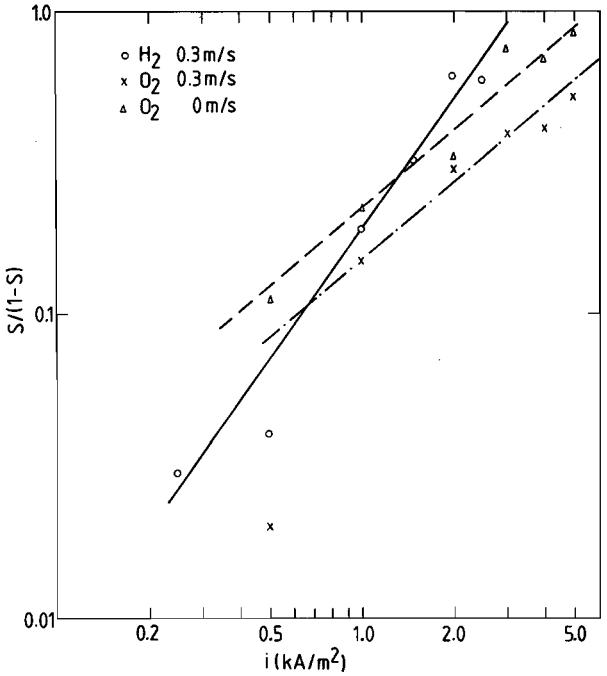

Fig. 2.4.2 s/(1-s) as a function of current density on a double logarithmic scale for a number of data obtained by Sillen.

2.4.1.3 Effect of solution flow velocity.

In Fig. 2.4.3 the degree of screening of the electrode surface by adhering bubbles, determined at 0.15 and 0.75 kA/m^2, is plotted in dependence of solution flow velocity together with results obtained by Sillen at 2 kA/m^2 [32]. The degree of screening decreases at increasing solution flow velocity for all current densities.

To describe the dependence of the degree of screening on the solution flow velocity, an approach similar to that of the previous section is used. In Fig. 2.4.4 the degree of screening divided by the difference between the maximum degree of screening at natural convection and the measured degree of screening, $s/(s_0-s)$, is plotted as a function of solution flow velocity on a double logarithmic scale, for a number of data obtained by Sillen [32].

From this Figure it follows that in the solution flow velocity range 0.1-1.0 m/s the dependence of the degree of screening on solution flow velocity may be represented by:

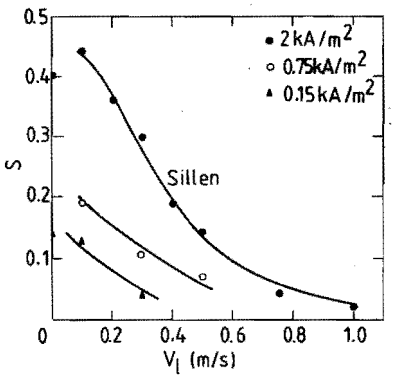

Fig. 2.4.3 The degree of screening of the electrode at various current densities in dependence of solution flow velocity.

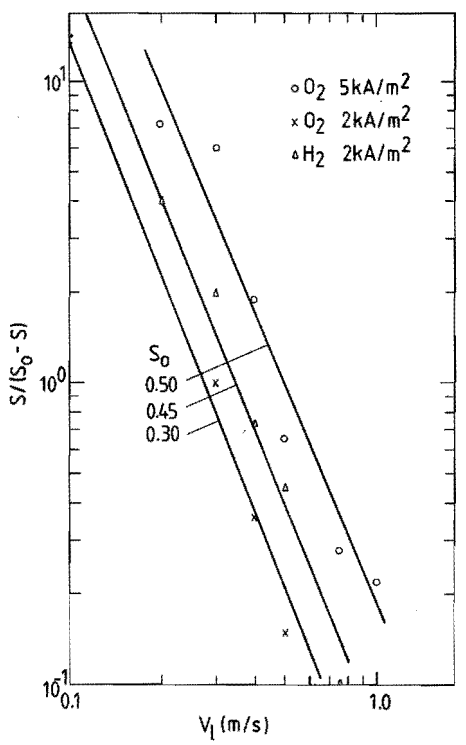

Fig. 2.4.4 s(1-s) as a function of solution flow velocity on a double logarithmic scale for a number of data obtained by Sillen.

$$\frac{s}{s_0 - s} \sim v_\ell^b \qquad (2.4.1.4)$$

where b is a constant independent of current density and nature of the gas evolved.

Rearranging Eq. 2.4.1.4 the degree of screening by bubbles adhering to the electrode is expressed as a function of the solution flow velocity by:

$$s = \frac{b_1 s_0 (v_\ell / v_{\ell,r})^{b_2}}{1 + b_1 (v_\ell / v_{\ell,r})^{b_2}} \qquad (2.4.1.5)$$

where $v_{\ell,r}$ is the reference solution flow velocity (= 1 m/s). The data of Sillen for a hydrogen evolving electrode at 2 kA/m^2 in Fig. 2.4.3 are fitted by:

$$s = \frac{0.08 \times 0.45 \times (v_\ell / v_{\ell,r})^{-2.5}}{1 + 0.08 (v_\ell / v_{\ell,r})^{-2.5}} \qquad (2.4.1.6)$$

2.4.1.4. Effect of height.

The effect of height on the degree of screening of the electrode surface by adhering bubbles is determined at approximately 7 cm from the bottom and 7 cm from the top of the 48 cm high electrode. It is only possible to establish this effect at very low current densities, because at higher current densities the illumination of the top of the electrode is insufficient due to the scattering of light by the numerous bubbles in the electrolyte.

At a current density of 0.15 kA/m^2 and a solution flow velocity of 0.1 m/s the degree of screening at 7 cm from the bottom of the electrode is approximately 0.13 while the corresponding value at 7 cm from the top of the electrode is approximately 0.14. This small difference can not be considered as a significant effect of height. It is, however, possible that, at greater current densities when the bubble population is dense, effects in height may occur.

2.4.1.5. Conclusions.

From the data presented in the previous sections it may be concluded that the degree of screening of the electrode surface by adhering bubbles increases at increasing current density in the current density range 0.25-2.5 kA/m^2 for a hydrogen evolving electrode and 0.5-5.0 kA/m^2 for an oxygen evolving electrode. The degree of screening decreases at increasing solution flow velocity in the velocity range 0.1-1.0 m/s.

The maximum degree of screening at free convection is determined by the current density. The dependence of the degree of screening on current density and solution flow velocity may be approximated by substituting Eq. 2.4.1.2 for s_0 in Eq. 2.4.1.5:

$$s = \frac{b_1 \cdot \dfrac{a_1(i/i_r)^{a_2}}{1 + a_1(i/i_r)^{a_2}} \cdot (v_\ell/v_{\ell,r})^{b_2}}{1 + b_1(v_\ell/v_{\ell,r})^{b_2}} \qquad (2.4.1.7)$$

where, a_1, a_2, b_1 and b_2 are constants that may depend on the nature of both the electrode surface and the gas evolved. Rearranging this equation yields:

$$s = \frac{a_1 b_1 (i/i_r)^{a_2} \cdot (v_\ell/v_{\ell,r})^{b_2}}{(1+b_1(v_\ell/v_{\ell,r})^{b_2}) \cdot (1+a_1(i/i_r)^{a_2})} \qquad (2.4.1.8)$$

For the hydrogen evolving transparent nickel electrode used by Sillen [32] the equation reads:

$$s = \frac{15.10^{-3} (i/i_r)^{1.4} (v_\ell/v_{\ell,r})^{-2.5}}{(1+0.08(v_\ell/v_{\ell,r})^{-2.5})(1+0.19(i/i_r)^{1.4})} \qquad (2.4.1.9)$$

It is tempting to use this equation to predict the degree of screening of the electrode surface at higher current densities and for non-transparent electrodes. It must, however, be noted, that Eq. 2.4.1.9 only approximates the degree of screening of a

transparent nickel electrode in a limited current density range.

At higher current densities, when the interaction of bubbles increases, other effects may dominate the bubble behaviour. Further it is a well known fact [32, 37, 38] that the bubble behaviour strongly depends on the nature of the electrode surface. The nature of a transparent electrode surface deviates significantly from the nature of a "technical" electrode surface. Consequently, the values of the constants in Eq. 2.4.1.9 will differ for a transparent and a technical electrode.

2.4.2. Bubble distribution in the electrolyte.

2.4.2.1. Introduction.

The transparency of the gold electrode used for bubble distribution experiments was only 1-2%. Therefore, the illumination of the bubbles in the electrolyte was insufficient to take high speed motion pictures. To determine the bubble distribution in the electrolyte, the thin gold layer was removed from the glass support at four spots, thus creating small windows through which the bubbles in the electrolyte could be studied.

Due to the large magnification used, the depth of field is limited. Only bubbles with sharply defined outlines (located in a thin layer of electrolyte of approximately 100 μm) are measured. The following quantities have been determined from the experiments.

- $\bar{R}$: the average bubble radius; $\bar{R} = (\sum_{i=1}^{N} R_i)/N$
  the sum of the bubble radii measured divided by the number of bubbles. The average bubble radius depends on the departure radius of the bubbles from the electrode and on the degree of coalescence in the electrolyte.

- $\bar{R}_s$: the volume-surface mean radius or the average Sauter radius [39], $\bar{R}_s = \overline{R^3}/\overline{R^2} = \sum_{i=1}^{N} R_i^3 / \sum_{i=1}^{N} R_i^2$. The degree of

coalescence affects the Sauter radius more than it does the average bubble radius. The Sauter radius occurs in the equation for the mass transfer coefficient for gas evolving electrodes [40].

- s_ℓ: the degree of screening in the electrolyte;
  $s_\ell = (\sum_{i=1}^{N} \pi R_i^2)/c.A_\ell$ the fraction of the electrolyte area covered by the projection of the bubbles.The proportionality factor, c, accounts for the depth of field of the optical system. At high values of s, the probability for coalescence to occur is high. The electrolyte resistance in this layer will be high too.

2.4.2.2. Effect of current density.

The effect of current density on the degree of screening in the electrolyte, s_ℓ, is illustrated in Fig. 2.4.5 at three current densities viz. 0.15, 0.75 and 1.5 kA/m^2 at a solution flow velocity of 0.3 m/s and a height of approximately 7 cm from the bottom of the electrode.

The Figure shows that two layers may be distinguished in the electrolyte. The first layer adjacent to the electrode, exhibits a sharp decrease in the degree of screening at increasing distance from the electrode surface. In the second layer, s_ℓ decreases only slightly with increasing distance from the electrode.

The width of the first layer is estimated by drawing by hand two straight lines, approximating the screening in the respective layers. The intersection of these lines marks the transition of the first to the second layer in the Figure. In Fig. 2.4.6 the so determined width of the first layer is plotted as a function of current density on a double logarithmic scale. The Figure shows a straight line with a slope of approximately 0.1, indicating a slight dependence of δ on i. The width of the layer adjacent to the electrode in dependence on current density can therefore be approximated by:

$$\delta \sim i^{0.1} \qquad (2.4.2.1)$$

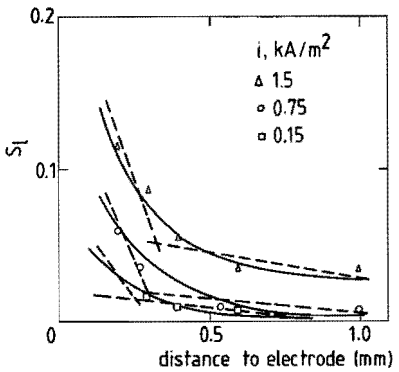

Fig. 2.4.5
The screening in the electrolyte as a function of the distance to the electrode surface.
v_ℓ = 0.3 m/s, h = 7 cm.

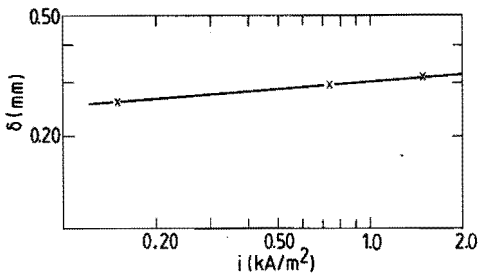

Fig. 2.4.6
The width of the bubble layer versus current density on a double logarithmic scale.

The degree of screening at a distance of 1 mm from the electrode surface, a solution flow velocity of 0.3 m/s and a height of 7 cm from the bottom of the electrode is plotted as a function of current density in Fig. 2.4.7, while the dependence of the average bubble radius and the average Sauter radius on current density is plotted in Fig. 2.4.8. From these Figures it follows that s_ℓ as well as $\bar{R}$ and $\bar{R}_s$ increase at increasing current density. The increase in s_ℓ is due to the increase in the total gas volume produced at higher current densities.
The increase in $\bar{R}$ could be due to an increase in departure radius from the electrode and/or to an increase in the degree of coalescence. From experiments by Sillen [32] it follows that the average departure radius of hydrogen bubbles from the electrode decreases at increasing current density. Therefore, the increase in average bubble radius must be due to an increase in the degree of coalescence at higher gas void fractions. This is confirmed by the relatively larger increase in the average Sauter radius, which is affected strongly by the degree of coalescence.

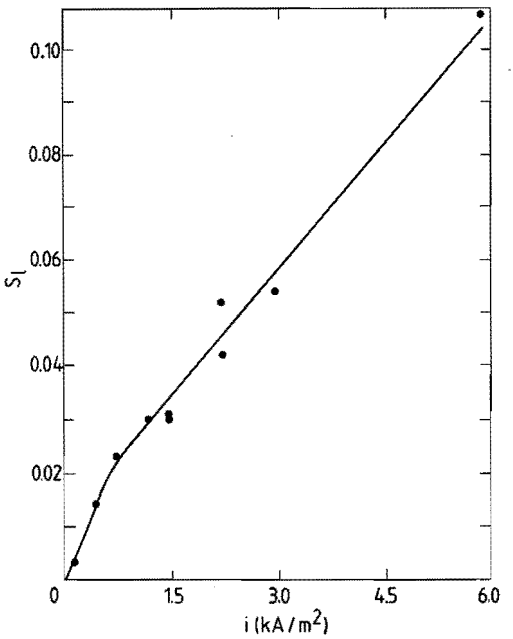

Fig. 2.4.7
Degree of screening at a distance of 1 mm from the electrode surface as a function of current density. v_ℓ = 0.3 m/s, h = 7 cm.

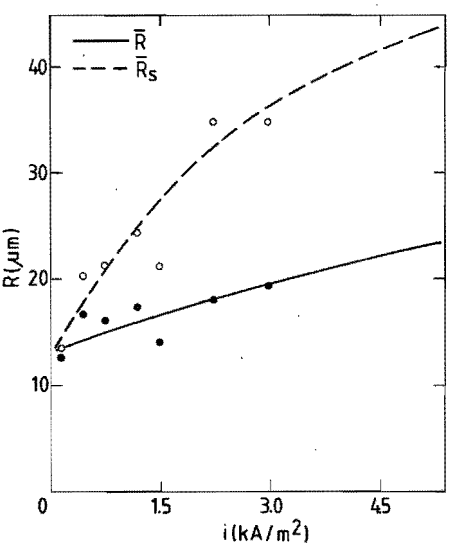

Fig. 2.4.8
The dependence of the average bubble radius and the average Sauter radius on current density. v_ℓ = 0.3 m/s, h = 7 cm, x = 1 mm.

2.4.2.3. Effect of solution flow velocity.

The effect of solution flow velocity on the degree of screening in the electrolyte is given in Fig. 2.4.9. From this Figure it follows that s_ℓ increases at decreasing solution flow velocity. The width of the first layer of electrolyte adjacent to the electrode is estimated as described in the previous section and depends on the flow velocity. Fig. 2.4.10 shows a plot of δ against v_ℓ on a double logarithmic scale. From this plot the following expression for the dependence of δ on v_ℓ is obtained:

$$\delta \sim v_\ell^{-0.2} \qquad (2.4.2.2)$$

In Fig. 2.4.11 the effect of solution flow velocity on the

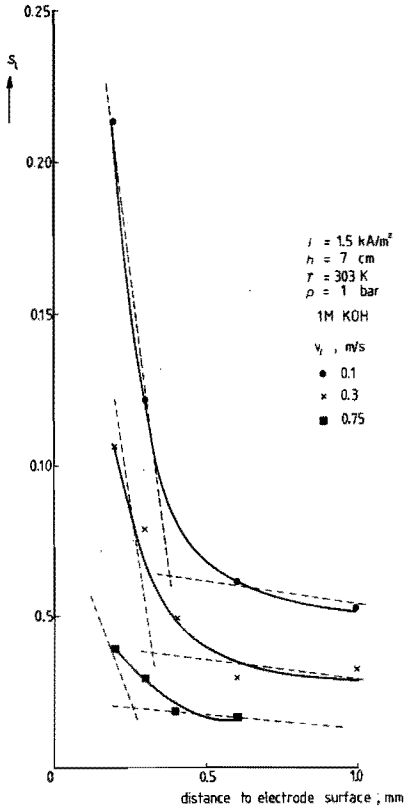

Fig. 2.4.9
The degree of screening as a function of distance to the electrode surface at various solution flow velocities.

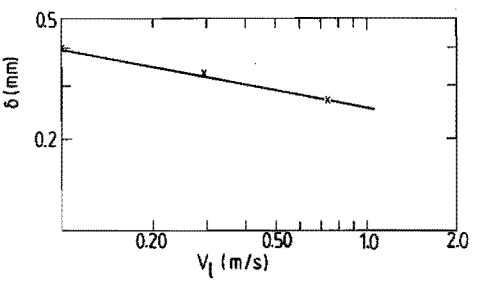

Fig. 2.4.10
The width of the first bubble layer in dependence on solution flow velocity on a double logarithmic scale.
i = 1.5 kA/m^2, h = 7 cm.

average bubble radius and on the average Sauter radius is illustrated at a current density of 1.5 kA/m^2, a height of approximately 7 cm from the bottom of the electrode and at a distance of approximately 0.3 mm from the electrode surface. Both $\bar{R}$ and $\bar{R}_s$ decrease at increasing solution flow velocity, due to the decrease in both the average departure radius from the electrode [32, 37] and the degree of coalescence at increasing flow velocity. The effect on the average Sauter radius is more pronounced due to its greater sensitivity to changes in coalescence behaviour.

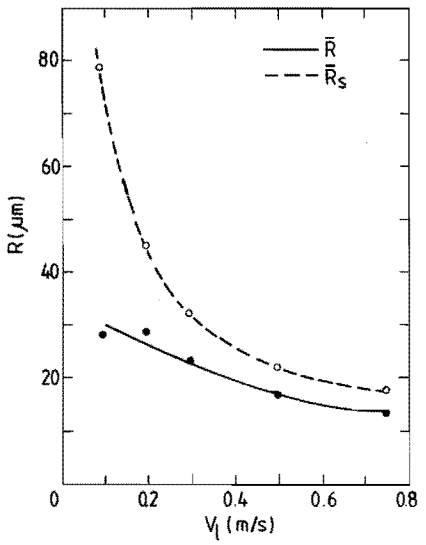

Fig. 2.4.11 The effect of solution flow velocity on the average bubble radius and the average Sauter radius at x = 0.3 mm, i = 1.5 kA/m^2, h = 7 cm.

2.4.2.4. Effect of height.

In Fig. 2.4.12 the degree of screening in the electrolyte is plotted versus the distance from the electrode surface at three heights, h, in the electrolysis cell viz. 7, 15 and 33 cm from the bottom of the electrode. As is to be expected, the degree of screening in the electrolyte increases at increasing height in the cell. It is noted that in section 2.4.1.4 it was stated that the degree of screening at the electrode surface is independent of the height in the electrolysis cell.

The width of the layer adjacent to the electrode, where the degree of screening decreases strongly, depends on the height in the electrolysis cell. A plot of δ versus h on a double logarithmic scale (cf. Fig. 2.4.13) shows a straight line with a slope of 0.3. The dependence of δ on h can therefore be estimated by:

$$\delta \sim h^{0.3} \qquad (2.4.2.3)$$

In Figs. 2.4.14 and 2.4.15 the average bubble radius and the average Sauter radius are plotted as a function of distance from

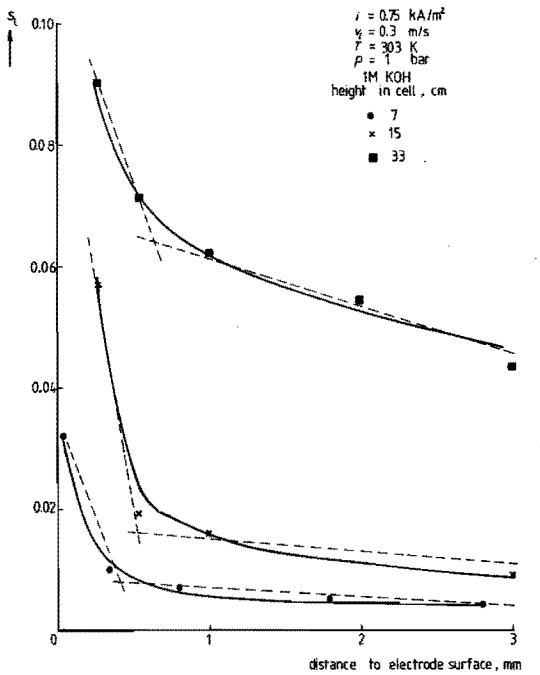

Fig. 2.4.12 The degree of screening as a function of distance to the electrode surface at various heights in the cell.

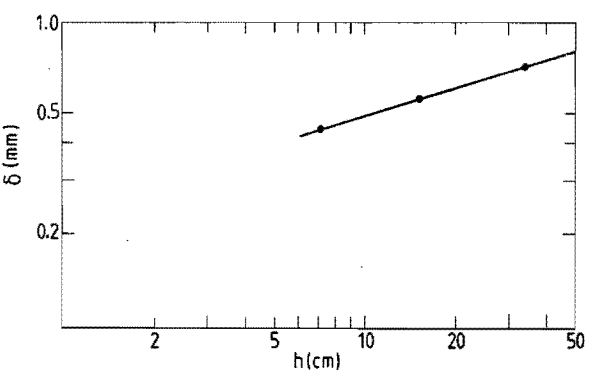

Fig. 2.4.13 The width of the first bubble layer as a function of height on a double logarithmic scale.
$i = 0.75\ kA/m^2$, $v_\ell = 0.3\ m/s$.

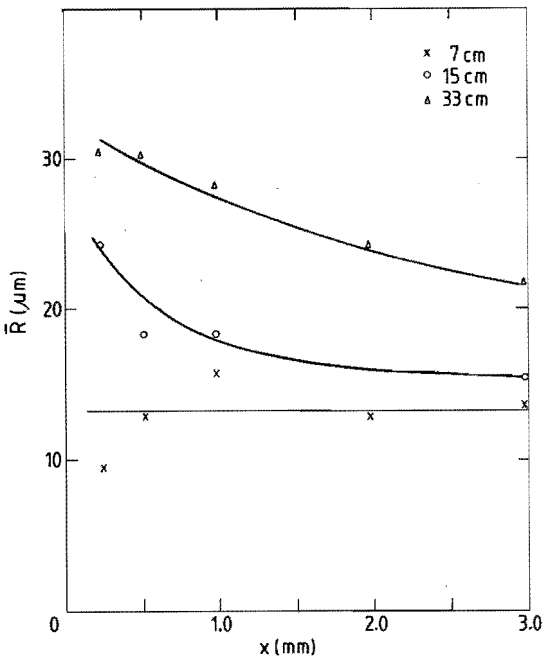

Fig. 2.4.14
The average bubble radius in dependence on distance to the electrode surface.
$i = 0.75$ kA/m^2, $v_\ell = 0.3$ m/s.

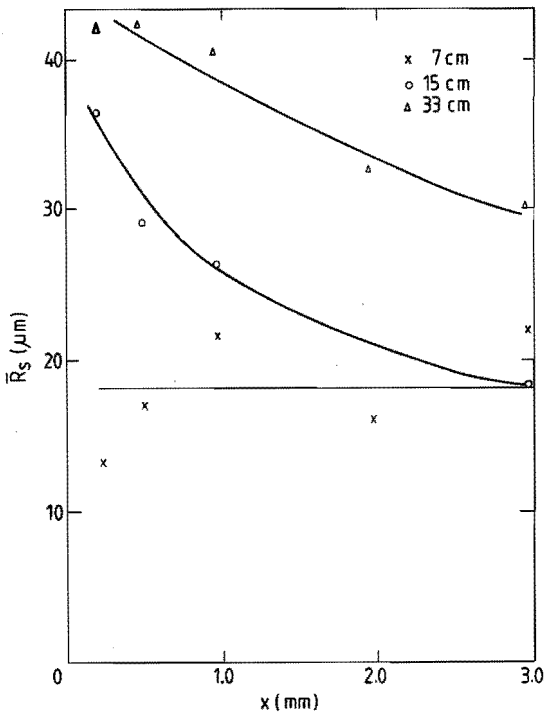

Fig. 2.4.15
The average Sauter radius in dependence on distance to the electrode surface.
$i = 0.75$ kA/m^2, $v_\ell = 0.3$ m/s.

the electrode surface at a current density of 0.75 kA/m^2, a solution flow velocity of 0.3 m/s and at three heights in the electrolysis cell. It is obvious that both radii increase at increasing height, due to an increase in the degree of coalescence.

In the bulk of the solution the gas void fraction in the electrolyte is smaller and the electrolyte velocity is larger than near the electrode surface. Consequently, coalescence will occur especially near the electrode surface and less further in the electrolyte. Therefore, $\bar{R}$ and $\bar{R}_s$ decrease at increasing distance from the electrode surface, except at relatively small heights in the cell where coalescence has hardly occured.

2.4.2.5. Conclusions.

Summarizing the previous results, the dependence of δ on current density, solution flow velocity and height is obtained from a combination of Eqs. 2.4.2.1, 2.4.2.2 and 2.4.2.3 and may in principle be represented by:

$$\delta \sim i^{c_1} . v_{\ell}^{c_2} . h^{c_3} \qquad (2.4.2.4)$$

The proportionality factor and the respective exponents probably depend on the cell geometry and the nature of the solution flow. In the present cell geometry the thickness of the first bubble layer adjacent to the electrode surface can approximately be represented by:

$$\delta/\delta_r = (i/i_r)^{0.1} . (v_{\ell}/v_{\ell,r})^{-0.2} . (h/h_r)^{0.3} \qquad (2.4.2.5)$$

The value of δ_r is determined, taking as a reference situation $i = 0.75$ kA/m^2, $v_{\ell} = 0.3$ m/s, $h = 7$ cm and $\delta = 0.30$ mm (cf. Fig. 2.4.6), to be 0.14 mm.

It should, however, be noted that this is only a rough approximation. The relative experimental uncertainty in the screening values is of the order of 10% and, the way in which δ has been estimated is questionable.

Therefore, Eq. 2.4.2.5 can only be considered as giving an indication of the effect of the respective parameters on δ.

CHAPTER 3: SPECIFIC RESISTANCE OF A BUBBLE ELECTROLYTE MIXTURE AND CURRENT DISTRIBUTION AT A SEGMENTED NICKEL ELECTRODE.

3.1. INTRODUCTION.

During alkaline water electrolysis oxygen and hydrogen bubbles, which are evolved on the electrodes, cause an increase in the ohmic resistance of the electrolysis cell. Consequently, the energy efficiency of the electrolysis process decreases. The current distribution in a vertical cell will also be affected by the evolved bubbles. The gas void fraction in the cell increases with increasing height and consequently, the current density is expected to decrease with increasing height. Insight in the effects of various parameters on the current distribution and on the ohmic resistance in the cell is of utmost importance for the optimization of the water electrolysis process.

In this chapter a brief literature survey on the effect of non-conducting particles on the ohmic resistance of electrolytes and on the current distribution in the cell is given (section 3.2).

In section 3.3 a new model relating the ohmic resistance to the bubble fraction in the cell is presented.

In section 3.4 experiments to determine the current distribution and the ohmic resistance in a vertical electrolysis cell are described. The results of these experiments are presented in section 3.5 and compared with the proposed model in section 3.6.

3.2. LITERATURE SURVEY.

3.2.1. Conductivity of dispersions.

In the past several models describing the effect of the presence of particles of conductivity K_d in a medium of conductivity K_c have been developed. At the end of the last century, Maxwell [41] obtained the following expression for the effective conductivity, K_e, of randomly dispersed spherical particles of uniform diameter and conductivity K_d in a continuous medium with conductivity K_c in relation to the volume fraction, f, of the dispersed phase

$$\frac{K_e/K_c - 1}{K_e/K_c + 2} = f \cdot \frac{K_d/K_c - 1}{K_d/K_c + 2} \qquad (3.2.1.1)$$

If the dispersed particles are non-conductors ($K_d = 0$). Eq. (3.2.1.1) simplifies to (cf. Fig. 3.2.1):

$$K_e/K_c = (1-f)/(1+\tfrac{1}{2}f) \qquad (3.2.1.2)$$

or in terms of resistances:

$$R/R_p = (1+\tfrac{1}{2}f)/(1-f) \qquad (3.2.1.3)$$

where R = the effective resistance of the dispersion and R_p = the resistance of the pure continuous medium.

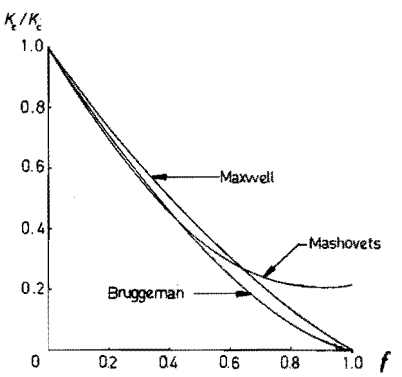

Fig. 3.2.1 Relative conductivity as a function of gas void fraction according to various models.

In his derivation, Maxwell assumed that the average distance between the dispersed particles is large in comparison to their radii, so that the fields surrounding each sphere do not perturb each other to any appreciable extent. Therefore, Maxwell's equation may accurately represent conductivity data for dispersions of spheres when the volume fraction of the dispersed phase is up to approximately 0.1. Although, the relation was derived only for these dilute dispersions, numerous workers have found that experimental data in moderately concentrated dispersions may be represented satisfactorily by Maxwell's

equations [42-44].

Similar and more extended relations were derived for different geometrical conditions by Rayleigh [45], Fricke [46], Runge [47] and Meredith and Tobias [48].

Bruggeman [49] considered the case where the dispersed phase consists of spheres with a wide diameter range. In his treatment he consideres that if one adds a relatively large sphere to a dilute dispersion containing much smaller particles, the disturbance of the field around the large sphere due to the small spheres may be assumed to be negligible. The surroundings of this particle may then be considered to be a continuum with effective conductivity K_e', which may be evaluated using Maxwell's equation. For each infinitesimal increment in volume fraction the effective conductivity changes according to:

$$dK_e'/df' = [-3K_e'/(1-f')][(K_e'-K_d)/(2K_e'+K_d)] \qquad (3.2.1.4)$$

Integrating Eq. 3.2.1.4 with the boundary conditions:

$$K_e' = K_c, \quad \text{when} \quad f' = 0$$
$$K_e' = K_e, \quad \text{when} \quad f' = f$$

he obtained:

$$\frac{K_e/K_c - K_d/K_c}{(K_e/K_c)^{1/3}(1-K_d/K_c)} = 1 - f \qquad (3.2.1.5)$$

With $K_d = 0$, Eq. 3.2.1.5 simplifies to (cf. Fig. 3.2.1):

$$K_e/K_c = (1-f)^{3/2} \qquad (3.2.1.6)$$

or in terms of resistances:

$$R/R_p = (1-f)^{-3/2} \qquad (3.2.1.7)$$

Experiments on suspensions of glass beads by De La Rue and Tobias [50] indicate, that Bruggeman's approximation represents the dependence of the effective conductivity on the volume fraction

very satisfactorily for the dispersed phase containing a broad range of particle sizes. Data for narrow size ranges fall in between the values predicted by the Maxwell and Bruggeman equations. In such mixtures the physical assumptions implicit in the Bruggeman approximation are not justified. De Vries [51] came to a similar conclusion on the basis of theoretical considerations and of experimental values for the dielectric permittivity, the electrical conductivity and the effective diffusivity for gas diffusion of porous media and mixtures.
Since all the theoretical expressions given above were derived for dilute dispersions, many semi-empirical and empirical equations have been developed for more concentrated dispersions and for dispersions of irregularly shaped particles.
So, Wiener [52] derived a semi-empirical relation for the conductivity of mixtures:

$$K_e/(K_e+u) = fK_D/(K_D+u) + (1-f)K_c/(K_c+u) \qquad (3.2.1.8)$$

where u is a constant depending on the form of the particles, to be determined experimentally for each mixture. Other semi-empirical relations were derived by e.g. Lichtenecker [53], Pearce [54] and Higuchi [55].
Mashovets [56] obtained an experimental relation for non-conducting spheres in a continuum by curve fitting (cf. Fig. 3.2.1).

$$K_e/K_c = 1 + 1.78f + f^2 \qquad (3.2.1.9)$$

However, in this relation the conductivity of the mixture, K_e, does not approach zero as f approaches one. Hence it can not be applied for f-values above approximately 0.70.

3.2.2. Current density distribution.

The distribution of current in an electrolytical reactor is determined by a number of parameters such as polarization and electrode geometry. In the absence of concentration differences and activation overpotentials and using Ohm's law, an expression for the current flowing between an electrode and the solution in

which it is emersed is:

$$i = -K_s(d\Phi/dx)_{x=0} \qquad (3.2.2.1)$$

where i = the current density, K_s = the specific conductivity of the solution and x = the coordinate normal to the electrode surface; $(d\Phi/dx)_{x=0}$ represents the potential gradient at the electrode surface.

With the expression for the continuity of electrical charge in the solution and the Laplace equation subject to the appropriate boundary conditions, the so-called primary current density distribution may be calculated.

For a flat plate electrode located opposite an identical electrode three characteristic distributions, depending on different boundary conditions are obtained (cf. Fig. 3.2.2).

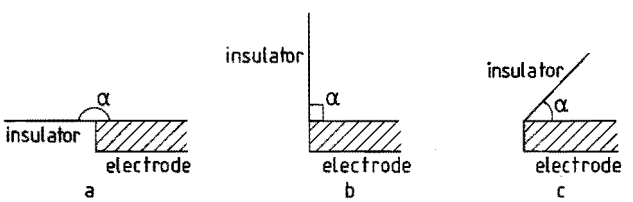

Fig. 3.2.2 Three different electrode geometries.

The current density at the edge of the electrode will approach infinity for $\alpha \to 180°$. For $\alpha = 90°$ the current density will be uniform over the entire electrode surface, while the current density at the edge of the electrode will approach zero for small values of α.

For a parallel plate reactor in which the electrodes do not fully occupy their respective sides of the reactor (cf. Fig. 3.2.2a) Parrish and Newman [57] derived the following primary current distribution:

$$\frac{i}{i_{av}} = \frac{\epsilon \cosh\epsilon \,/B(\tanh^2\epsilon)}{[\sinh^2\epsilon - \sinh^2(2h-H)\epsilon/H]^{\frac{1}{2}}} \qquad (3.2.2.2)$$

where $\epsilon = \pi H/2d$ and B = the complete elliptic integral of the first kind; h = the distance to the beginning of the electrode,

H = the total length of the electrode and d = the distance between the electrodes.

In the limiting cases of d >> H and d << H Eq. 3.2.2.2 simplifies to respectively:

$$\frac{i}{i_{av}} = \frac{2/\pi}{(1-(\frac{2h-H}{H})^2)^{\frac{1}{2}}} \qquad (3.2.2.3)$$

and:

$$\frac{i}{i_{\infty}} = (1-\exp(-2\pi h/d))^{-\frac{1}{2}} \qquad (3.2.2.4)$$

In Fig. 3.2.3 the primary current distribution in a parallel plate reactor for short and long electrodes is illustrated. For relatively long electrodes the current density is reasonably uniform over a substantial part of the electrode surface. Only at h = 0 and h = H infinite current densities are predicted.

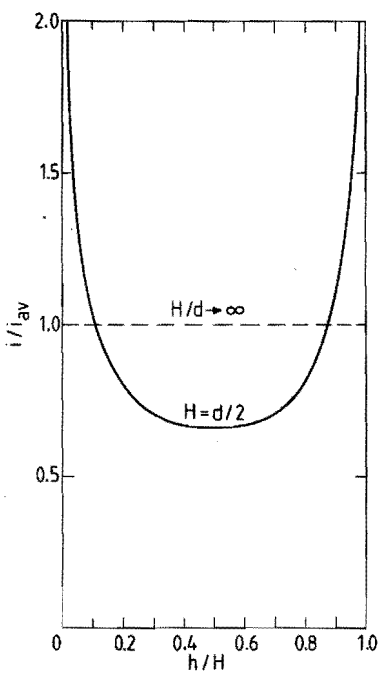

Fig. 3.2.3 Primary current distributions in a parallel plate reactor for long and short electrodes.

When the activation overpotential, η, is taken into account, the boundary condition for the Laplace equation becomes:

$$\Phi_0 = V_0 - \eta \qquad (3.2.2.5)$$

where Φ_0 = the potential in the solution at the electrode/solution interphase, V_0 = the potential for the primary distribution and η = the overpotential which depends on the current density. In the simple case of linear polarization the relation between i and η may be written as:

$$i = \eta\left(\frac{di}{d\eta}\right) = \left(\frac{\alpha\, i_0\, F}{R_G T}\right)\eta \qquad (3.2.2.6)$$

From Eqs. 3.2.2.1, 3.2.2.5 and 3.2.2.6 it follows that:

$$\Phi_0 = V_0 + \frac{K_s R_G T}{\alpha\, i_0\, F}\left(\frac{d\Phi}{dx}\right)_{x=0} \qquad (3.2.2.7)$$

The second term on the right hand side in Eq. 3.2.2.7 is a correction term on the primary potential, due to the activation overpotential. The modified current distribution that occurs with activation polarization is known as the secondary current distribution. When the primary current distribution is uneven, the secondary distribution will tend to be more uniform. High current densities will cause lowered solution potentials because of the increase in the values of the overpotentials. When the primary current distribution is uniform over the entire electrode surface, the secondary distribution will also be uniform, since the overpotential will have the same value over the entire electrode surface.

If both the transport of active species to or from the electrode surface as well as the activation polarization affect the reaction, this gives rise to the so-called tertiary current distribution. The boundary conditions for the Laplace equation become very complicated, because $(d\Phi/dx)_0$ depends on concentration as well as on potential. Except for simple electrode geometries,

numerical solutions for this problem are very voluminous and time-consuming.

The current density distribution may also be affected by variations in the ohmic resistance of the bulk electrolyte in the electrolysis cell. This may be the case when conducting species from the electrolyte are consumed in the reaction or when ill- or non-conducting species are produced. The concentration of these various species is a function of location in the electrolytic cell. In these cases the conductivity, K_s, can not be taken as a constant.

3.2.3. Application to electrolysis processes.

Tobias [9] applied the Bruggeman approximation to a stagnant bubble-electrolyte mixture between two gas evolving vertical plate electrodes. The volume fraction of gases in the electrolyser increases at increasing height in the cell, causing a corresponding increase in the ohmic resistance between the electrodes. Consequently, there will be a non-uniform current distribution over the electrodes.

In order to describe the effect of gas evolution on current distribution and cell tension quantitatively, Tobias made the following physical assumptions:

a) The electrode on the metal side is equipotential.
b) The bubble size distribution may be regarded as constant in time and at all levels.
c) Immediately after detaching from the electrode the bubbles rise at a constant (steady state) velocity, independent of the height in the cell and of the gas volume fraction.
d) Secondary effects on bubble motion such as those due to coalescence are disregarded.
e) Polarization is linear over the current density range considered $E_p = b' . i_h$ (3.2.3.1)
f) The curvature of the lines of current flow is negligible.
g) At a level h, the height from the bottom of the electrode, the bubbles are distributed randomly in the inter-electrode gap. The dependence of the ohmic resistance, R_h, at level h on the volume fraction, f_h, is given by the Bruggeman equation:
$R_h" = R_p"(1-f_h)^{-3/2}$ (3.2.3.2)

The volume fraction of gas in a volume element w d dh is given by:

$$f_h = \frac{dV_h}{w.d.dh} = (R_G T/PnFdv) \int_0^h i_h dh = C \int_0^h i_h dh \qquad (3.2.3.3)$$

where w = the width of the electrodes, d = the distance between the electrodes, P = the partial pressure of the evolved gas and v = the average rising velocity of bubbles. The dependence of potential on current density, polarization and resistance is obtained by combination of Eqs. 3.2.3.1 and 3.2.3.2

$$E = (b'+R_h'')i_h \qquad (3.2.3.4)$$

Since the unit surface resistance of the solution without bubbles, R", equals $R_p'.d$, combination of Eqs. 3.2.3.2 and 3.2.3.4 yields

$$E/R_p'd = [\mu+(1-f_h)^{-3/2}]i_h \qquad (3.2.3.5)$$

where the polarization parameter $\mu = b'/R_p'd$.
The current density may be eliminated in Eq. 3.2.3.5 using a differentiated form of Eq. 3.2.3.3

$$i_h = df_h/C.dh \qquad (3.2.3.6)$$

Integrating the resulting equation yields

$$(CE/R_p'd) \int_0^h dh = \int_0^{f_h} [\mu+(1-f)^{-3/2}]df_h \qquad (3.2.3.7)$$

Assuming no polarization (μ=0) a closed solution for this equation can be obtained:

$$f_h = [(KH^*)^2 + 4KH^*]/[KH^*+2]^2 \qquad (3.2.3.8)$$

where K = the gas effect parameter ($= R_G TEH^*/PnFR_p'vd^2$) and
H^* = the dimensionless height (= h/H).
Combination of this equation with Eq. 3.2.3.6 leads to an

expression for the local current density:

$$i_h = 8K/H^* C(KH^*+2)^3 \qquad (3.2.3.9)$$

If the effect of polarization is considered ($\mu \neq 0$) integration of Eq. 3.2.3.7 yields:

$$KH^* = \mu f_h + 2(1-f_h)^{-\frac{1}{2}} - 2 \qquad (3.2.3.10)$$

which is not explicit in f_h. Therefore, i_h can not be expressed in closed form either. For low gas volume fractions a reasonable approximation is obtained by replacing the term $(1-f_h)^{-3/2}$ in the Bruggeman equation by the first two terms of its binomial expansion, i.e. $1 + 3/2 f_h$. The following expression can then be obtained for the current density variation:

$$i_h/i_{av} = \frac{3}{2} \cdot K\left[(\mu+1)^2+3KH^*\right]^{-\frac{1}{2}} \cdot \left\{\left[(\mu+1)^2+3K\right]^{\frac{1}{2}}-(\mu+1)\right\}^{-1} \qquad (3.2.3.11)$$

Fig. 3.2.4 shows the leveling effect of polarization on the non-uniform current distribution caused by gas evolution.

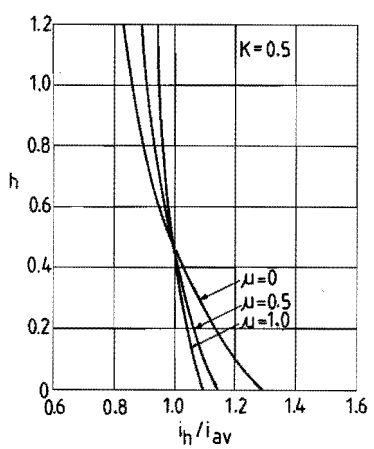

Fig. 3.2.4 Leveling effect of polarization on the non-uniform current distribution caused by gas evolution.

Similar to Tobias' approach, Nagy [58] calculated the effect of gas evolution on current distribution for an electrode built of blades. This geometry allows the inclusion of linear polarization and gas effects in the mathematical treatment without the necessity to use approximate or numerical solutions for the differential equations.
Using the laws of conservation of mass, motion and energy, Ohm's law and Mashovets' equation (3.2.1.9), Funk and Thorpe [36] determined the theoretical gas void fraction and current density distribution in an electrolysis cell with two vertical plate electrodes, separated by a membrane, under forced convection conditions. In their derivation they assumed that:

a) Both gas and liquid are incompressible and isothermal.
b) The bubble layers extend completely across the channels between the electrodes and the membrane.
c) The membrane is permeable only to ions and not to liquid or gases.

They find:

$$f = \frac{1}{1 + \frac{\rho_2}{\rho_1} \cdot \frac{v_g}{v_\ell} \cdot \frac{\Gamma_0}{I}} \qquad (3.2.3.12)$$

where v_g/v_ℓ = the slip ratio, $\Gamma_0 = (\frac{d}{H}).(\frac{\rho_1 \, v_\ell nF}{i_0 M_g})$, M_g = the atomic mass of the gas and $I = \int_0^h i/i_0 \, dh$.

Experimentally the slip ratio is determined to be near unity. Rousar et.al. [59, 60] calculated current density distributions and terminal tensions for monopolar and bipolar electrolysers, used for chlorate production. For a system with forced convection they calculated the resistance of the electrolyte containing bubbles from a modified Maxwell equation

$$R/R_p = 1 + 1.5 \, V_g/V_\ell \qquad (3.2.3.13)$$

Hine et.al. [61] studied the effect of bubbles on the ohmic potential drop in a vertical rectangular cell with stainless steel plate electrodes. The following experimental equation relating the resistance of electrolyte, containing hydrogen bubbles, halfway the vertical cell, to current density, operating temperature, electrolyte flow rate and channel geometry was obtained:

$$R/R_p = K_1 \left(\frac{V_g}{V_\ell}\right)^{\alpha} \cdot \left(\frac{d_{wm}}{w}\right)^{\beta} \qquad (3.2.3.14)$$

where K_1 is an empirical coefficient.
Halfway up the cell the gas void fraction is given by:

$$f = \frac{V_g/2}{V_g/2 + V_\ell} \qquad (3.2.3.15)$$

Substituting this in Eq. 3.2.3.14 yields:

$$\frac{R}{R_p} = K_1 \left(\frac{2f}{1-f}\right)^{\alpha} \left(\frac{d_{wm}}{w}\right)^{\beta} \qquad (3.2.3.16)$$

Experimentally α and β are determined to equal respectively 0.12 and -0.65. The authors propose that the assumption of uniform distribution of bubbles in the inter-electrode gap is not justified, which accounts for the deviation from the Bruggeman equation (3.2.1.7). Especially under flow conditions, the major part of the bubbles is crowded in the vicinity of the electrode surface, while the electrolyte flows mainly through the center of the channel.
In subsequent papers [11, 62], Hine et al. report experimental results that agree with the Bruggeman equation. They state that the different conclusions are due to different methods of experimentation. Initially, the IR-drop was measured between the working electrode and a Luggin probe located near the counter electrode. Consequently, the IR-drop in a thin solution layer in the vicinity of the electrode, crowded with bubbles, was included in the measurements. In subsequent work, the IR-drop was measured between a Luggin probe located near the working electrode and a second one located near the counter electrode. In this

configuration the IR-drop over the thin solution layer adjacent to the electrode is excluded from the measurements.

Based on the idea that the total ohmic resistance may be affected by a "fixed layer" or "bubble curtain" of accumulated bubbles, Vogt [63] developed a hydrodynamic model in which the assumption of uniformly distributed bubbles at each sectional area was dropped. The interelectrode space is divided in several sections:

a) Stagnant layers of thickness δ_A and δ_C close to the gas evolving electrodes from where bubbles protrude into a moving section. These layers, covering the electrodes, are strongly enriched in gas and thus cause an increased potential drop. The thickness of the layers is assumed to equal the break-off diameter of the bubbles and a void fraction of 0.6-0.7 is considered realistic.

b) A centre section of thickness $(d-\delta_A-\delta_C)$ with a flowing dispersion of gas bubbles in the electrolyte. The bubbles in this section are assumed to be uniformly distributed over the whole sectional area.

The mean relative resistance at given current density is:

$$R/R_p = 0.4(1-Y)\frac{V_G}{V_L}\left[(1+\frac{V_G}{V_L})^{2.5} - 1\right] + YQ \qquad (3.2.3.17)$$

where $Y = (\delta_A+\delta_C)/d$ and Q = the relative resistance of the bubble layer calculated from Bruggeman's equation. Using values of 0.01 for Y and 5 for K, Vogt reports satisfactory agreement between his theory and recent experiments by Hine and Murakami [11]. Older experiments of Hine et al. [61] however, can not be interpreted satisfactorily.

Recently, Sillen [32] developed a model for calculating the effect of bubble evolution on the specific resistance of the electrolyte at forced flow. The electrode-diaphragm gap is divided in three sections:

a) The first sublayer adjacent to the electrode, containing the attached bubbles.

b) The second sublayer containing the detached bubbles.

c) The bubble-free electrolyte.

The thickness of the first sublayer is determined by the larger bubbles and has been taken equal to the average bubble departure diameter, $2\bar{R}_d$. The flow velocity in this layer is taken zero. The resistance of the layer is derived using the following expression proposed by Janssen et al. [64]:

$$R/R_p = \frac{1}{2\bar{R}_d} \int_0^{2\bar{R}_d} (1-s(x))^{-3/2} dx \qquad (3.2.3.18)$$

where s(x) is the degree of screening of the electrode at a distance x from the electrode by adhering bubbles. The thickness of the second sublayer is related to the velocity boundary layer in a turbulent one-phase flow, with modifications for the presence of bubbles. The bubbles are assumed to remain in this layer after detachment from the electrode. For the modified thickness of the velocity boundary layer, $\delta_{v,bu}$, the following expression is proposed:

$$\delta_{v,bu} = C_{bu} \cdot h \cdot Re_h^{-1/5} \qquad (3.2.3.19)$$

where C_{bu} depends on the volumetric gas production rate. The thickness of the second sublayer equals $\delta_{v,bu} - 2\bar{R}_d$. The average velocity of the two phase mixture in this layer is assumed to be (7/8)v. The gas volume fraction in this layer is given by:

$$f_h = \frac{8}{7} \frac{R_G T i}{n\ p\ F} \frac{h}{v(\delta_{v,bu} - 2\bar{R}_d)} \qquad (3.2.3.20)$$

The resistance is determined using the Bruggeman equation. The total relative resistance between the electrode and the diaphragm at height h is given by:

$$R/R_p = \frac{1}{d_{wm}} \left\{ \int_0^{2\bar{R}_d} (1-s(x))^{-3/2} dx + (\delta_{v,bu} - 2\bar{R}_d)(1-f(h))^{-3/2} + \right.$$

$$\left. + (d_{wm} - \delta_{v,bu}) \right. \qquad (3.2.3.21)$$

In this model a uniform current density distribution is assumed.

In table 3.2.1 a summary of the above mentioned models to calculate the ohmic resistance in an electrolysis cell is given:

	vertical electrode	electrolyte	relative resis-tivity	current distrib-ution	gas fraction distrib-ution
Tobias	planar	stagnant	Bruggeman	varying	uniform
Funk and Thorpe	planar	flowing	Mashovets	varying	uniform
Rousar	planar	flowing	Maxwell	varying	uniform
Nagy	blades	stagnant	Bruggeman	varying	uniform
Vogt	planar	flowing	Bruggeman	varying	two layers
Sillen	planar	flowing	Bruggeman	uniform	three layers

Table 3.2.1 Various models to calculate the ohmic resistance in an electrolysis cell.

Except for the models of Vogt [63] and Sillen [32] the above mentioned models assume a uniform gas fraction distribution in the interelectrode gap, thus neglecting the fact that in the vicinity of the bubble source, the electrode, the gas fraction will be higher than in the bulk electrolyte. According to Bruggeman's equation, the effect of the bubbles in this region on the effective resistance of the electrolyte will be substantially higher.

In the models proposed by Vogt and Sillen, the assumption of a uniformly distributed gas fraction in the entire interelectrode gap is dropped. Based on hydrodynamic considerations Vogt proposes a two layer model while Sillen distinguishes three layers. However, both authors assume a discontinuity in the gas fraction distribution between the first and the second layer, which is unrealistic. Since in both models the thickness of the bubble layer adjacent to the electrode is confined to only one average bubble diameter, the contribution of this layer to the total ohmic resistance is still underestimated.

3.3. BUBBLE DIFFUSION MODEL.

To a large extent the performance of an electrolytic cell is governed by transport phenomena. Therefore, insight in the flow situation in the reactor is of great importance to model development. A favourite approach is to apply boundary layer theory [65] to the regions adjacent to an electrode.
The common boundary layer equations are, however, simplifications of the Navier-Stokes equations, derived for a surface in contact with an unbounded free stream, as illustrated in Fig. 3.3.1. In most electrolytic reactors, the flow situation is very different. For the water electrolysis cell, operated under forced flow described in section 3.4, with the 2 cm wide and 50 cm high working electrode placed against the backwall of a rectangular compartment, leaving a cross-sectional area of 2 x 0.8 cm^2 between the electrode surface and the diaphragm, the conditions to apply this theory are not fulfilled.

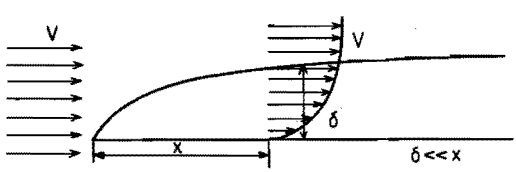

Fig. 3.3.1 Flow situation for an unbounded free stream in contact with a surface.

The transport of bubbles in the electrolytic cell takes place through the motion of the bubbles relative to and together with the electrolytic flow and through turbulent diffusion. The problem is too complicated to find an exact solution. Therefore, the best approach is to solve a simplified version of the problem first and then gradually extend it to match the real situation as much as possible. The first step in this approach is to consider the motion of a single bubble in the vicinity of a wall in an upward electrolyte flow [66, 67].
The bubble will experience an upward force, F_{up}, due to the density difference between the gas and the electrolyte and to the pressure gradient opposite to the direction of the flow. The bubble will

accelerate upward in the electrolyte and, in reaction, a drag force opposing the upward force will act on the bubble, limiting its velocity relative to the electrolyte (cf. Fig. 3.3.2a).
Due to the electrolyte velocity gradient perpendicular to the wall, the bubble will experience an additional force, F_G, towards the wall perpendicular to the drag force (cf. Fig. 3.3.2b). This force will cause the bubble to move in the direction of the wall. F_{drag} and F_G will adjust so that, in a steady state, apart from a small inertia force that is neglected, together they compensate for F_{up} (cf. Fig. 3.3.2c).

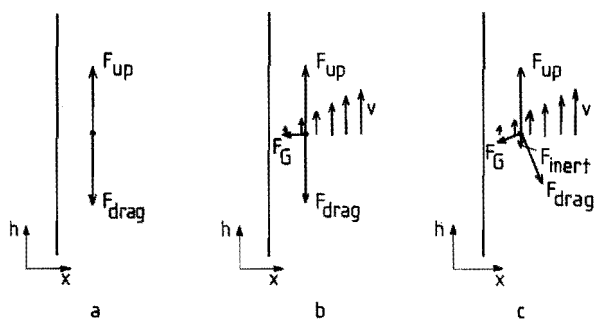

Fig. 3.3.2 Forces acting on a bubble in the vicinity of a wall in an upward electrolyte flow.

The forces are then given by [65, 67, 68, 69]:

$$\vec{F}_{up} = \frac{\pi}{6} d_b^3 (\rho_1-\rho_2)(g - \frac{1}{(\rho_1-\rho_2)} \frac{dp}{dh}) \vec{e}_h \qquad (3.3.1)$$

$$\vec{F}_{drag} = -3\pi\rho_1 \nu d_b (1 + \frac{3}{16} \frac{|u_b| d_b}{\nu}) \vec{u}_b \qquad (3.3.2)$$

$$\vec{F}_G = 20.3\rho_1 d_b^2 (\nu \frac{dv_\ell}{dx})^{\frac{1}{2}} (u_x \vec{e}_h - u_{b,h} \vec{e}_x) \qquad (3.3.3)$$

where g = the gravitational acceleration, d_b = the bubble diameter, ν = the kinematic viscosity and u_b = the velocity of the bubble relative to the electrolyte.

Bubbles will therefore tend to accumulate in the vicinity of the wall. This effect has been confirmed by experimental observations [70].

To solve the diffusion problem the following assumptions are made:

- Immediately after detachment from the electrode surface, the bubbles attain the steady state velocity.
- Quantities are independent of the y-coordinate.
- The channel has smooth walls.
- The electrolyte velocity increases linearly with increasing distance to the electrode surface ($= \frac{dv_\ell}{dx} \cdot x$) with dv_ℓ/dx independent of x and proportional to the average flow velocity.
- The velocity of the bubbles relative to the electrolyte is negligible, which is acceptable for small bubbles.
- The turbulent diffusion coefficient, K_T, of the bubbles is uniform in the entire cell.
- The number of bubbles generated per unit surface area and unit time, ψ, is constant over the entire electrode; $\psi = -K_T(\partial N/\partial x)_{x=0}$ with N = the number of bubbles per unit of volume.

In the stationary case the diffusion equation for N reads:

$$\frac{1}{K_T}\left(\frac{dv_\ell}{dx}\, x\right)\frac{\partial N}{\partial h} = \frac{\partial^2 N}{\partial x^2} + \frac{\partial^2 N}{\partial h^2} \qquad (3.3.4)$$

With boundary conditions:

$$\text{for } x = 0 \begin{cases} h < 0 \quad (\partial N/\partial x) = 0 \\ h > 0 \quad (\partial N/\partial x) = -\psi/K_T \end{cases}$$

$$\text{for } x \to \infty \quad (\partial N/\partial x) = 0$$

$$\text{for } h < 0 \quad N = 0$$

Neglecting $\frac{\partial^2 N}{\partial h^2}$, the equation can be solved, yielding [67]:

$$N = \frac{3\psi}{K_T\,(1/3)}\,\frac{1}{A}\int_{A.x}^{\infty} \{t - A.x\}e^{-t^3}dt \qquad (3.3.5)$$

With $A = \left(\frac{dv_\ell/dx}{9K_T h}\right)^{1/3}$

The thickness of the bubble layer, δ_T, is assumed small in comparison to the width of the compartment and is taken to equal the x-value at the intersection of the tangent to the curve of N(x,h) in x = 0 and the x-axis. Since $(\partial N/\partial x)_{x=0} = -\psi/K_T$ this thickness given by:

$$\delta_T = \left(\frac{NK_T}{\psi}\right)_{x=0} \qquad (3.3.6)$$

The thickness of the bubble layer can now be approximated by:

$$\delta_T = \left(\frac{K_T h}{dv_\ell/dx}\right)^{1/3} \qquad (3.3.7)$$

The dependence of the thickness of the bubble layer on height and velocity follows directly from this equation. Its thickness is proportional to $h^{1/3}$ and, since it is assumed that dv_ℓ/dx is proportional to v_ℓ, it is proportional to $v_\ell^{-1/3}$. The dependence of δ_T on current density can, however, not be obtained from this equation. It is likely that the generation of bubbles affects the turbulent diffusion coefficient and has a slight effect on the electrolyte velocity gradient. However, no quantitative relations describing these effects are available.

Comparing the obtained theoretical relation to the experimental expression for the thickness of the bubble layer adjacent to the electrode (section 2.4.2, Eq. 2.4.2.5) it is noted that, for the effect of height, the relations agree well. There is, however, a discrepancy between the relations where the solution flow velocity is concerned, but from both relations it follows that δ decreases with increasing solution flow velocity.

Substituting the experimentally obtained value δ = 0.6 mm at h = 35 cm, i = 6 kA/m^2 and v_ℓ = 0.3 m/s into Eq. 3.3.10 and assuming a velocity gradient of 500 s^{-1} for this situation a value for K_T of 3.10^{-7} m/s^2 is obtained. In Fig. 3.3.3 N is plotted as a function of x for various heights in the cell for these values of

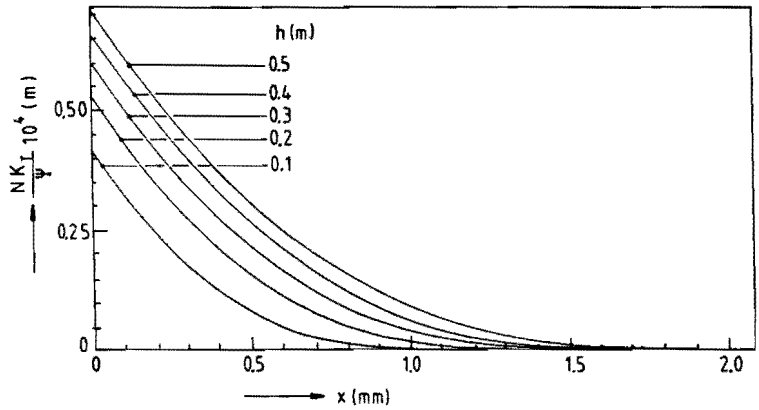

Fig. 3.3.3 Bubble density as a function of distance to the electrode surface at various heights. $K_T = 3.10^{-7}$ m/s^2.

K_T and dv_ℓ/dx. From this figure it follows that the bubble density at $x > 1.5$ mm is negligible. Experimentally it is found that the bubbles spread over the entire gap between the electrode and the diaphragm. This may be caused by flow patterns which extend over a relatively large distance, for which the diffusion theory is not applicable. The local bubble density then equals the bubble density due to the diffusion process superposed on the bubble density caused by the long range transport process.

From the aforesaid it follows that two bubble regions can be distinguished. The first region, the bubble layer adjacent to the electrode, is crowded with bubbles and the average solution flow velocity in this layer is relatively low, whilst in the second region the bubble population is much lower and the average solution flow velocity is higher. The gas void fraction in the first layer is assumed to decrease linearly over the width of the layer. The gas void fraction at the electrode surface is denoted by f_0. The gas void fraction at the boundary of this layer, f_b, equals the gas void fraction in the second layer (cf. Fig. 3.3.4). Applying the Bruggeman equation the resistance of the bubble layer is given by:

$$R_l = R_p' \int_0^{\delta} (1-f_0+(f_0-f_b)x/\delta)^{-3/2} dx \qquad (3.3.8)$$

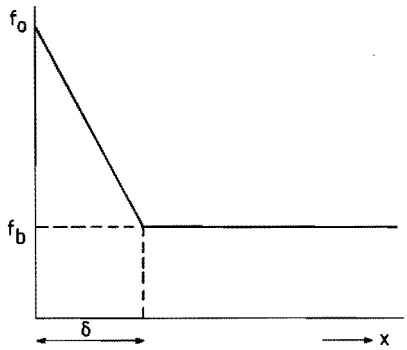

Fig. 3.3.4 Assumed gas void distribution perpendicular to the electrode surface.

The gas void fraction in the second region, the rest of the cross-sectional area, f_b, is assumed constant over the entire width. Its value is approximated by dividing the volume of gas produced per unit time by the volume of electrolyte flowing through the compartment per unit time and depends on current density, solution flow velocity and height in the electrolysis cell. The resistance of this section is given by:

$$R_2 = R_p'(1-f_b)^{-3/2}(d_{wm}-\delta) \qquad (3.3.9)$$

The relative resistance in the electrolysis cell between the working electrode and the diaphragm can then be expressed as:

$$R/R_p = \frac{\int_0^{\delta} (1-f_0+(f_0-f_b)x/\delta)^{-3/2}dx + (1-f_b)^{-3/2}(d_{wm}-\delta)}{d_{wm}} \qquad (3.3.10)$$

3.4. EXPERIMENTAL SET-UP.

The experimental set-up used for the determination of current density distributions and ohmic resistance measurements is shown in Fig. 3.4.1. The electrolysis cell consists of stainless steel and is divided into two parts, the working and the counter electrode compartment, by an asbestos diaphragm. The counter electrode is a nickel venetian blind electrode of 50 x 2 cm^2 and is placed against

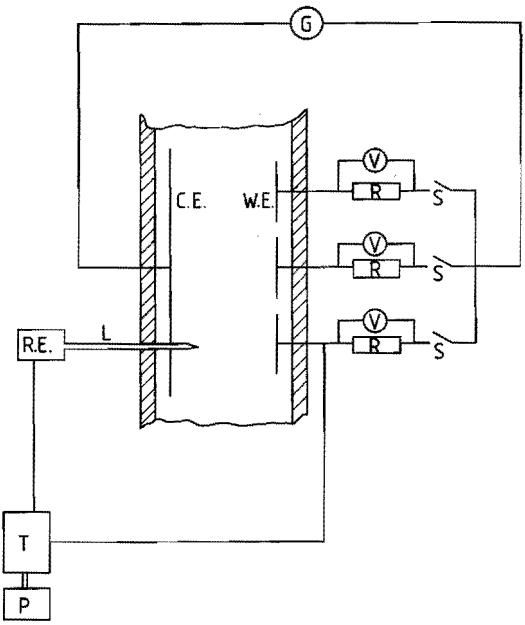

Fig. 3.4.1 Experimental set-up used for the determination of current density distributions and ohmic resistance measurements.

the asbestos diaphragm. Details of this electrode are given in chapter 4. The working electrode (cf. Fig. 3.4.2) consists of 20 nickel plates of 2.30 x 1.85 cm^2 embedded in an acrilate plate. To each nickel plate two wires are attached, viz. a tinned copper wire used as a current feeder and a nickel wire for "currentless" potential measurements. The working electrode is placed against the backwall of the working electrode compartment, leaving a distance of 8 mm between the working electrode surface and the diaphragm.
For the electrode consisting of 20 separate electrode segments to resemble one flat equipotential plate electrode, it is of utmost importance to keep all the electrode segments at the same potential. For this purpose a special potentiostat has been designed. The current through each segment is adjusted so, that the potential differences between the segments and the counter electrode all equal a set value. The current through each segment is determined by measuring the potential drop over a calibrated resistance of 0.1 Ω. The maximum possible current through a segment is restricted to approximately 6 A.

Five glass Luggin capillaries, with an outer tip-diameter of approximately 0.8 mm enter the cell at various heights through the backwall of the counter electrode compartment and prick through little holes in the midst of the counter electrode and the diaphragm. The capillaries are situated at 5, 15, 25, 35 and 45 cm from the lower edge of the working electrode. The distance from the tips of the Luggin capillaries to the working electrode can be varied and measured by means of micro-screws. Each capillary is connected to a reference electrode consisting of Hg/HgO/KOH.
The ohmic potential drops between various segments of the working electrode and the Luggin capillaries are measured simultaneously, using the current interruptor technique. A schematic outline of the electrical circuit is shown in Fig. 3.4.1. The current through each segment is interrupted simultaneously by electronic switches and the potential drops are recorded by a four channel transient recorder (Difa TR-1010) and printed.

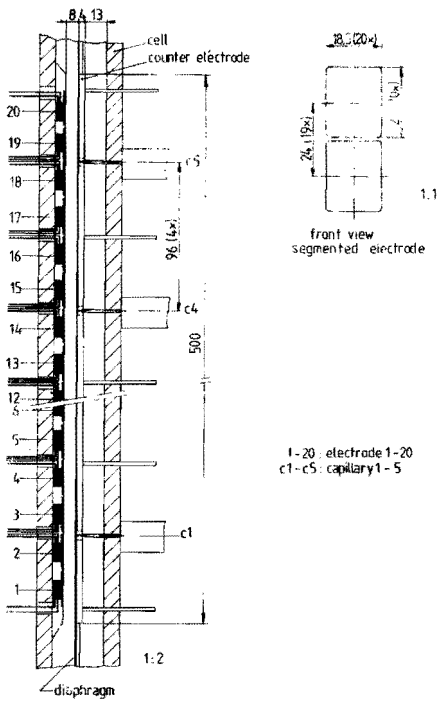

Fig. 3.4.2 Schematic outline of the segmented nickel electrode.

The electrolysis cell is connected to a circuit for forced flow which consists of stainless steel. After passing through a heat exchanger the flow is divided in an anolyte and a catholyte flow before entering the electrolysis cell. The solution flow rates in the anode and cathode compartments can be controlled separately and are measured by flow meters. At the outlet of the cell the flows come together. The electrolytically generated hydrogen and oxygen gases are separated from the electrolyte in a hydrocyclone. After passing an expansion vessel and a cooling device, the electrolyte is pumped back to the heat exchanger.
Unless stated otherwise, the experiments have been carried out potentiostatically at atmospheric pressure in a 30 wt% KOH solution at 313 K. Hydrogen as well as oxygen evolution have been studied at various current densities and solution flow velocities. The distances between the tips of the Luggin capillaries and the working electrode equal 4 mm.

3.5. RESULTS.

3.5.1. Current density distribution.

3.5.1.1. Effect of current.

The effect of the current through the electrolysis cell on the current density distribution over the working electrode is illustrated in Fig. 3.5.1 for oxygen and hydrogen evolution at the working electrode at a solution flow velocity of 0.05 m/s. The current density decreases with increasing height in the electrolysis cell. The effect is more pronounced at high current densities when the gas production is high. The relatively high values of the current density for both the top and the bottom segments result from the inhomogeneous primary and secondary current density distribution in a parallel flat plate reactor in which the electrodes do not fully occupy their respective sides of the reactor (cf. section 3.2.2). The relative difference in the current density, obtained by linear extrapolation, between the bottom and the top of the electrolysis cell is approximately 20% at an average current density of 8 kA/m^2.

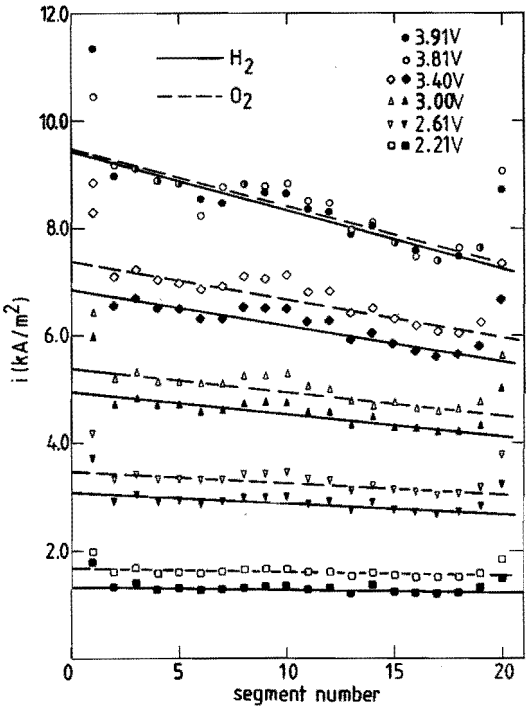

Fig. 3.5.1 Current density distributions for oxygen and hydrogen evolution at various current densities and a solution flow velocity of 0.05 m/s.

3.5.1.2. Effect of solution flow velocity.

In Fig. 3.5.2 the current density distribution over the working electrode for hydrogen evolution at this electrode is shown at various solution flow velocities at a constant potential of 3.60 V between the segments of the working electrode and the counter electrode.

At low solution flow velocities the differences in current density between the bottom and the top of the electrode are clearly visible. At solution flow velocities higher than approximately 0.3 m/s the current density becomes constant over the entire electrode, except for the already mentioned deviations at the bottom and top segments.

In Fig. 3.5.3 the current density distribution in the absence of forced convection is shown at various cell potentials. The differences in current density between the bottom and the top of

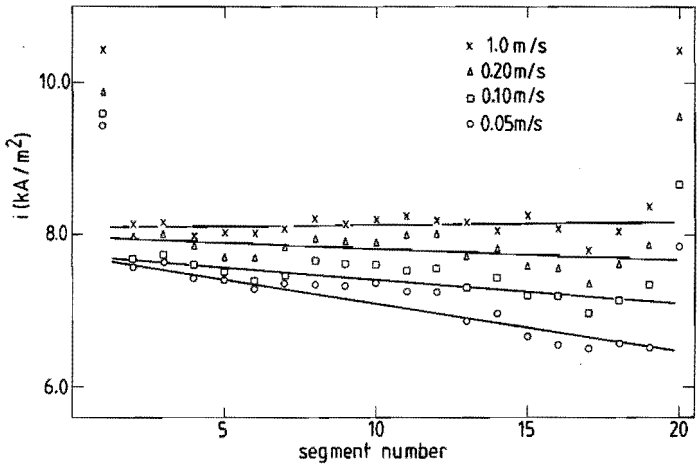

Fig. 3.5.2 Current density distribution for hydrogen evolution at various solution flow velocities at a potential of 3.60 V.

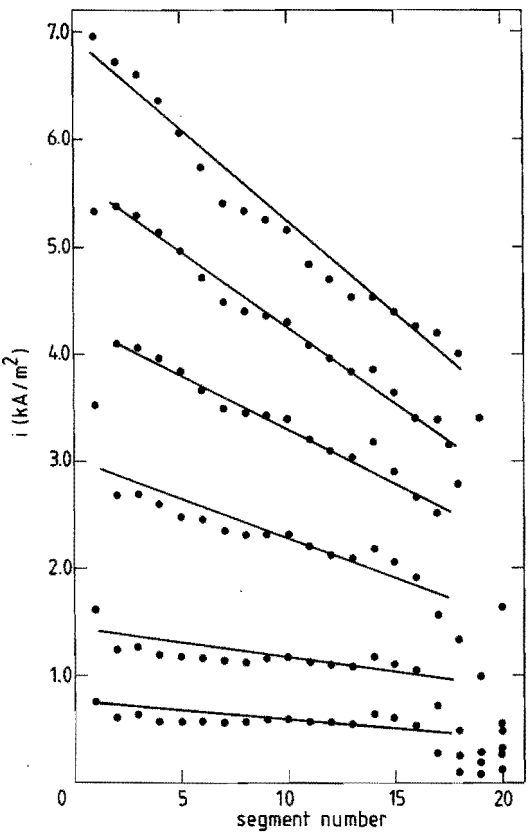

Fig. 3.5.3 Current density distributions in the absence of forced convection.

the electrode are high, due to the accumulation of bubbles in the upper part of the electrolysis cell. In the absence of forced flow the bubbles rise in the electrolyte, but they can be dragged down in the electrolyte flow induced by rising bubbles. Therefore, the gas holdup in the cell will be very much larger than in the case of even a small applied forced flow through the cell.

3.5.1.3. Effect of electrolyte concentration.

The effect of electrolyte concentration has only been studied for hydrogen evolution at the working electrode. In Fig. 3.5.4 the current density distribution at potential differences between the working and the counter electrode of 3.9 and 3.0 V are given for various KOH-concentrations. The differences in current density, relative to the average current density, between the bottom and the top of the electrolysis cell decrease at decreasing concentration.

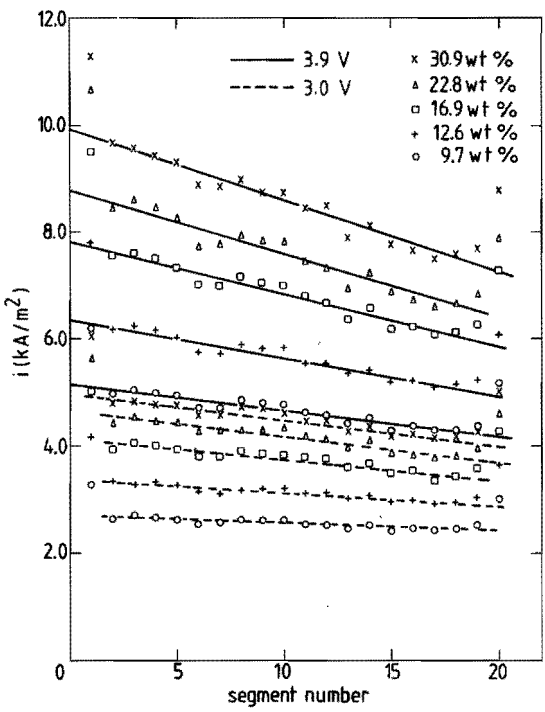

Fig. 3.5.4 Current density distribution at potential differences of 3.9 and 3.0 V for various KOH-concentrations.

However, at a constant potential difference between anode and cathode and decreasing electrolyte concentration, the average current density decreases. Since the current density distribution at a cell potential difference of 3.0 V and a KOH-concentration of 30.9 wt% almost equals the distribution at 3.9 V and 9.7 wt% KOH, the effect can be contributed to the simultaneous decrease in average current density (cf. section 3.5.1.1). No detectable effect of electrolyte concentration remains.

3.5.1.4. Effect of nature of gas evolved at the working electrode.
From Fig. 3.5.1 it follows that, at a fixed potential between the working and the counter electrode, the average current density through the electrolysis cell is higher if oxygen instead of hydrogen gas is evolved at the working electrode. This can easily be understood from the fact that the gas volume of the evolved oxygen is half the corresponding value for hydrogen. The gas bubbles evolved at the working electrode rise in the interelectrode gap, while the gas bubbles evolved at the venetian blind counter electrode which is placed against the diaphragm are deviated to the back of the electrode. Hence, when oxygen is evolved at the working electrode, the average gas holdup in the interelectrode gap will be less than the holdup when hydrogen is evolved at this electrode.
However, the nature of the gas evolved at the working electrode has no effect on the relative current distribution in the electrolysis cell. This indicates that under these conditions the current distribution is hardly affected by the bubbles rising in the interelectrode gap, but is probably determined by bubble layers adjacent to both electrodes.

3.5.2. Ohmic resistance.

3.5.2.1. Effect of current density.
The effect of current density on the ohmic resistance in the cell has been studied for hydrogen and oxygen evolution at the working electrode at various solution flow velocities and heights in the electrolysis cell. In Fig. 3.5.5 the ohmic

resistance between two segments of the hydrogen evolving working electrode, at respective heights of 15 and 35 cm from the bottom of the electrode and the tips of Luggin capillaries located at a distance of 4 mm perpendicular to the electrode, is given as a function of current density at various solution flow velocities.

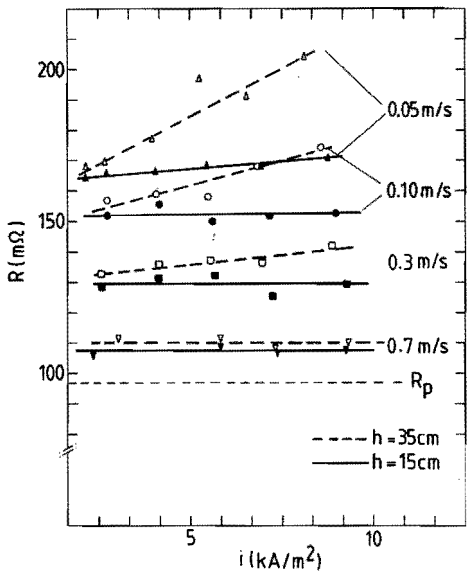

Fig. 3.5.5 Ohmic resistance as a function of current density at various solution flow velocities at two heights in the electrolysis cell.

From this figure it follows that, at low solution flow velocities, the ohmic resistance increases at increasing current density. At high solution flow velocities, the ohmic resistance is almost independent of current density.
When the gas production rate is low, viz. at low current density, one would expect the resistance of the bubble-electrolyte mixture to approximate the resistance of the pure electrolyte. This is, however, not confirmed by the experimental results. Especially at low solution flow velocities, the ohmic resistance at low current densities is considerably higher than the resistance of the pure electrolyte. This indicates that the resistance is not simply determined by the rate of

gas production. Possibly a crowded bubble layer adjacent to the electrode is formed almost immediately, causing a substantial increase in resistance. For oxygen evolution on the working electrode the effect of current density on the ohmic resistance is similar. The absolute value of the resistance is, however, lower.

3.5.2.2. Effect of solution flow velocity.

In Fig. 3.5.6 the ohmic resistance between two segments of the working electrode at respective heights of 15 and 35 cm from the bottom of the working electrode are given as a function of solution flow velocity at a fixed potential difference between the hydrogen evolving working electrode and the counter electrode of 3.6 V.

From this figure it follows that the ohmic resistance decreases at increasing flow velocity. At a solution flow velocity of 1 m/s the bubbles in the bubble-electrolyte mixture hardly affect the ohmic resistance which approximates the resistance of the pure electrolyte even at high current densities.

For oxygen evolution at the working electrode the effect of solution flow velocity on the ohmic resistance is essentially the same as for the hydrogen evolving electrode.

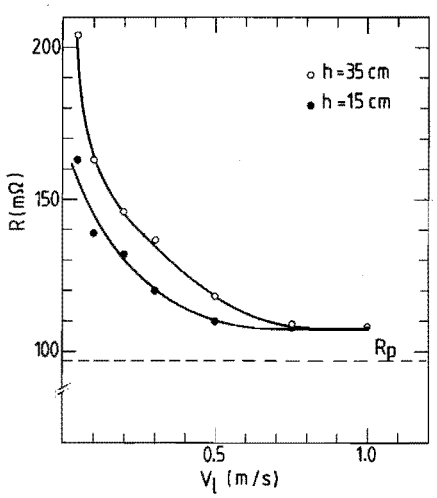

Fig. 3.5.6 Ohmic resistance at two heights as a function of solution flow velocity. E = 3.60 V.

3.5.2.3. Effect of height.

An indication about the effect of height on the ohmic resistance variations in the electrolysis cell is obtained from the current density distribution measurements presented in section 3.5.1. The current density in the cell decreases at increasing height which is to be expected since the gas volume fraction increases with height.

Ohmic resistance measurements between segments of the working electrode and Luggin capillaries confirm that the ohmic resistance increases with increasing height in the cell, cf. Figs. 3.5.5 and 3.5.6. The effect is more pronounced at high current densities and low solution flow velocities.

3.6. DISCUSSION.

In section 3.3 a new model, relating the gas void fraction distribution to the ohmic resistance in the electrolysis cell, is proposed. With this model redictions for the ohmic resistance in the electrolysis cell can be made, provided that the values of f_0, f_b, δ and d_{wm} are known.

The value of d_{wm} follows directly from the experimental set-up and equals 4 mm. The assumed value of δ follows from measurements in chapter 2 and is given by Eq. 2.4.2.5.

From measurements by Janssen [40] it follows that, for electrolytically evolved hydrogen and oxygen, only approximately 60% of the produced gas leaves the electrode in the form of gas bubbles. The rest is carried off in the form of supersaturated electrolyte. The average gas void fraction in the second region, f_b, is approximated according to the following equation:

$$f_b = 0.6 \frac{w.h.i_{av}.V_M}{nF} / \left(V_\ell + 0.6 \frac{w.h.i_{av}.V_M}{nF}\right) \qquad (3.6.1)$$

where w = the width of the electrode, V_M = the molar gas volume and V_ℓ = the volume of liquid flow per unit time.

The void fraction f_0 is high, but its value is not known. As a first approximation it is assumed independent of current density and height and only slightly dependent on solution flow velocity. It is

taken to vary between 0.85 at v_ℓ = 0.05 m/s and 0.60 at v_ℓ = 1.0 m/s.

In table 3.6.1 values for f_0, f_b and δ are given for a hydrogen evolving electrode at various current densities, solution flow velocities and heights in the electrolysis cell, together with the calculated relative resistances. In Fig. 3.6.1 the calculated relative resistance is plotted as a function of current density for various situations. The measured values (section 3.5.2) are also indicated in the figure.

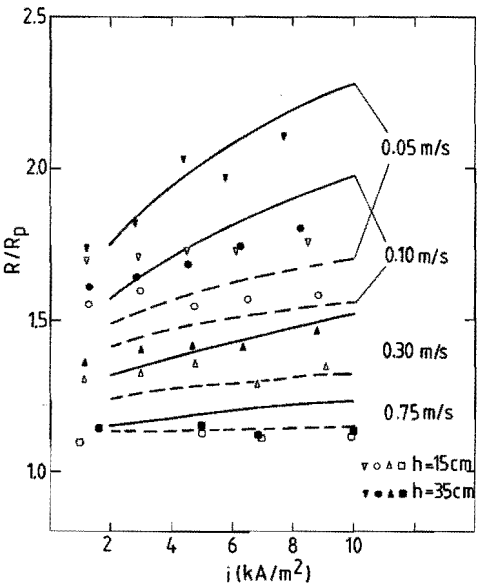

Fig. 3.6.1 Calculated and measured relative resistance as a function of current density for various situations.

From this figure it follows that the qualitative agreement between the predicted and the measured results is relatively good. There are some discrepancies in a quantitative sense, but this is not surprising since the numerical values used to calculate R/R_p are taken rather arbitrarily.

In the approach used, the Bruggeman equation has been applied at very high gas void fractions. As stated in chapter 2, the Bruggeman equation has been derived only for low gas void fractions, where the bubbles do not influence each other. Recently, Janssen [64] found that the Bruggeman equation could be applied to gas bubbles attached

	i	h = 15 cm			h = 35 cm		
	KA/m^2	f_b	δ mm	R/R_p	f_b	δ mm	R/R_p
	10	0.11	0.69	1.70	0.26	0.88	2.28
v_ℓ=0.05 m/s	8	0.10	0.67	1.66	0.24	0.87	2.20
	6	0.09	0.65	1.62	0.21	0.84	2.08
f_0=0.85	4	0.07	0.63	1.56	0.17	0.81	1.94
	2	0.05	0.59	1.49	0.11	0.76	1.75
	10	0.08	0.60	1.56	0.19	0.78	1.97
v_ℓ=0.10 m/s	8	0.07	0.59	1.53	0.17	0.76	1.90
	6	0.06	0.57	1.50	0.14	0.74	1.81
f_0=0.85	4	0.05	0.55	1.47	0.11	0.71	1.71
	2	0.03	0.52	1.41	0.06	0.67	1.57
	10	0.04	0.49	1.32	0.10	0.63	1.52
v_ℓ=0.30 m/s	8	0.04	0.48	1.32	0.08	0.62	1.47
	6	0.02	0.47	1.28	0.06	0.60	1.42
f_0=0.80	4	0.02	0.45	1.27	0.04	0.58	1.37
	2	0.01	0.42	1.24	0.02	0.54	1.32
	10	0.02	0.44	1.18	0.06	0.57	1.29
v_ℓ=0.50 m/s	8	0.02	0.43	1.18	0.05	0.56	1.27
	6	0.02	0.42	1.17	0.04	0.55	1.25
f_0=0.70	4	0.01	0.41	1.15	0.02	0.52	1.21
	2	0.01	0.38	1.14	0.01	0.49	1.18
	10	0.01	0.40	1.11	0.03	0.51	1.17
v_ℓ=1.0 m/s	8	0.01	0.39	1.11	0.02	0.50	1.15
	6	0.01	0.38	1.10	0.02	0.49	1.15
f_0=0.60	4	0.01	0.36	1.10	0.01	0.47	1.13
	2	0.01	0.34	1.09	0.01	0.44	1.12

Table 3.6.1 Calculated values of f_b (Eq. 3.6.1), δ (Eq. 3.3.7) and R/R_p (Eq. 3.3.10) in dependence of i and h.

to the electrode surface. It is therefore assumed that the validity range of the equation is much larger than the limited range for which it has been derived.

The effect of the calculated resistance on the current density distribution can only be compared to the experimental current density distribution in a qualitative way, since the calculated resistance is only a part of the total cell resistance which governs the current density distribution. It is obvious that when differences in resistance are large, viz. at high current densities and low solution flow velocities, the differences in current density will also be large. This is in agreement with experimental results (cf. section 3.5.1).

Approximating the current density distribution by a straight line, the local current distribution is expressed by the following relation:

$$i_h = i_{av} + (\frac{H-2h}{2H})\Delta i \qquad (3.6.2)$$

where Δi = the difference in the extrapolated values of i between $h = 0$ and $h = H$.

In Fig. 3.6.2 Δi is plotted as a function of i_{av} on a double logarithmic scale for various solution flow velocities. The figure shows straight lines with a slope of approximately 1.6, independent of solution flow velocity. Therefore, Δi can be expressed in dependence on i_{av} by:

$$\Delta i = c.i_{av}^{1.6} \qquad (3.6.3)$$

where c depends on the solution flow velocity.

A plot of c_0-c versus v_ℓ on a double logarithmic scale shows a straight line with a slope of 0.06. Therefore, c can be expressed in dependence on solution flow velocity by:

$$c = c_0 - 0.24\ v_\ell^{0.06} \qquad (3.6.4)$$

with $c_0 = 0.24$.

Combination of Eqs. 3.6.2, 3.6.3 and 3.6.4 yields the following

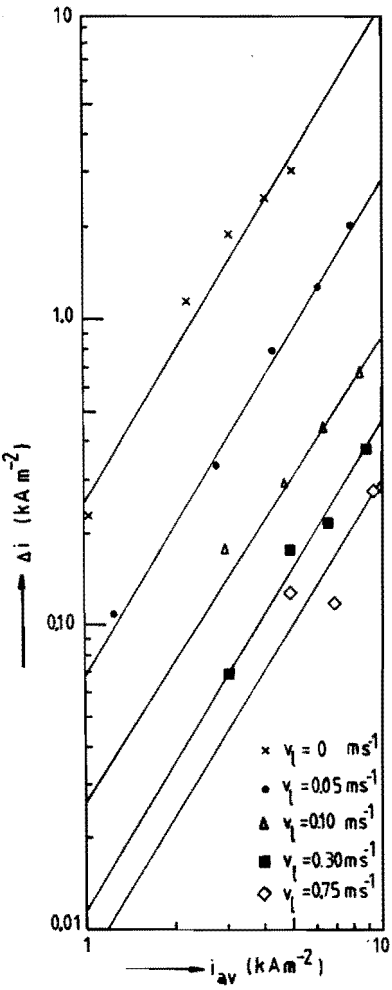

Fig. 3.6.2 Δi as a function of i_{av} on a double logarithmic scale for various solution flow velocities.

empirical expression for the local current density in dependence on i_{av} and v_ℓ in the current density and solution flow velocity ranges studied:

$$i_h = i_{av} + 0.24\,(\frac{H-2h}{2H})(1-v_\ell^{0.06})i_{av}^{1.6} \qquad (3.6.5)$$

It may be concluded that as an approximation the proposed model can be used satisfactorily. Additional research is needed to decide whether the gas void fraction in the layer adjacent to the electrode does indeed decrease linearly with distance or that another profile, e.g. a parabolic profile, describes the decrease in gas void better. A small dependence of f_b on distance may be introduced to improve the relation.

CHAPTER 4: SPECIFIC RESISTANCE OF A BUBBLE-ELECTROLYTE MIXTURE DURING WATER ELECTROLYSIS UNDER PRACTICAL CONDITIONS.

4.1. INTRODUCTION.

In chapter 3 the electrolysis process has been studied at a flat plate working electrode, serving as the backwall of the compartment. This geometry is relatively simple and bubbles evolved on the electrode are obliged to rise in the interelectrode gap, resulting in a relatively well defined average gas volume fraction but also in a high ohmic resistance at various heights in the electrolysis cell.

Under practical conditions efforts are made to diminish the ohmic resistance e.g. by deviating the evolved bubbles to the back of the electrode. Insight in the effects of various parameters on the gas bubble behaviour and on the ohmic resistance is of utmost importance for the optimization of the alkaline water electrolysis.

In this study, the following parameters have been varied: current density (1-10 kA/m^2), solution flow velocity (0.1-1.0 m/s), electrolyte concentration (5-40 wt% KOH), temperature (333-353 K), pressure (1-10 bar), distance between working electrode and diaphragm (0-10 mm) the nature of the nickel working electrode (bare nickel, nickel-teflon, teflon bonded nickel cobalt oxide, Raney type nickelsulfide) and the geometry of the working electrode (plate, venetian blind, Veco gauze (10 N and 25 M), woven gauze and expanded metal gauze).

From the experimental results, a dimensionless correlation for the reduced ohmic resistance between working electrode and diaphragm is derived as a function of the above mentioned parameters.

4.2. EXPERIMENTAL SET-UP.

4.2.1. Electrolysis cells.

The experiments have been carried out in two electrolysis cells. One cell (Fig. 4.2.1), suitable for measurements at atmospheric pressure, consists of a transparent acrylate compartment for the counter electrode and a non-transparent acrylate compartment for the working electrode.

The working electrode is a nickel Veco-type gauze, 50 cm in height. The edges have been bent backward to reinforce the electrode. The width of the electrode is 18 mm. This electrode serves as a support when the effect of the nature of the electrode surface is studied. The counter electrode is a nickel venetian blind electrode of the same dimensions, which is pressed against the woven asbestos diaphragm.

Each electrode is fixed on six nickel bars. These bars also serve as current feeders. The distance between the electrode and the diaphragm is varied, without dismounting the cell, by moving the six bars. Three glass Luggin capillaries, with an outer tip-diameter of approximately 0.8 mm, enter the cell at various heights through the backwall of the counter electrode compartment and prick through little holes in the midst of the counter electrode and the diaphragm. The capillaries are situated at 5 (capillary 1), 25 (capillary 2) and 45 cm (capillary 3) from the lower edge of the working electrode. The distance from the tip of the Luggin capillaries to the working electrode can be varied and measured with micrometer screws. Each capillary is connected to a reference electrode consisting of Hg/HgO/KOH.

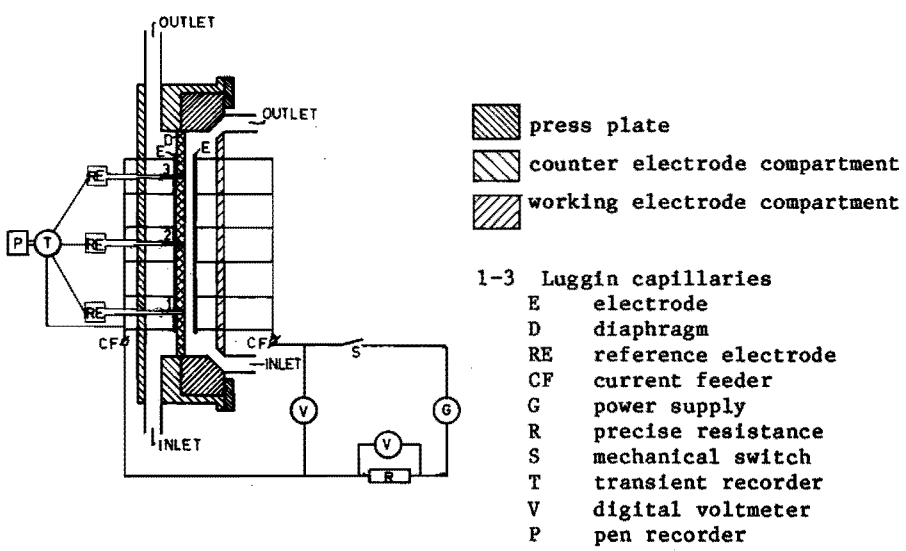

Fig. 4.2.1 Schematic outline of the electrolysis cell and the electrical circuit as used for potential drop measurements.

The temperature in the cell is measured with thermocouples located at the top and at the bottom of the cell in both compartments.

The second electrolysis cell for potential drop measurements, suitable at pressures up to 10 bar, is essentially the same as the one used at atmospheric pressure, except that it is made of stainless steel. To be able to study the gas bubbles in the electrolysis cell at various heights, the cell contains five glass windows.

Five instead of three Luggin capillaries, situated at 5, 15, 25, 35 and 45 cm from the lower edge of the working electrode are used.

4.2.2. Electrolytic flow circuits.

The electrolytic flow circuits for water electrolysis at atmospheric pressure and at elevated pressures are respectively sketched in Fig. 4.2.2 and Fig. 4.2.3.

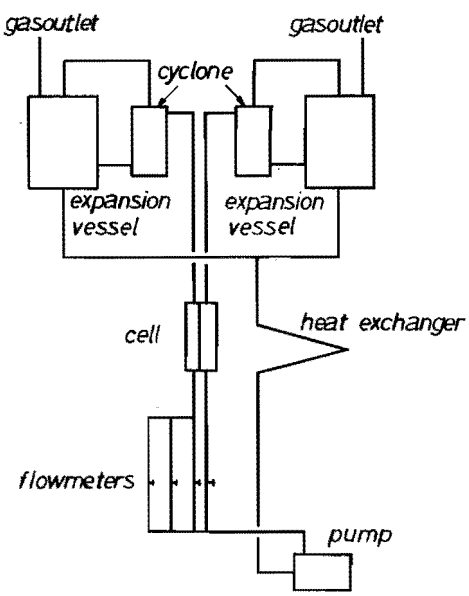

Fig. 4.2.2
Scheme of the circuit for water electrolysis at forced flow and atmospheric pressure.

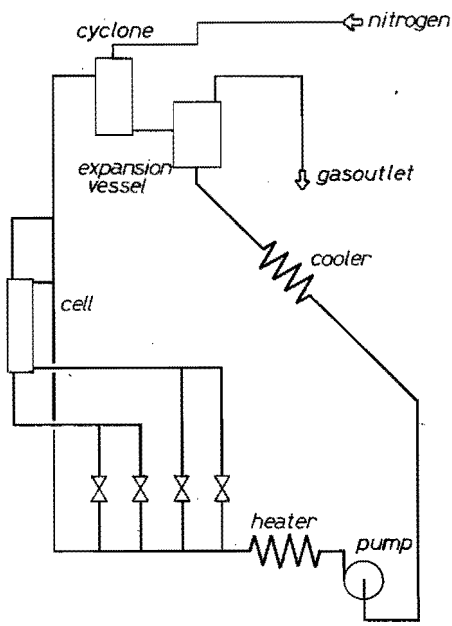

Fig. 4.2.3
Scheme of the circuit for water electrolysis at forced flow and elevated pressure.

The anolyte and catholyte flows are separated before entering the cell. The solution flow rates in the anode and the cathode compartment can be adjusted separately and are measured with flow meters.
In the circuit for atmospheric pressure the electrolytically generated hydrogen and oxygen gas are separated from the electrolyte in two acrylate hydrocyclones. After passing through expansion vessels the two flows join. In the circuit for elevated pressure, the two flows are joined before entering the stainless steel hydrocyclone, where the gases are separated from the electrolyte.
After being brought to the required temperature the gas-free electrolyte is forced through the cell again.
The pressure in the circuit for elevated pressure is maintained by a nitrogen flow from a cylinder in combination with a pressure valve.

4.2.3. Determination of ohmic potential drop.

The ohmic potential drops between the working electrode and the Luggin capillaries and sometimes between the anode and the cathode are measured simultaneously, using the current interruptor technique. The schematic outline of the electrical circuit is shown in Fig. 4.2.1.
The current is interrupted by a mechanical switch (max. 100 A) and the potential drop is recorded by a four channel transient recorder (Difa TR-1010) and is written out by a recorder (YEW type 3066). The constant current is supplied by a SCR Power Supply 0-40 V, 0-150 A. The current is measured by means of a resistance of 1 mΩ and a digital voltmeter (Fluke type 8200 A).

4.2.4. Experimental conditions.

Unless stated otherwise, the experiments are carried out in a 30 wt% KOH solution at atmospheric pressure, 353 K, 3 mm distance between the working electrode and the asbestos diaphragm, 12 mm distance between the working electrode and the backwall of the compartment and a solution flow velocity of 0.5 m/s.
Before starting a series of experiments the electrode is pre-polarized for approximately 1.5 hours at a current density of 5 kA/m^2.

The current density is calculated by dividing the total current by the geometrical surface area of the working electrode. The solution flow velocity is calculated by dividing the volumetric rate of the solution by the cross-section area of the cell compartment diminished by the cross-section area of the electrode in the compartment.
The ohmic potential drop is determined subsequently for a series of experiments with current density decreasing from 10 kA/m^2 to 1 kA/m^2.

4.3. Results.

4.3.1. Effect of the gas to liquid volumetric ratio at the outlet of the electrolysis cell.

The gas to liquid volumetric ratio at the outlet of the cell can be varied by changing either the current density or the solution flow velocity in the cell. The gas/liquid volumetric ratio is usually expressed in terms of a gas void fraction. A gas/liquid volumetric ratio of 1 corresponds with a gas void fraction of 0.5.
In Fig. 4.3.1 the ohmic potential drop, ΔV, is plotted as a function of the current density, i, for various solution flow velocities, v_ℓ. Only the results for capillary 1 are shown in this figure, since similar results were found for the other capillaries and for the ohmic potential drop between anode and cathode.
The figure shows that ΔV is proportional to the current density. Consequently, the resistance, $R = \Delta V/i$, between the capillary and the working electrode is independent of the current density in the current density range studied. This result has been found for both hydrogen and oxygen evolving electrodes.
From the same figure it follows that the ohmic resistance decreases at increasing solution flow velocity. In Fig. 4.3.2 the resistance is plotted as a function of the solution flow velocity on a double logarithmic scale for electrodes of various materials. From this figure it follows that the log R vs log v_ℓ curves are straight and the slopes depend on the nature of the electrode material. They are, however, almost independent of distance between electrode and diaphragm, temperature, pressure and height

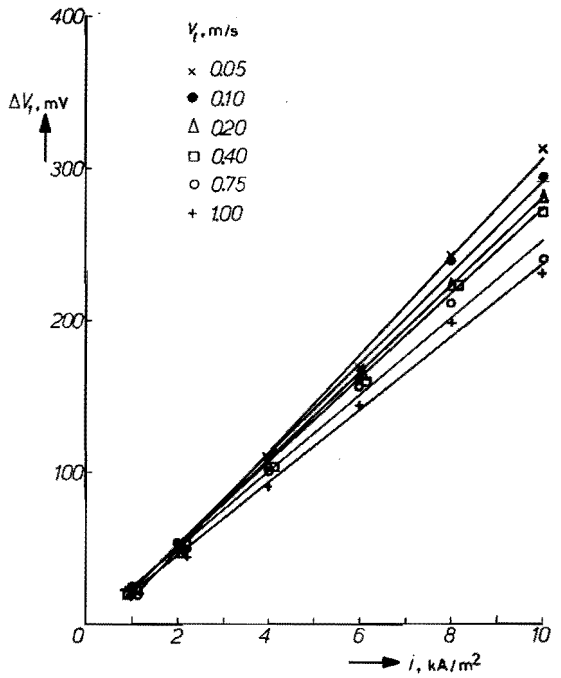

Fig. 4.3.1 ΔV_1 as a function of current density for a hydrogen evolving nickel electrode at [KOH] = 30 wt%, T = 353 K, d_{wm} = 3 mm and various solution flow velocities.

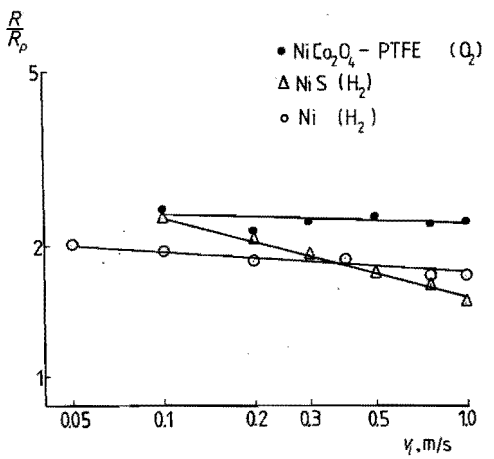

Fig. 4.3.2 The reduced ohmic resistance as a function of solution flow velocity on a double logarithmic scale at [KOH] = 30 wt%, T = 353 K, d_{wm} = 3 mm for various electrodes.

in the cell. They vary between approximately -0.05 for an oxygen evolving teflon bonded nickel cobalt oxide electrode and -0.15 for a hydrogen evolving Raney type nickelsulfide electrode.
Since the resistance does depend on the solution flow velocity but does not depend on the current density, the average gas void fraction cannot be used to describe the resistance between working electrode and diaphragm.

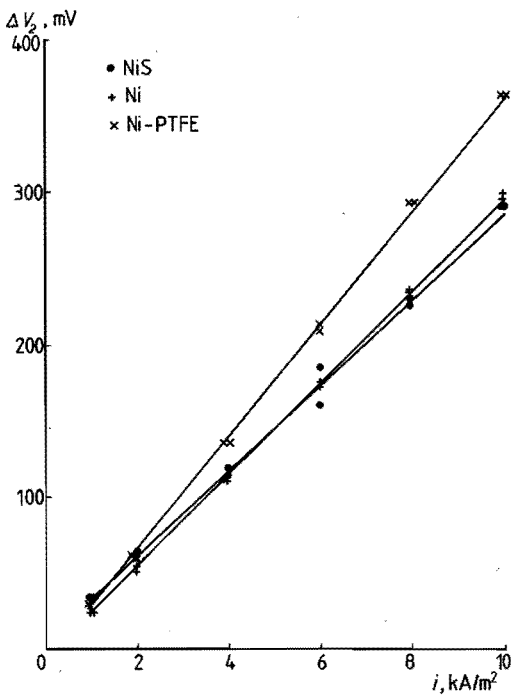

Fig. 4.3.3
The ohmic potential drop as a function of current density for a nickel, a nickel-sulfide and a nickel-teflon cathode at [KOH] = 30 wt%, T = 353 K, d_{wm} = 3 mm and v_ℓ = 0.5 m/s.

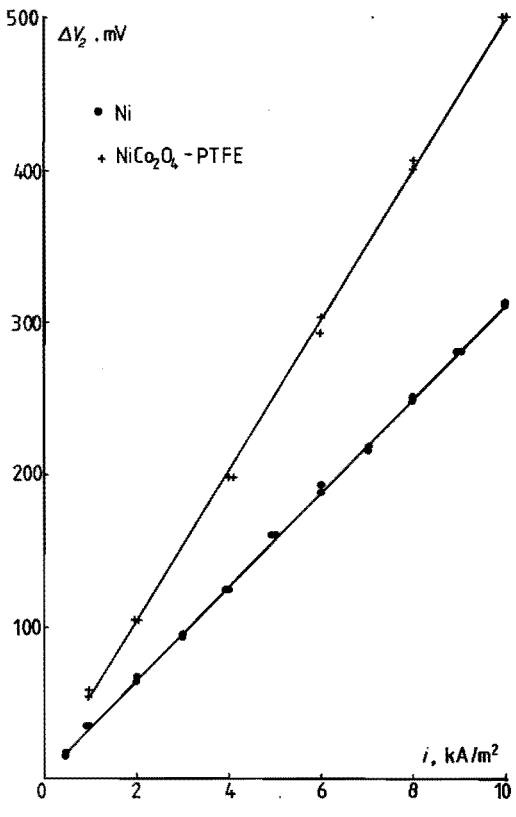

Fig. 4.3.4
The ohmic potential drop as a function of current density for a nickel and a teflon bonded nickel cobalt oxide anode at [KOH] = 30 wt%, T = 353 K, d_{wm} = 3 mm and v_ℓ = 0.5 m/s.

4.3.2. Effect of nature of the electrode surface.

The effect of the nature of the cathode has been studied on three different kinds of electrodes, viz. a nickel electrode, a nickel-teflon electrode and a Raney type nickelsulfide electrode. Fig. 4.3.3 shows the ohmic potential drops between capillary and the respective working electrodes, as a function of current density. The ohmic potential drop is largest for the nickel-teflon electrode. At relatively high solution flow velocities, the ohmic potential drop for a nickelsulfide electrode is slightly lower than for a bare nickel electrode cf. Fig. 4.3.2. The activation overpotential for this electrode, however, is significantly lower than for the nickel electrode.

Nickel and teflon bonded nickel cobalt oxide have been used as anode materials. Fig. 4.3.4 shows the results obtained for these electrodes. The ohmic potential drop for an oxygen evolving teflon bonded nickel cobalt oxide electrode exceeds the corresponding value for a nickel anode. No significant differences in activation overpotential between these electrodes have been found.

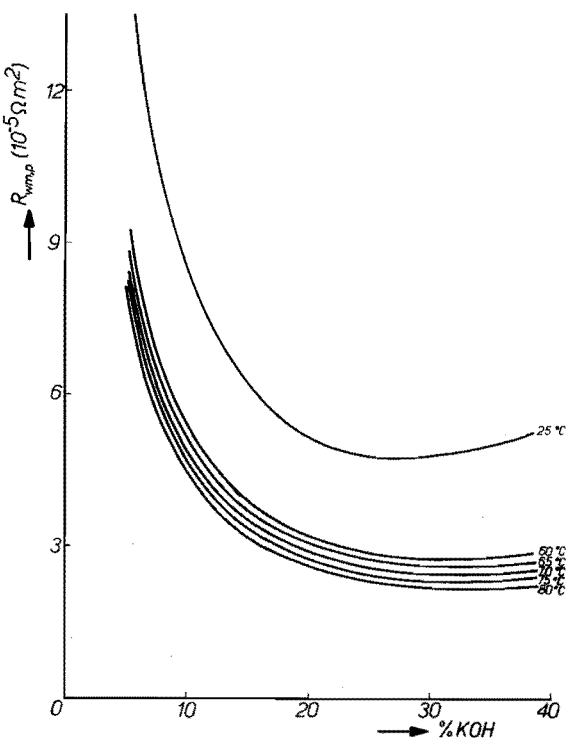

Fig. 4.3.5
The resistance of a solution layer of 3 mm pure electrolyte as a function of KOH-concentration.

The large ohmic resistance for teflon containing electrodes is probably due to a different bubble behaviour on these electrodes. Because of the poor wettability of the teflon, relatively large bubbles are formed which remain on the electrode for a longer period than in the case of a nickel electrode.

4.3.3. Effect of temperature.

The ohmic potential drop between working electrode and diaphragm decreases at increasing temperature. The reduced resistance, R/R_p, is calculated from the potential drop measurements in combination with the experimental R_p values given in Fig. 4.3.5. In Fig. 4.3.6, the reduced resistance is plotted as a function of temperature. This figure shows, that the reduced resistance is practically independent of temperature in the range 333-353 K. Since the reduced resistance does depend on the nature of the electrode surface, a slight hysteresis effect may occur when the electrode surface is modified during the experiment, cf. NiS-electrode. This effect also occurs when a fresh nickel electrode is used as an anode.

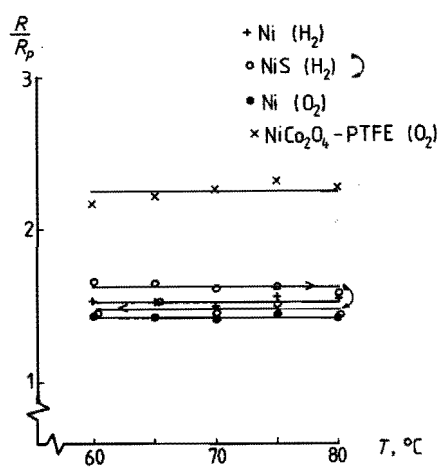

Fig. 4.3.6 The reduced resistance as a function of temperature for various electrodes at [KOH] = 30 wt%, d_{wm} = 3 mm and v_ℓ = 0.5 m/s. For the NiS electrodes results at increasing and decreasing T (indicated by arrows) are presented.

4.3.4. Effect of KOH-concentration.

The effect of KOH-concentration has only been determined for a hydrogen evolving nickel working electrode. The reduced resistance between capillary 2 and the working electrode and between anode and cathode are plotted as a function of the electrolyte concentration for two solution flow velocities in Fig. 4.3.7. Although the ohmic resistance decreases at increasing KOH-concentration up to a value of approximately 30 wt%, the reduced resistance shows a maximum at approximately 16 wt% KOH, because of the ohmic resistance decrease of the pure electrolyte with increasing KOH-concentration (Fig. 4.3.5).

In Fig. 4.3.8, the reduced resistance is plotted versus $[KOH]/\left|[KOH] - [KOH]_{max}\right|$ on a double logarithmic scale. The figure shows straight lines with a slope of approximately 0.05.

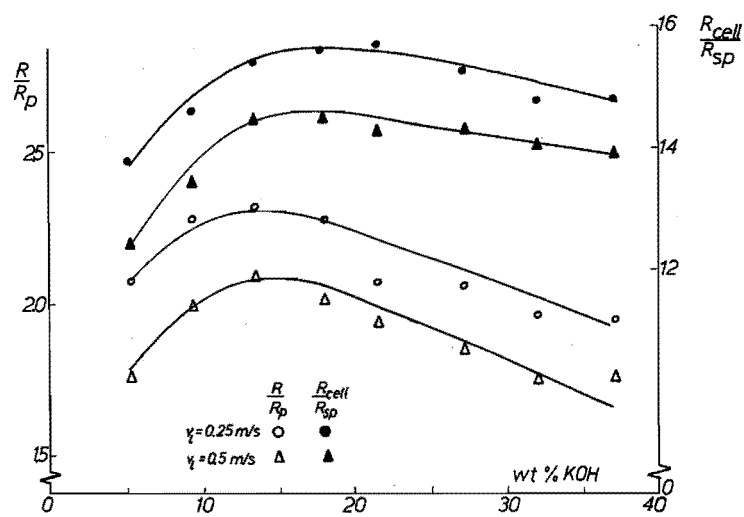

Fig. 4.3.7 The reduced resistance between cathode and diaphragm and between anode and cathode as a function of KOH-concentration at T = 353 K, d_{wm} = 3 mm and v_{ℓ} = 0.5 and 0.25 m/s.

4.3.5. Effect of pressure.

At elevated pressures up to 10 bar, the ohmic potential remains proportional to the current density. In Fig. 4.3.9 the ohmic resistance is plotted in dependence on pressure for a hydrogen

evolving nickel electrode. From this figure it follows, that the ohmic resistance decreased at increasing pressure. This effect is more pronounced at lower pressures than at higher pressures. A plot of log R versus log p shows a straight line with a slope of approximately -0.03.

This slope is practically independent of solution flow velocity, distance between electrode and diaphragm and height in the electrolysis cell and only slightly dependent on the nature of the electrode surface.

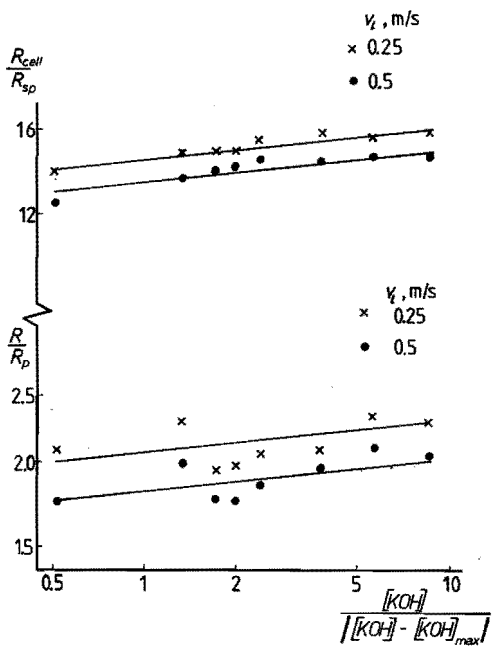

Fig. 4.3.8
The reduced resistance versus $[KOH]/\ KOH\text{-}KOH_{max}$ on a double logarithmic scale at T = 353 K, d_{wm} = 3 mm and v_ℓ = 0.5 and 0.25 m/s.

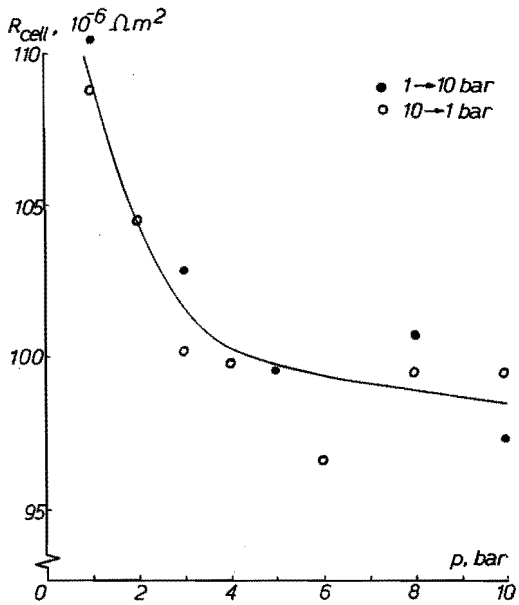

Fig. 4.3.9
The ohmic resistance between anode and cathode as a function of pressure. T = 353 K, d_{wm} = 3 mm v_ℓ = 0.5 m/s and [KOH] = 30 wt%.

4.3.6. Effect of distance between working electrode and diaphragm.

The distance between working electrode and diaphragm, d_{wm}, has been varied from 10 mm to 0 mm. Fig. 4.3.10 shows the

resistance and the reduced resistance as a function of distance for a hydrogen evolving nickel electrode. The ohmic resistance decreases almost linearly, with decreasing distance. The curve has the same slope as the curve for the pure electrolyte. This indicates that the bubbles near the electrode determine the increase in ohmic potential drop. The reduced resistance, however, increases at decreasing distance.

Experiments show that the slope of the log R/R_p - log d_{wm} plot depends on both the height in the cell and the nature of the electrode. It is, however, independent of solution flow velocity. The slopes vary from approximately -0.20 to -0.50.

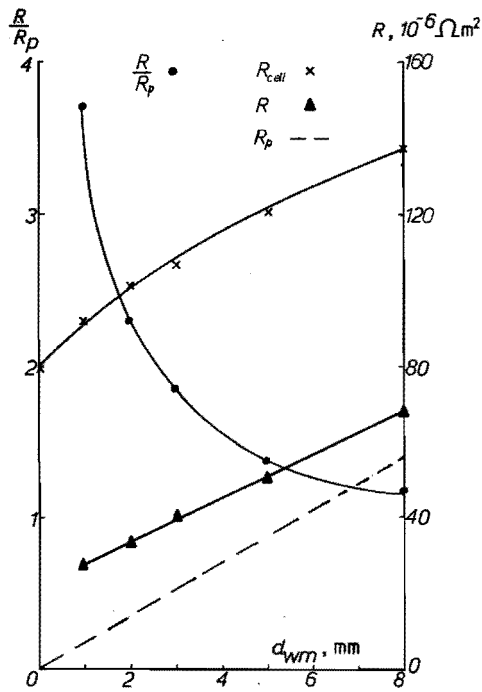

Fig. 4.3.10 The resistance and the reduced resistance between cathode and diaphragm and the resistance between anode and cathode as a function of distance between cathode and diaphragm. T = 353 K, v_ℓ = 0.5 m/s, [KOH] = 30 wt%.

4.3.7. Effect of the geometry of the electrode.

The effect of the geometry of the electrodes has been studied at various solution flow velocities and pressures. Six different electrode geometries have been used, i.e., a plate electrode, a venetian blind electrode, a woven gauze electrode, an expanded metal gauze electrode and two types of Veco gauze electrodes. Detailed information on these elctrodes is shown in Fig. 4.3.11.

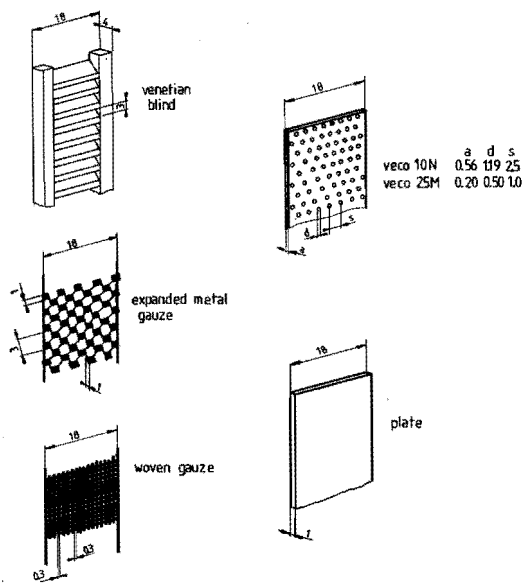

Fig. 4.3.11 Different types of working electrodes as used for potential drop measurements. Dimensions are given in mm. The electrodes are 50 cm in length.

To ensure that only the electrode configuration effect and not the effect of the nature of the electrode surface is studied, each electrode is nickel plated in a Watts bath at a current density of $2A/dm^2$ for one hour. During this process a nickel layer of approximately 20 μm is deposited on the electrode surface.
In Fig. 4.3.12 and Fig. 4.3.13 the ohmic potential drop between anode and cathode is shown in dependence on current density for various electrodes in case of gap widths between the working electrode and the diaphragm, d_{wm}, of 3 and 0 mm and at solution flow velocities, v_{ℓ}, of 0 and 0.4 m/s. Fig. 4.3.12 shows that, at

free convection (v_ℓ=0 m/s) and d_{wm} = 3 mm, the ohmic resistance for the expanded metal gauze electrode is smaller than the corresponding values for the other electrodes. The ohmic potential drop measured for various electrodes increases in the sequence expanded metal gauze electrode, woven gauze electrode, Veco gauze 25 M electrode, venetian blind electrode, plate electrode and Veco gauze 10 N electrode.

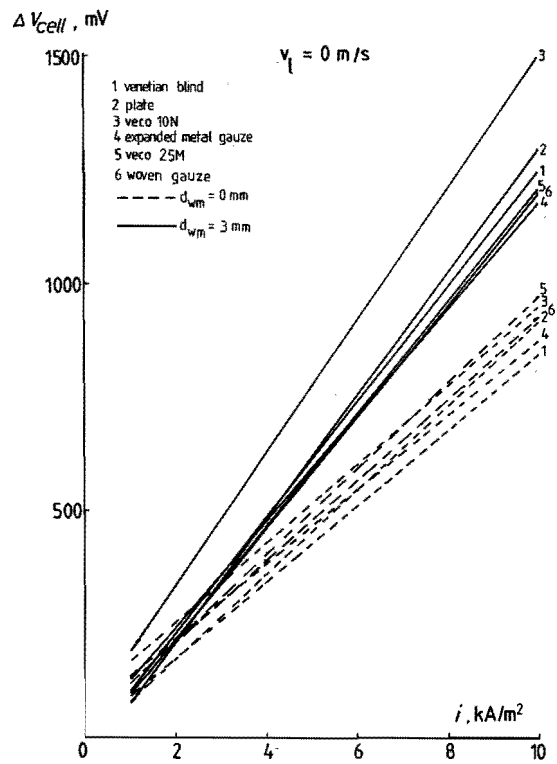

Fig. 4.3.12 Ohmic potential drop between anode and cathode as a function of current density for various electrode geometries. [KOH] = 30 wt%, T = 353 K, v_ℓ = 0 m/s.

At d_{wm} = 0 mm, the venetian blind electrode is more favourable in comparison to the expanded metal gauze electrode. For this configuration the ohmic potential drop for the plate electrode is surprisingly low. Possibly hydrogen gas diffuses through the asbestos diaphragm, where it is carried to the back of the counter electrode together with the evolved oxygen gas.

A comparison of Fig. 4.3.12 and Fig. 4.3.13 shows that, at d_{wm} = 3 mm, the differences between the different electrodes decrease at increasing solution flow velocity. The effect of solution flow velocity on the ohmic potential drop at d_{wm} = 0 mm, is small. Apparently, for all electrodes studied, the ohmic resistances between anode and cathode at d_{wm} = 3 mm exceed those at d_{wm} = 0 mm.

The effect of pressure on the ohmic resistance in the cell has been found to be independent of electrode geometry. For all electrodes studied the ohmic resistance decrease at increasing pressure. The effects are more pronounced at lower than at higher pressures.

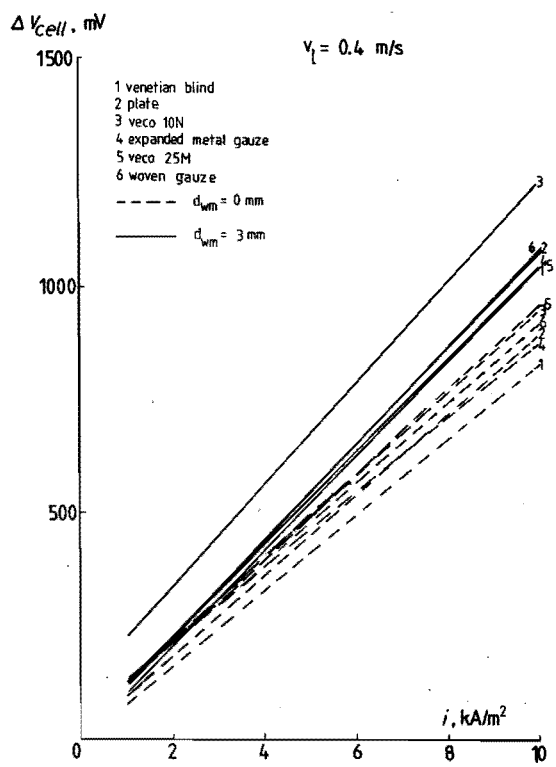

Fig. 4.3.13 Ohmic potential drop between anode and cathode as a function of current density for various electrode geometries. [KOH] = 30 wt%, T = 353 K, v_ℓ = 0.4 m/s.

4.4. Discussion.

Compared to chapter 3 the flow situation and the gas void distribution in the electrolysis cell under practical conditions are very complicated. Although one may argue that the average solution flow velocity in the 3 mm wide area between the electrode and the diaphragm will be substantially lower than the velocity in the 12 mm wide area at the back of the electrode, the flow profile, the value of the average flow velocity and the width of the bubble layer adjacent to the electrode are not known. Further it is unknown which part of the evolved gas volume is deviated to the back of the electrode.

For these reasons it is practically impossible to use the model proposed in section 3.3 to predict the effect of various parameters. Therefore, a dimensionless correlation is derived from the experimental results obtained in this situation.

It is noted that the current is assumed to be distributed uniformly over the entire electrode surface.

Janssen et al. [13] have proposed a dimensionless correlation, which describes the reduced ohmic resistance increase due to the presence of bubbles in the solution layer between working electrode and diaphragm, during alkaline water electrolysis. This relation has to be extended to include the effects of electrolyte concentration, temperature and pressure. To diminish the number of empirical constants, a correlation describing the reduced ohmic resistance, instead of the reduced ohmic resistance increase, is proposed.

It has been found that, within experimental scatter, the reduced resistance is independent of current density (4.3.1.) and of temperature (4.3.3.) in the ranges investigated. Consequently, these parameters do not occur in the dimensionless correlation.

Analysing the experimental results, the effects of the other parameters on the reduced ohmic resistance are represented by the following relation:

$$R/R_p = K_1^* . v_\ell^{n_1} . d_{wm}^{n_2} . p^{n_3} \left([KOH] / \left| [KOH]_{max} \right| \right)^{n_4}$$

where K_1^*, n_1, n_2, n_3 and n_4 are empirical constants. To obtain a

dimensionless correlation the Reynolds number, Re, the reduced distance between working electrode and diaphragm, D_{wm}, and the reduced pressure, P, are introduced.

The Reynolds number for a flowing liquid is defined by $Re = d_{hyd} \cdot v_{\ell} / \nu$. The hydraulic diameter, d_{hyd}, equals 4× cross sectional area of the working electrode compartment divided by the circumference of the rectangular compartment and is constant during all experiments. The variations in the kinematic viscosity, ν, of the electrolyte are relatively small in the range studied. Consequently, within experimental scatter, the Reynolds number can be used to describe the dependence of the reduced resistance on the solution flow velocity.

The reduced distance between working electrode and diaphragm is defined by the distance between working electrode and diaphragm divided by the distance between the backwall of the working electrode compartment and the diaphragm. The latter quantity has been chosen because the bubbles evolved on the electrode can spread over the entire compartment.

The reduced pressure is obtained by relating the pressure to the atmospheric pressure , p_0.

Using the forementioned parameters, the following dimensionless correlation is obtained:

$$R/R_p = K_1 \cdot Re^{n_1} \cdot D_{wm}^{n_2} \cdot P^{n_3} \cdot ([KOH]/|[KOH]-[KOH]_{max}|)^{n_4} \quad \text{where}$$

$Re = d_{hyd} \cdot v_{\ell} / \nu$

$D_{wm} = d_{wm} / d_{bm}$

$P = p / p_0$

K_1 = empirical constant, dependent on the nature of the electrode surface and the gas evolved.

n_1 = empirical constant, dependent on the nature of the electrode surface. For the electrodes studied n_1 varies from -0.05 to -0.15.

n_2 = empirical constant, dependent on the nature of the electrode surface and on the height in the electrolysis cell and varies between -0.20 and -0.50.

n_3 = empirical constant of approximately -0.03.

n_4 = empirical constant of approximately 0.05.

In Table 4.4.1, the numerical values of K_1, n_1, n_2, n_3 and n_4 are given for the 4 kinds of electrodes in the present experiments.

nature of electrode	gas evolved	K_1	n_1	n_2	n_3	n_4
Veco gauze	H_2	1.9	-0.08	-0.30	-0.03	0.05
NiS	H_2	2.9	-0.15	-0.40	-0.03	n.d.
Ni-PTFE	H_2	2.1	-0.08	-0.30	-0.03	n.d.
Veco gauze	O_2	1.3	-0.06	-0.35	-0.03	n.d.
$NiCo_2O_4$-PTFE	O_2	1.7	-0.05	-0.45	-0.03	n.d.

Table 4.4.1 Numerical values of empirical constants for various electrodes.

CHAPTER 5: AVERAGE RADII AND RADIUS DISTRIBUTIONS OF BUBBLES EVOLVED DURING WATER ELECTROLYSIS AT THE OUTLET OF THE CELL.

5.1. INTRODUCTION.

In chapter 2 the screening by bubbles and the bubble radius distributions have been studied in the electrolysis cell, since these quantities affect the ohmic resistance in the cell. If it is impossible to study the bubble behaviour in the electrolysis cell, knowledge of the bubble radius distribution at the outlet of the cell may contribute to the understanding of the bubble behaviour in the cell. It further helps to solve the bubble electrolyte separation problem.

In this chapter, a study on the effects of the parameters mentioned in chapter 4 on the bubble radius distribution at the outlet of the cell is described. From the experimental results a dimensionless correlation for the average bubble radius at the outlet of the electrolysis cell is derived as a function of the above mentioned parameters.

5.2. EXPERIMENTAL SET-UP.

The experimental set-up is essentially the same as described in chapter 4.

Pictures of gas bubbles at the outlet of the electrolysis cell are taken in an auxiliary transparent cell, with a rectangular cross section of 36 × 3.5 mm^2, which is connected to the compartment of the working electrode. The experimental set-up is shown in Fig. 5.2.1.

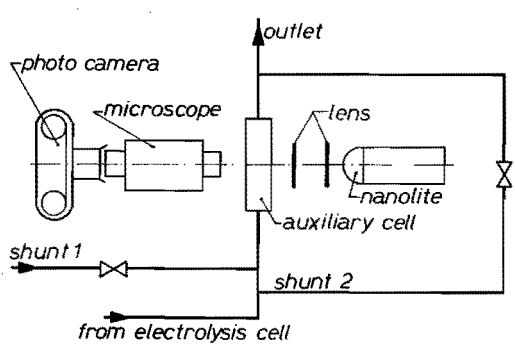

Fig. 5.2.1
Experimental set-up to photograph bubbles in an auxiliary cell at the outlet of the working electrode compartment of the electrolysis cell.

The photographs have to be taken through a microscope because of the very small sizes of the bubbles (10-100 μm diameter). In order to take sharp pictures of the moving bubbles, a very short exposure time and a very intensive illumination are essential. For this reason a nanolite flashlight with a flash time of approximately 20 nanoseconds is used. A set of lenses is necessary to concentrate the light in the auxiliary cell.

To be able to determine the sizes of the bubbles from the photograph, the number of bubbles on a picture has to be limited. Therefore, the two-phase mixture at the outlet of the cell is diluted (shunt 1) with bubble free electrolyte, before entering the auxiliary cell. To decrease the flow velocity in this cell, a large part of the mixture is passed by through a shunt (shunt 2) parallel to the auxiliary cell.

Usually, six pictures are taken of each situation; this results in the investigation of a total of approximately 400 bubbles at each condition.

5.3. RESULTS.

5.3.1. Introduction.

The average bubble radius and the bubble radius distribution at the outlet of the cell depend on two main factors, i.e. the departure radius of the bubbles from the electrode surface and the coalescence behaviour of the detached bubbles in the electrolyte.

The importance of the coalescence behaviour is illustrated in Fig. 5.3.1, where two radius distribution curves for oxygen bubbles are shown. The bubbles of series 1 obviously have coalesced more frequently before entering the auxiliary cell than the bubbles of series 2.

When a parameter of the electrolysis process is varied both the departure radius and the coalescence behaviour, may be affected. Consequently the interpretation of the results is very difficult; especially for oxygen bubbles, because they coalesce more frequently than hydrogen bubbles. For hydrogen, the bubble radius distribution curves are similar to the curve for series 2 in Fig. 5.3.1.

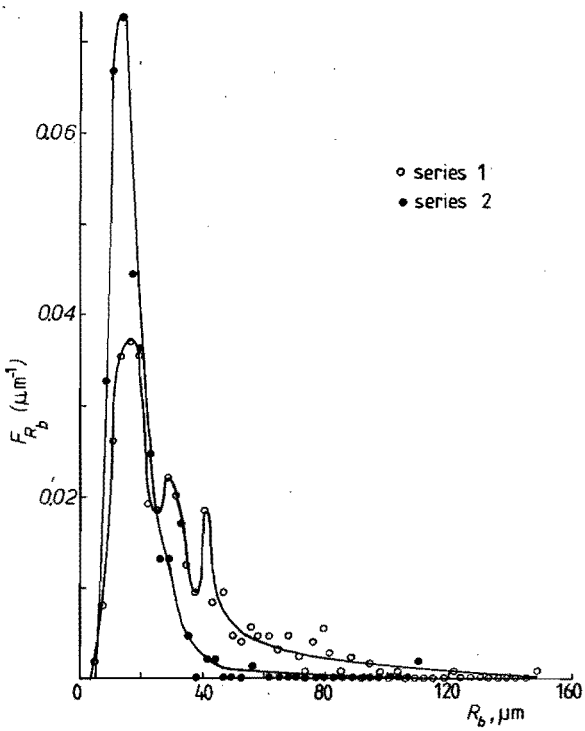

Fig. 5.3.1 Two bubble radius distribution curves for oxygen bubbles evolved on a nickel electrode at i = 2 kA/m^2, T = 353 K, v_ℓ = 0.5 m/s, d_{wm} = 3 mm and [KOH] = 30 wt%.

NiS and $NiCo_2O_4$-PTFE electrodes with different sulfur or PTFE contents have been used. Since the bubble behaviour depends on these contents some differences in average bubble radii may occur.

5.3.2. Effect of current density.

In Fig. 5.3.2, the average radii, $\bar{R}_b$, for oxygen and hydrogen bubbles evolved on various electrodes are shown in dependence on current density. It has been found that the average radius for hydrogen bubbles evolved on a nickel electrode is independent or only slightly dependent on current density. The average bubble radii for oxygen bubbles generated on a nickel and on a teflon bonded nickel cobalt oxide electrode and for hydrogen bubbles evolved on a nickelsulfide electrode increase at increasing current density.

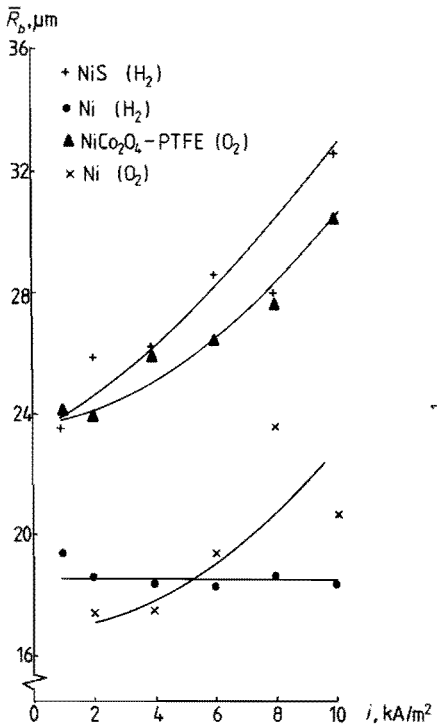

Fig. 5.3.2
The average bubble radius for oxygen and hydrogen bubbles evolved on various electrodes as a function of current density.
T = 353 K, v_ℓ = 0.5 m/s, d_{wm} = 3 mm and [KOH] = 30 wt%

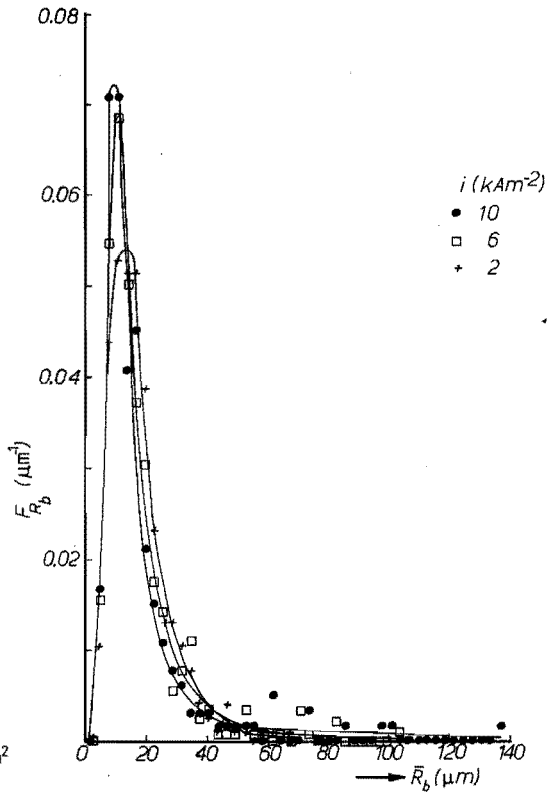

Fig. 5.3.3
Bubble radius distribution curves for hydrogen bubbles evolved on a nickel electrode at 2,6 and 10 kA/m^2.
T = 353 K, v_ℓ = 0.5 m/s, d_{wm} = 3 mm and [KOH] = 30 wt%

Fig. 5.3.3 shows the bubble size distribution for a hydrogen evolving nickel electrode for i = 10 kA/m^2, i = 6 kA/m^2 and i = 2 kA/m^2. At high current density there is a sharp peak with a top at 9 µm and the maximal bubble radius is about 150 µm. At lower current densities the peak broadens and its top shifts to 13 µm. The maximal bubble radius decreases to about 80 µm. The small bubbles probably detached from the electrode surface without coalescence while the larger bubbles are due to coalescence of small bubbles.
Since the gas void fraction is larger at higher current densities

it is obvious that more bubbles coalesce, resulting in larger bubbles at high current densities. The shifting of the peak at increasing current densities to smaller bubble radii may indicate that the average departure radius decreases at increasing current density. A similar result was reported for hydrogen bubbles growing on a vertical transparent gold electrode at forced convection and at room temperature and atmospheric pressure during electrolysis in a 30 wt% KOH solution for $i = 0.5 - 2.5$ kA/m^2 [32].

In Fig. 5.3.4 the bubble size distribution curves for an oxygen evolving nickel electrode are shown at $i = 10$ kA/m^2 and $i = 2$ kA/m^2. The peak of the curve becomes lower and broader at high current densities, probably because of the increase in coalescence of the bubbles. The position of the peak does not change markedly.

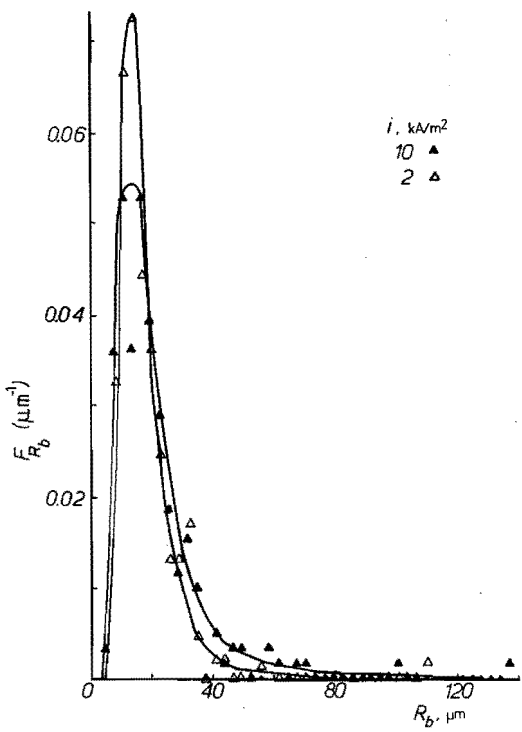

Fig. 5.3.4 Bubble radius distribution curves for oxygen bubbles evolved on a nickel electrode at 2 and 10 kA/m^2.
T = 353 K, v_ℓ = 0.5 m/s, d_{wm} = 3 mm and [KOH] = 30 wt%

The effect of current density on the average bubble radius at the outlet of the cell is determined by both the average radius of bubbles departing from the electrode surface and the degree in which coalescence of detached bubbles in the electrolyte occurs. For hydrogen bubbles evolved on a nickel electrode the decrease in departure radius at high current densities is practically cancelled out by the increase in radius due to the increase in the degree of coalescence. For oxygen bubbles the increase in the occurrence of coalescence outweighs a possible decrease in peak radius. This is also the case for hydrogen bubbles evolved on a nickelsulfide electrode.

Because of the porous structure of the electrode, a considerable degree of coalescence may already occur at the electrode surface and effect the average departure radius. A plot of $\bar{R}_b$ versus i on a double logarithmic scale shows straight lines with slopes varying from 0 for a hydrogen evolving nickel electrode to 0.16 for an oxygen evolving electrode.

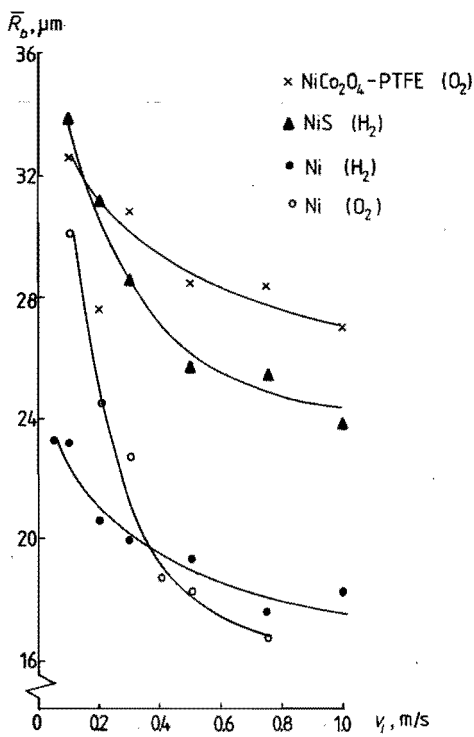

Fig. 5.3.5
The average bubble radius for oxygen and hydrogen bubbles evolved on various electrodes as a function of solution flow velocity.
T = 353 K, i = 4 kA/m^2,
d_{wm} = 3 mm and [KOH] = 30wt%

5.3.3. Effect of solution flow velocity.

In Fig. 5.3.5 the average bubble radii for oxygen and hydrogen bubbles evolved on various electrodes are shown as functions of solution flow velocity. At increasing solution flow velocity, the average bubble radius for both oxygen and hydrogen bubbles decreases. This effect is most pronounced at low solution flow velocities.

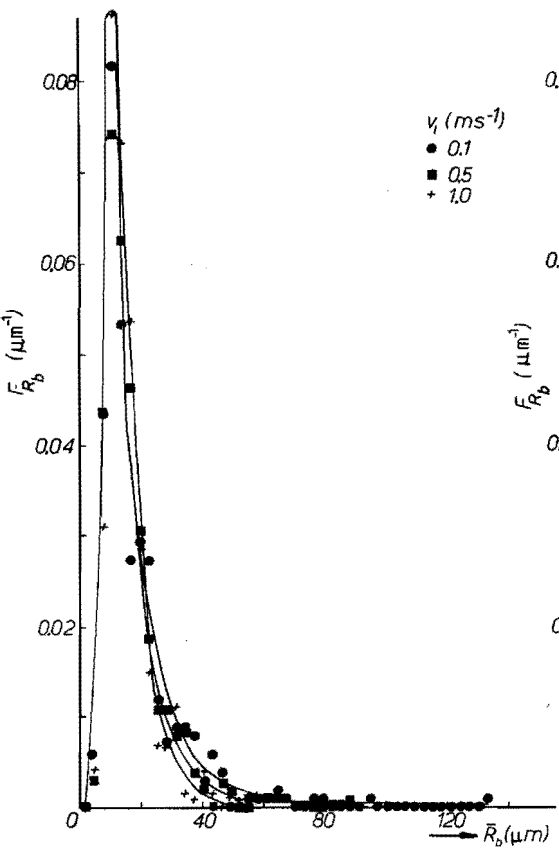

Fig. 5.3.6
Bubble radius distribution curves for hydrogen bubbles for three solution flow velocities.
T = 353 K, i = 4 kA/m^2,
d_{wm} = 3 mm and [KOH] = 30 wt%.

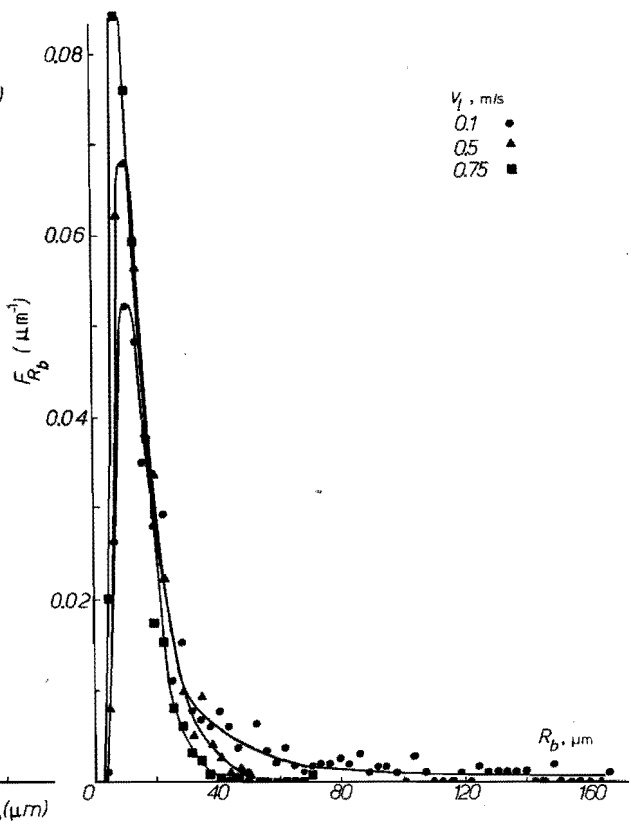

Fig. 5.3.7
Bubble radius distribution curves for oxygen bubbles for three solution flow velocities.
T = 353 K, i = 4 kA/m^2,
d_{wm} = 3 mm and [KOH] = 30 wt%.

Fig. 5.3.6 and Fig. 5.3.7 show bubble radius distribution curves at various solution flow velocities for respectively hydrogen and oxygen bubbles evolved on nickel electrodes. The position of the peak is almost independent of solution flow velocity. The average bubble radius increases at decreasing flow velocity because of the increase in large bubbles due to an increase in the number of coalescences at lower solution flow velocities. Plots of $\log \bar{R}_b$ as a function of $\log v_\ell$ show straight lines with slopes varying between -0.06 for both an oxygen evolving teflon bonded nickel cobalt oxide electrode and a hydrogen evolving nickel electrode and -0.40 for an oxygen evolving nickel electrode.

5.3.4. Effect of the nature of the electrode surface.

Bubbles evolved on teflon containing electrodes e.g. teflon bonded nickel cobalt oxide and nickel-teflon electrodes or on an nickelsulfide electrode show a larger average bubble radius than bubbles evolved on nickel electrodes.

In Fig. 5.3.8 characteristic bubble radius distribution curves for hydrogen evolving nickel, nickel-teflon and nickelsulfide electrodes are shown. The distribution curve for the nickel-teflon electrode shows a peak at a value of approximately 11 μm and a shoulder to the peak at about 25 μm. This shoulder becomes a second peak at low solution flow velocities in the electrolysis cell. Contrarily, the curve for the nickel electrode exhibits only one maximum at approximately 11 μm. If we assume that the position of the peak is a measure for the average value of the departure radius, two peaks indicate the existence of two types of bubbles departing from the electrode.

Apparently, this behaviour is due to the nucleation properties of the electrode surface. On a nickel-teflon electrode two types of active sites generating growing bubbels are present. The first type consists of nickel sites which are surrounded by nickel. These sites are comparable to the sites on a pure nickel electrode. The second type consists of nickel sites which are surrounded by teflon. The bubbles growing on the latter sites may grow to a larger size; this results in a secondary peak in the bubble distribution curve.

For bubbles evolved on a nickelsulfide electrode the bubble radius distribution curve shows a maximum at a value of approximately 15 μm.

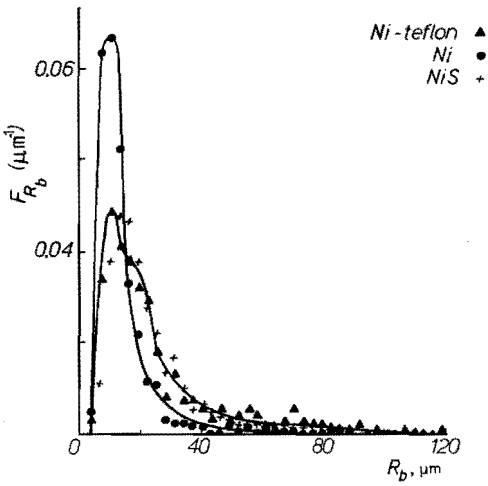

Fig. 5.3.8 Characteristic bubble radius distributions for hydrogen bubbles evolved on a nickel, a nickel-teflon and a nickel-sulfide electrode. T = 353 K, i = 8 kA/m^2, v_ℓ = 0.5 m/s, d_{wm} = 3 mm and [KOH] = 30 wt%.

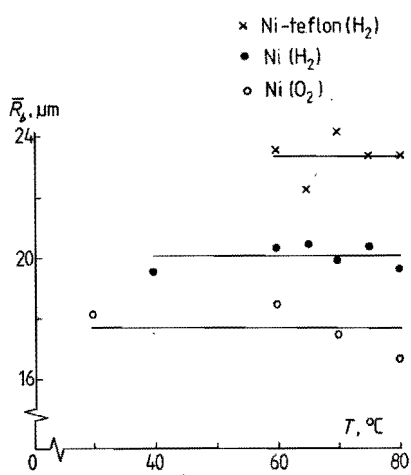

Fig. 5.3.9 The average bubble radius for oxygen and hydrogen bubbles evolved on various electrodes in dependence on temperature. i = 4 kA/m^2, v_ℓ = 0.5 m/s, d_{wm} = 3 mm and [KOH] = 30 wt%.

5.3.5. Effect of temperature.

Fig. 5.3.9 shows the average bubble radius as a function of temperature in the temperature range 30 - 80 ^{0}C at i = 4 kA/m^2 and v_ℓ = 0.5 m/s for various electrodes. From this figure it follows that the average bubble radius for oxygen as well as for hydrogen bubbles is practically independent of temperature in the investigated range. The bubble size distribution curves are also independent of temperature.

5.3.6. Effect of KOH-concentration.

The effect of KOH-concentration on the average bubble radius has been investigated using a hydrogen evolving nickel electrode. Results are shown in Fig. 5.3.10. The average radius decreases at increasing KOH-concentration.

A plot of $\bar{R}_b$ in dependence on KOH-concentration on a double logarithmic scale shows a straight line with a slope of -0.22 at a solution flow velocity of 0.25 m/s and a slope of -0.12 at 0.5 m/s.

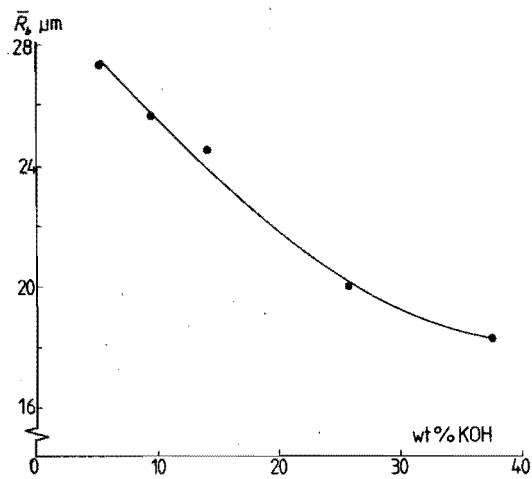

Fig. 5.3.10 The average bubble radius for hydrogen bubbles evolved on a nickel electrode in dependence on KOH-concentration. T = 353 K, v_ℓ = 0.5 m/s, i = 4 kA/m^2 and d_{wm} = 3 mm.

5.3.7. Effect of pressure.

In Fig. 5.3.11 the effect of pressure on the average radius of

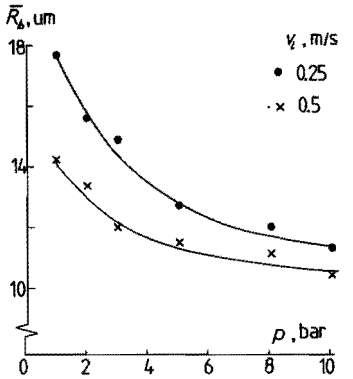

Fig. 5.3.11 The average radius for hydrogen bubbles evolved on a nickel electrode as a function of pressure at two solution flow velocities. T = 353 K, i = 4 kA/m^2, d_{wm} = 3 mm and [KOH] = 30 wt%.

hydrogen bubbles evolved on a nickel electrode is illustrated. The average radius decreases at increasing pressure, due to the decrease in the occurrence of coalescence at elevated pressures. The effect is more pronounced at lower solution flow velocities. Plots of $\bar{R}_b$ versus p on a double logarithmic scale show straight lines with slopes varying from -0.24 at a solution flow velocity of 0.1 m/s to -0.09 at a velocity of 0.5 m/s. The slopes are practically independent of the nature of the gas evolved.

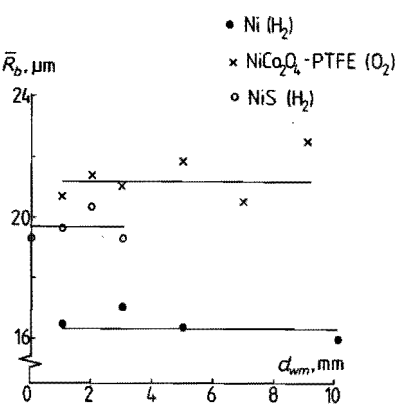

Fig. 5.3.12 The average bubble radius for oxygen and hydrogen bubbles evolved on various electrodes in dependence on distance between the working electrode and the diaphragm. T = 353 K, i = 4 kA/m^2, v_ℓ = 0.5 m/s and [KOH] = 30 wt%.

5.3.8. Effect of distance between working electrode and diaphragm.

The distance between working electrode and diaphragm has been varied from 10 to 0 mm. Fig. 5.3.12 shows the average bubble radius as a function of this distance for a hydrogen evolving nickel and nickelsulfide electrode and for an oxygen evolving teflon bonded nickel cobalt oxide electrode. The average radii are found to be independent of distance between the working electrode and the diaphragm.

5.4. DISCUSSION.

From the experiments it has been found that the average bubble radius at the outlet of the electrolysis cell is practically independent of temperature and distance between working electrode and diaphragm in the ranges studied. Consequently, these parameters do not appear in the dimensionless correlation.
The effect of the other parameters can be represented by the following relation:

$$\bar{R}_b = K_2^* . i^{n_5} . v_\ell^{n^*_6} . p^{n^*_7} . [KOH]^{n_8} \quad \text{where}$$

K^*_2, n_5, n_6, n_7 and n_8 are empirical constants, depending on the nature of the electrode and the gas evolved and possibly on the solution flow velocity in the electrolysis cell. n_5 varies between 0 and 0.16, n_6 varies from -0.06 to -0.40, n_7 from -0.09 to -0.24 and n_8 from -0.22 to -0.12.

To obtain a dimensionless correlation the reduced average bubble radius and the gas to liquid volumetric ratio at the outlet of the electrolysis cell, V_g/V_ℓ, the Reynolds number and the reduced pressure are used. The KOH-concentration is already dimensionless because it is expressed in wt%.
The reduced average bubble radius at the outlet of the cell is defined by the average bubble radius divided by the distance between the backwall of the working electrode compartment to the diaphragm. The gas to liquid volumetric ratio at the outlet of the cell is proportional to $i/p.v_\ell$. Incorporating the dimensionless parameters in the relation, the following dimensionless correlation results:

$\bar{R}_b/d_{bm} = K_2 \cdot (V_g/V_\ell)^{n_5} \cdot Re^{n_6} \cdot p^{n_7} \cdot [KOH]^{n_8}$ where

$\bar{R}_b/d_{bm}$ = reduced average bubble radius at the outlet of the electrolysis cell.

V_g/V_ℓ = gas to liquid volumetric ratio at the outlet of the electrolysis cell.

$Re = d_{hyd} \cdot v_\ell/\nu$

$P = p/p_0$

K_2 = empirical constant, dependent on the nature of the electrode and the gas evolved.

n_5 = empirical constant, dependent on the nature of the electrode and the gas evolved; n_5 varies between 0 and 0.16.

$n_6 = n_6^* + n_5$ = empirical constant, dependent on the nature of the electrode and the gas evolved; n_6 varies between 0.03 and -0.24.

$n_7 = n_7^* + n_5$ = empirical constant, dependent on the nature of the electrode and on the solution flow velocity; n_7 varies from -0.25 at low solution flow velocities to 0.10 at high solution flow velocities.

n_8 = empirical constant, dependent on solution flow velocity; n_8 varies between -0.22 at low velocities and -0.12 at high velocities.

In Table 5.4.1 the numerical values of K_2, n_5, n_6, n_7 and n_8, obtained from our experiments, are given for the cases of the 4 kinds of electrodes studied.

nature of electrode	gas evolved	K_2 v_ℓ= 0.5 m/s	n_5	n_6	n_7 v_ℓ= 0.25	n_7 v_ℓ= 0.5 m/s	n_8 v_ℓ= 0.25	n_8 v_ℓ= 0.5 m/s
Veco gauze	H_2	5.1×10^{-3}	0	-0.10	-0.20	-0.13	-0.22	-0.12
NiS	H_2	3.6×10^{-3}	0.11	-0.04	n.d.		n.d.	
Ni-PTFE	H_2	4.6×10^{-3}	0	-0.11	n.d.		n.d.	
Veco gauze	O_2	1.8×10^{-2}	0.16	-0.24	0	+0.07	n.d.	
$NiCo_2O_4$-PTFE	O_2	2.1×10^{-3}	0.09	+0.03	n.d.		n.d.	

Table 5.4.1 Numerical values of empirical constants for various electrodes.

n.d. = not determined

CHAPTER 6: SUGGESTIONS FOR FURTHER WORK.

In the previous chapters the gas fraction distribution, the ohmic resistance and the current density distribution in the cell during water electrolysis have been discussed.
An attempt has been made to relate the turbulent diffusion theory to the gas bubble distribution and, using Bruggeman's equation, to the ohmic resistance in the cell. However, to come to a more extended and quantitative relation a number of additional experiments has to be carried out.
To obtain insight into the bubble behaviour at a technical electrode, optical measurements should be performed by illuminating and photographing the bubbles from the front of the electrode.
The value of the gas fraction in the cell, in the steady state under various conditions, is important for the determination of the ohmic resistance in the cell. The introduction of local gas void probes [71] may be useful to obtain additional information on the value of the local gas void fraction and on its distribution in the cell.
The flow situation in the cell is very complicated. Measurements to come to a better understanding of the transport phenomena e.g. the determination of the turbulent diffusion coefficient of the bubbles will help to improve the bubble diffusion model proposed in chapter 3.
For practical application it will be very interesting to study the electrolysis process at free convection, using a cell geometry in which the flow induced by the rising gas bubbles has a pronounced effect.

REFERENCES

1) C.A. Hampel, The encyclopedia of electrochemistry, Reinhold Publishing Corporation, New York (1964).

2) R. Hooykaas, Geschiedenis der natuurwetenschappen, Bohn, Scheltema en Holkema, Utrecht (1976).

3) A. Schmidt, Angewandte Electrochemie, Verlag Chemie Weinheim (1976).

4) U. Landan, E. Yeager and D. Kortan, Electrochemistry in Industry, Plenum Press, New York (1982).

5) H. Vogt, Electrochemical reactors with gas evolution, Fortschr. Verfahrenstechnik, 20, (1982), p. 369-404.

6) N. Ibl, Stofftransport bei der Elektrolyse mit Gasrührung, Chem.-Ing.-Tech., 43, (1971), p. 202-215.

7) L.J.J. Janssen and E. Barendrecht, The effect of electrolytic gas evolution on mass transfer at electrodes, Electrochim. Acta, 24, (1979), p. 693-699.

8) L.J.J. Janssen and S.J.D. van Stralen, Bubble behaviour on and mass transfer to an oxygen-evolving transparent nickel electrode in alkaline solution, Electrochim. Acta, 26, (1981), p. 1011-1022.

9) C.W. Tobias, Effect of gas evolution on current distribution and ohmic resistance in electrolyzers, J. Electrochem. Soc., 106, (1959), p. 833-838.

10) L. Sigrist, O. Dossenbach and N. Ibl, On the conductivity and void fraction of gas dispersions in electrolyte solutions, J. Appl. Electrochem., 10, (1980), p. 223-228.

11) F. Hine and K. Murakami, Bubble effects on the solution IR drop in a vertical electrolyzer under free and forced convection, J. Electrochem. Soc., 127, (1980), p. 292-297.

12) G. Kreysa and H.-J. Külps, Experimental study of the gas bubble effects on the IR drop at inclined electrodes, J. Electrochem. Soc., 128, (1981), p. 979-984.

13) L.J.J. Janssen, J.J.M. Geraets, E. Barendrecht and S.J.D. van Stralen, Ohmic potential drop during alkaline water electrolysis, Electrochim. Acta, 27, (1982), p. 1207-1218.

14) E. Hausmann, Technischer Stand der Wasser-Elektrolyse, Chem.-Ing.-Tech., 48, (1976), p. 100-103.

15) N. Gethoff, Wasserstof als Energieträger, Springer Verlag, Wien (1978).

16) M.V.C. Sastri, Hydrogen energy - a prophesy comes true, Int. J. Hydrogen Energy, 5, (1980), p. 365-367.

17) K.E. Cox and K.D. Williamson, Hydrogen: its technology and implications; Vol. 1, Hydrogen production technology, C.R.C. Press, Cleveland (1977).

18) M.S. Cooper, Hydrogen manufacture by electrolysis, thermal decomposition and other unusual techniques, Noyes Data Corporation, New Yersey (1978).

19) F. Deneuve and J.R. Roncat, Thermochemical and hybride cycles of hydrogen production - Technico-economical comparison with water electrolysis, Int. J. Hydrogen Energy, 6, (1981), p. 9-23.

20) E. Barendrecht, Electrochemie, Lecture Notes nr. 6.676, Eindhoven University of Technology, Eindhoven (1982).

21) G.J. Brug, The kinetics of some electrode reactions at the gold/electrolyte solution interface, Ph.D.-Thesis, Ch. 3, Utrecht (1984).

22) A.J. Appleby, M. Chemla, H. Kita and G. Bronoël in (A.J. Bard ed.) Encyclopedia of Electrochemistry of the Elements, Vol. IXa, Marcel Dekker, New York, (1982), p. 413-556.

23) P. Rasiyah, A.C.C. Tseung and D.B. Hibbert, A mechanistic study of oxygen evolution on $NiCo_2O_4$, J. Electrochem. Soc., 129, (1982), p. 1724-1727.

24) H. Dieng, O. Contamin and M. Savy, Oxygen evolution study on porous Molybdenum Naphthalocyanine Electrodes, J. Electrochem. Soc., 131, (1984), p. 1635-1639.

25) K.J. Vetter, Elektrochemische Kinetik, Springer Verlag, Berlin (1961).

26) S.J.D. van Stralen and R. Cole, Boiling Phenomena, Hemisphere Publishing Corporation, Washington (1979).

27) D.E. Westerheide and J.W. Westwater, Isothermal growth of hydrogen bubbles during electrolysis, A.I. Ch. E. Journal, 7, (1961), p. 357-362.

28) L.E. Scriven, On the dynamics of phase growth, Chem. Eng. Sci., 10, (1959), p. 1-13.

29) W. Zijl, Departure of a bubble, growing on a horizontal wall, Ph.D.-Thesis, Eindhoven University of Technology, Eindhoven (1979).

30) H.F.A. Verhaart, R.M. de Jonge and S.J.D. van Stralen, Gas bubble growth during electrolysis, Ing. J. Heat Mass Transfer, 23, (1980), p. 293-299.

31) J.P. Glas and J.W. Westwater, Measurements of the growth of electrolytic bubbles, Int. J. Heat Mass Transfer, 7, (1964), p. 1427-1443.

32) C.W.M.P. Sillen, The effect of gas bubble evolution on the energy efficiency in water electrolysis, Ph.D.-Thesis, Eindhoven University of Technology, Eindhoven (1983).

33) W. Fritz, Berechnung des maximal Volumes von Dampfblasen, Phys. Zeitschrift, 11, (1935), p. 379-384.

34) P.C. Slooten, Departure of vapor- and gas-bubbles in a wide pressure range, Ph.D.-Thesis, Eindhoven University of Technology, Eindhoven (1984).

35) R. Cole and H.L. Shulman, Bubble departure diameters at subatmospheric pressures, Chemical Engineering Progress Symposium Series, Heat Transfer, Los Angeles, 62, (1966), p. 6-16.

36) J.E. Funk and J.F. Thorpe, Void fraction and current density distributions in a water electrolysis cell, J. Electrochem. Soc., 116, (1969), p. 48-54.

37) L.J.J. Janssen, C.W.M.P. Sillen, E. Barendrecht and S.J.D. van Stralen, Bubble behaviour during oxygen and hydrogen evolution at transparent electrodes in KOH-solution, Electrochim. Acta, 29, (1984), p. 633-642.

38) L.J.J. Janssen and S.J.D. van Stralen, Bubble behaviour on and mass transfer to an oxygen evolving transparent nickel electrode in alkaline solution, Electrochim. Acta, 26, (1981), p. 1011-1022.

39) R. Bruckhart and W. Deckwer, Bubble size distribution and interfacial areas in electrolyte solutions in bubble columns, Chem. Eng. Sci., 30, (1975), p. 354-355.

40) L.J.J. Janssen and E. Barendrecht, Mass transfer at gas evolving electrodes, International meeting on electrolytic bubbles, London, Sept. 1984.

41) J.C. Maxwell, A treatise on electricity and magnetism, 2nd ed., Vol. 1, Clarendon Press, Oxford (1881).

42) H. Fricke and S. Morse, Phys. Rev., 25, (1925), pp. 361.

43) A. Eucken, VDI-Forschungsheft, no. 353, (1932), pp. 353.

44) C. Orr and J.M. Dalla Valla, Chem. Eng. Progr. Symposium Ser. no. 9, 50, (1954), pp. 29.

45) Lord Rayleigh, On the influence of obstacles arranged in rectangular order upon the properties of a medium, Phil. Mag., 34, (1892), p. 481-502.

46) H. Fricke, Phys. Rev., 24, (1924), pp. 575.

47) I. Runge, 2. Teck. Phys., 6, (1925), pp. 61.

48) R.E. Meredith and C.W. Tobias, Conduction in heterogeneous systems, Advances in electrochemistry and electrochemical engineering, Vol. 2, John Wiley and Sons, New York (1962).

49) D.A.G. Bruggeman, Berechnung verschiedener physikalischer Konstanten von heterogenen Substanzen, Ann. Physik, 24, (1935), pp. 659.

50) R.E. de la Rue and C.W. Tobias, On the conductivity of dispersions, J. Electrochem. Soc., 106, (1959), p. 827-833.

51) D.A. de Vries, Het warmtegeleidingsvermogen van de grond, Mededelingen van de Landbouw Hogeschool te Wageningen/Nederland, 52 (1), (1952), p. 1-73; The thermal conductivity of granular materials, Annexe 1952-1 an Bulletin de l'Institut du Froid, Paris (1952), p. 115-131.

52) O. Wiener, Abhandl. sächs. Ges. Wiss., Math.-Physik, 32, (1912), pp. 509.

53) K. Lichtenecker, Physik. Z., 27, (1926), pp. 115.

54) C.A.R. Pearce, Brit. J. Appl. Phys., 6, (1955), pp. 113.

55) W.I. Higuchi, J. Phys. Chem., 62, (1958), pp. 649.

56) V.P. Mashovets, J. Appl. Chem. (USSR) (English translation), 24, (1951), pp. 391.

57) W.R. Parrish and J. Newman, J. Electrochem. Soc., 117, (1970), pp. 43.

58) Z. Nagy, Calculations on the effect of gas evolution on the current-overpotential relation and current distribution in electrolytic cells, J. Appl. Electrochem., 6, (1976), p. 171-181.

59) I. Rousar, V. Cezner, J. Nejepsova, M.M. Jacksic, M. Spasojevic and B.Z. Nikolic, Calculation of local current densities and terminal voltage for a monopolar sandwich electrolyzer; Application to chlorate cells, J. Appl. Electrochem., 7, (1977), p. 427-435.

60) I. Rousar, Calculation of current density distribution and terminal voltage for bipolar electrolyzers; Application to chlorate cells, J. Electrochem. Soc., 116, (1969), p. 676-683.

61) F. Hine, M. Yasuda, R. Nakamura and T. Noda, Hydrodynamic studies of bubble effects on the IR drops in a vertical rectangular cell, J. Electrochem. Soc., 122, (1975), p. 1185-1190.

62) F. Hine, M. Yasuda, Y. Ogata and K. Hara, Hydrodynamic studies on a vertical electrolyzer with gas evolution under forced circulation, J. Electrochem. Soc., 131, (1984), p. 83-89.

63) H. Vogt, A hydrodynamic model for the ohmic interelectrode resistance of cells with vertical gas evolving electrodes, Electrochim. Acta, 26, (1981), p. 1311-1317.

64) L.J.J. Janssen and E. Barendrecht, Electrolyte resistance of solution layers at hydrogen and oxygen evolving electrodes in alkaline solution, Electrochim. Acta, 28, (1983), p. 341-346.

65) J.A. Roberson and C.T. Crowe, Engineering Fluid Mechanics, Houghton Mifflin Company, Boston (1975).

66) C.W.M. van der Geld, Ph.D.-Thesis, Eindhoven University of Technology, Eindhoven (to be published).

67) R. Blokland, Private communications (1984).

68) R.S. Scorer, Environmental aerodynamics, Ellis Horwood, Chichester (1978).

69) P.G. Saffman, The lift on a small sphere in a slow shear flow, J. Fluid Mech., 22, (1965), p. 385-400.

70) D.A. Drew and R.T. Lahey, Phase-distribution mechanisms in turbulent low-quality two-phase flow in a circular pipe, J. Fluid Mech., 117, (1982), p. 91-106.

71) C.W.M. van der Geld, Flow regime recognition at elevated pressures, Eindhoven University of Technology (1984).

ABSTRACT

During water electrolysis oxygen and hydrogen bubbles evolved on the electrodes, cause an increase in the ohmic resistance of the electrolysis cell. Consequently, the energy efficiency of the electrolysis process decreases. The aim of the present study is to acquire insight into the effect of various process parameters on the bubble behaviour, the gas void distribution, the ohmic resistance and the current density distribution in the electrolysis cell.

To obtain information on the bubble behaviour and the gas void distribution in a vertically placed cell with forced convection, high speed motion pictures of bubbles on the electrode surface and at various locations in the electrolyte have been taken through a transparent gold electrode (Ch. 2). It has been found that the bubble-electrolyte mixture in the gap between the electrode and the diaphragm can be divided in two regions. In the first region, i.e. the layer adjacent to the electrode, the gas fraction decreases sharply with increasing distance to the electrode surface. In the second region, the gas fraction decreases only slightly with increasing distance to the electrode surface. The width of the first layer depends on current density, solution flow velocity and height in the cell.

A theoretical model for the gas void distribution in the cell, based on the idea of turbulent diffusion of bubbles from the electrode surface, is proposed in chapter 3. Starting from the Bruggeman equation for the resistance of homogeneously dispersed non-conducting particles in a continuous phase an expression, relating the gas void distribution to the ohmic resistance in the electrolysis cell, is obtained. To test the proposed model, the ohmic resistance and current density distributions in the electrolysis cell have been determined, using a segmented nickel working electrode. The predicted and experimental results are found to be in qualitative agreement.

The above mentioned model can not be applied directly to industrial processes, since in these processes the flow in the cell is much more complex than in the experimental set-up. This makes a theoretical approach practically infeasible. To predict the effects of the various process parameters, empirical relations must be derived. Therefore, a number of experiments have been carried out under semi-industrial conditions. The obtained results are expressed in dimensionless empirical relations.

In chapter 4 a dimensionless correlation for the reduced ohmic resistance between the working electrode and the diaphragm and the parameters of the electrolysis process is derived. The relation may be used to determine the optimum electrolysis conditions. In chapter 5 a similar relation is derived for the reduced average bubble radius at the outlet of the electrolysis cell. Knowledge of the average bubble radius and the bubble radius distribution at the outlet of the cell can help to solve the bubble-electrolyte separation problem.

SAMENVATTING

Zuurstof- en waterstofbellen die tijdens waterelektrolyse aan de elektroden ontstaan, veroorzaken een verhoging van de ohmse weerstand van de elektrolysecel. Dientengevolge neemt het energetisch rendement van het elektrolyseproces af. Het doel van het onderhavige onderzoek is het verwerven van inzicht in de effecten van verschillende grootheden op het belgedrag, de gasvolumeverdeling, de ohmse weerstand en de stroomdichtheidsverdeling in de elektrolysecel.

Om informatie te verkrijgen over het belgedrag en de gasvolumeverdeling in een verticaal geplaatste cel met geforceerde convectie, zijn "high speed" filmopnamen gemaakt van bellen op het elektrode-oppervlak en op verschillende plaatsen in de elektrolyt, door een transparante goud-elektrode (Hfst. 2). Het is gebleken dat het bel-elektrolietmengsel in de ruimte tussen de elektrode en het diafragma verdeeld kan worden in twee gebieden. In het eerste gebied, een laag grenzend aan de elektrode, neemt de gasvolumefractie sterk af met toenemende afstand tot het elektrode-oppervlak. In het tweede gebied neemt de gasvolumefractie slechts weinig af met toenemende afstand tot het elektrode-oppervlak. De breedte van de eerste laag is afhankelijk van de stroomdichtheid, de vloeistofsnelheid en de hoogte in de cel.

Een theoretisch model voor de gasvolumeverdeling in de cel, gebaseerd op het idee van turbulente diffusie van bellen van het elektrode-oppervlak wordt voorgesteld in hoofdstuk 3. Uitgaande van de Bruggeman-vergelijking voor de weerstand van homogeen gedispergeerde niet-geleidende deeltjes in een medium, is een uitdrukking verkregen die de gasvolumeverdeling relateert aan de ohmse weerstand in de cel. Om het voorgestelde model te testen zijn de ohmse weerstand en de stroomdichtheidsverdeling in de cel bepaald, gebruik makend van een gesegmenteerde nikkel-werkelektrode. De voorspelde en experimentele resultaten blijken kwalitatief in overeenstemming te zijn.

Het bovengenoemde model kan niet direct worden toegepast op industriële processen, aangezien in deze processen de stroming in de cel veel gecompliceerder is dan in de experimentele opstelling. Dit maakt een theoretische aanpak praktisch ondoenlijk. Om de effecten van de verschillende procesgrootheden te voorspellen, moeten empirische relaties worden afgeleid. Daarvoor zijn een aantal experimenten uitgevoerd onder semi-industriële omstandigheden.

De verkregen resultaten zijn weergegeven in dimensieloze correlaties. In hoofdstuk 4 is een dimensieloze relatie afgeleid voor de gereduceerde weerstand tussen de werkelektrode en het diafragma en de grootheden van het elektrolyseproces. De relatie kan gebruikt worden om de optimale elektrolyse-omstandigheden te bepalen. In hoofdstuk 5 is een soortgelijke relatie afgeleid voor de gereduceerde gemiddelde belstraal aan de uitgang van de elektrolysecel. Kennis van de gemiddelde belstraal en de belstraalverdeling aan de uitgang van de cel kan het bel-elektrolyt-scheidingsprobleem helpen oplossen.

CURRICULUM VITAE

Bernadette Schlenter werd op 19 september 1957 geboren te Eindhoven. Zij doorliep het Gemeentelijk Lyceum aldaar en deed in 1976 eindexamen Atheneum-B. Aansluitend begon zij met de studie scheikunde aan de Rijksuniversiteit te Utrecht, waar zij in december 1981 afstudeerde. Een week hierna trouwde zij met Kees Bongenaar.
In februari 1982 trad zij in dienst van de Technische Hogeschool te Eindhoven bij de interafdelingswerkgroep "Gasontwikkelende elektroden" van de vakgroepen Elektrochemie (Scheikundige Technologie) en Transportfysica (Technische Natuurkunde), in het kader van een contract tussen de Technische Hogeschool en de commissie van de Europese Gemeenschap te Brussel. Het dienstverband werd in juli 1983 door de Technische Hogeschool verlengd, om gelegenheid te geven voor het doen van aanvullend onderzoek, hetgeen heeft geleid tot de totstandkoming van dit proefschrift.

Stellingen
behorende bij het proefschrift
van B.E. Bongenaar-Schlenter
7 december 1984

I

De verklaring door Ibl en Landolt voor het verschil in de verwachte en gemeten snelheid van de chloraatvorming bij lage NaCl concentratie (factor 7-65) met een kinetisch model is aan bedenkingen onderhevig.
(N. Ibl and D. Landolt, J. Electrochem. Soc., 115, (1968), p.713-720.)

II

Het is onjuist dat ten gevolge van convectie de effecten van verwarming op de respons bij demodulatie-voltammetrie overgewaardeerd worden.
(J. Struys et al., J. Electroanal. Chem., 143, (1983), p. 61-71.)

III

Townsend en Hart tonen onvoldoende aan dat de chromaat-passiveringslaag op Al-Zn deklagen en op Zn deklagen verschillend van samenstelling zijn.
(H.E. Townsend and R.G. Hart, J. Electrochem. Soc., 131, (1984), pp. 1345.)

IV

De aanname dat een ladingsoverdrachtscoëfficiënt α ongeveer 0,5 dient te zijn, leidt te gemakkelijk tot allerlei typen complexe reactieschema's voor bestudeerde elektrodereacties.
(F. v.d. Pol et al., J. Electroanal. Chem., 58, (1975), pp. 177;
C.P.M. Bongenaar et al., J. Electroanal. Chem., 111, (1980), p. 139-155;
J. Struys, Ph.D.-Thesis, (1984), Utrecht.)

V

Of de vergelijkingen voor de schatting van de ohmse weerstand ten gevolge van gasbellen aan het elektrode-oppervlak, zoals deze door Vogt worden gegeven, werkelijke verbeteringen zijn vergeleken met de benadering door Sides en Tobias, is twijfelachtig.
(H. Vogt, J. Appl. Electrochem., 13, (1983), p. 87-88;
P.J. Sides and C.W. Tobias, J. Electrochem. Soc., 127, (1980), p. 288-291;
Dit proefschrift, hfst. 3.)

VI

Bossen als natuurlijke begroeiing in grondwaterwingebieden zijn ongewenst.
(H. Loman et al., Publicatiereeks Milieubeheer, 1984.)

VII

Het overheidsbeleid zou consistenter zijn, indien door het bedrijfsleven gevraagde ambtenaren voor de overheidsdienst behouden werden door het bieden van extra arbeidstijdverkorting bij gelijkblijvende beloning in plaats van hogere beloning bij gelijkblijvende arbeidstijd.

VIII

Terwijl de invoering van personal computers op grote schaal in menig opzicht als een vooruitgang beschouwd wordt, loopt hierdoor de kwaliteit van de software terug.